Development and biophysical characterization of a hyaluronic acid – vitamin E conjugate as a subcutaneous delivery platform

By

Kenneth Ryan Moulder

Submitted to the graduate degree program in Pharmaceutical Chemistry and the Graduate Faculty of the University of Kansas in partial fulfillment of the requirements for the degree of Doctor of Philosophy.

_____

Chairperson M. Laird Forrest, Ph.D.

_____

Cory Berkland, Ph.D.

_____

C. Russell Middaugh, Ph.D.

_____

Teruna Siahaan, Ph.D.

_____

Arghya Paul, Ph.D.

Date defended: July 18, 2019

The Dissertation Committee for Kenneth Ryan Moulder certifies that this is the approved version of the following dissertation:

Development and biophysical characterization of a hyaluronic acid – vitamin E conjugate as a subcutaneous delivery platform

Chairperson M. Laird Forrest, Ph.D.

Date approved: July 18, 2019

Abstract

The inherent properties of protein therapeutics (e.g. high molecular weight, charged, conformationally dependent) has historically limited their administration to parenteral routes which presents new challenges to their controlled delivery. Hydrogel and nanoparticle drug delivery systems can parenterally deliver a wide variety of drugs in a controlled manner while sustaining their therapeutic efficacy. Nanogels, formed from amphiphilic polymers, combine the unique and tunable properties of hydrogels and nanoparticles into one drug delivery system and have the potential to drastically improve the clinical applicability of protein therapeutics delivered subcutaneously.

Hyaluronic acid, a ubiquitous polysaccharide of the extracellular matrix often used in drug delivery applications, was hydrophobically functionalized by the addition of glycine-modified vitamin E (α-tocopherol) to form a self-assembling nanogel (HAtoco). The characterization of HAtoco was further developed by modifying its molecular weight and tocopherol substitution towards an optimum 33 kDa backbone with a 10mol% substitution. Physical and chemical characterization of the optimum HAtoco demonstrated its polydisperse effective size, stable colloidal and chemical stability and continued biodegradability by the endogenous enzyme hyaluronidase. In addition, HAtoco doubled the *in vitro* release half-life of three model proteins (BSA, RNase, Lysozyme) and the *in vivo* release half-life of the clinical protein therapeutic Coversin when delivered subcutaneously to mice. Structural studies of HAtoco bound Coversin demonstrated destabilization of the protein upon adsorption, but released Coversin from the HAtoco nanogel demonstrated complement inhibition for at least 73 hours *in vitro*. Overall, HAtoco has demonstrated the ability to bind protein therapeutics in a reversible manner capable of prolonging their release in a therapeutically efficacious state.

Acknowledgements

I would like to first thank my advisor and mentor, Dr. Laird Forrest. I have had the fortune of learning from Laird for the past eight years through undergraduate and doctoral research. He has given me the opportunity to work on many translational research projects that have the potential to directly affect patients, human and canine, in the near future. These projects have inspired me to be creative in the way I approach problems and to always have an entrepreneurial eye towards future translational applications. He believed in me and invested his time and resources to see that I become the scientist I am today and for that I will be forever grateful.

I would also like to thank my dissertation committee members: Dr. Cory Berkland, Dr. Russ Middaugh, Dr. Teruna Siahaan and Dr. Arghya Paul. They have all provided helpful guidance and suggestions as I progressed through my research and their critical review of my dissertation was invaluable to its completion. I would also like to thank the entire Department of Pharmaceutical Chemistry for the world-class education and network they have provided me, I am truly blessed to be part of its great history.

To all the current and past members of the Forrest lab and Hylapharm: Dr. Dan Aires, Allie Brachtenbach, Dr. Shuang Cai, Mark Craven, Melanie Forrest, Dr. Chad Groer, Jordan Hunt, Dr. Jaden Jun, Peter Kleindl, Ruolin Lu, Derek Mull, Dr. Abby Petrulis, Dr. Sanjeewa Senadheera, Jacob Thompson, Dr. Ninad Varkhede, Dr. Qiuhong Yang, Dr. Ti Zhang and Dr. Yunqi Zhao, your mentoring and discussions form the heart of what I've learned here and I cannot thank you all enough.

Thank you to all the collaborators who have supported my research including Nick Larson, Dr. Yangjie Wei, Dr. Siva Angalakurthi, Dr. Sanjeev Agarwal, Dr. Vishal Toprani, Dr. Derek

White, Dr. Ishan Shah, Dr. Björn-Hendrick Peters, Stephanie Johnson, Aric Huang, Mellissa Pressnall, Brian Kopec, Dr. Peter Rowe, Dr. Lesya Zelenchuck, Dr. Joe Gadzia, Dr. Todd Williams, Dr. Justin Douglas, Sarah Neuenswander, Dr. Eduardo Rosa-Molinar, Dr. Noraida Martinez-Rivera, Heather Shinogle, Dr. Prem Thapa and Dr. Irma Torres-Vazquez.

Finally, I would like to thank my family including my brother and sister, parents, grandparents, aunts, uncles and cousins for their support and encouragement. You all have made me the person I am today and are a big part of my successes. To my dear wife Kaitlyn, you have empowered me to this moment with your support, patience and love. You have sacrificed so much for me to achieve this and I could not have done it without you. I love you and cannot wait to start the next chapter of our lives together.

Table of Contents

Chapter I: Introduction

1.1 Advantages to Modified Release Strategies of Pharmaceuticals

Medicines can be considered drug delivery systems (DDS) which strive to deliver a desired effect in a safe, efficient, reproducible and convenient way.[1] Although the medicinal application of slow release coatings has been in use since twelfth century China[2], the modern western design of modified or slow release systems began in the 1950's[3] with the introduction of Spansule by Smith-Kline & French.[4] Prior to the introduction of Spansule, all medicines constructed in pill or capsule formulations released the drug or active pharmaceutical ingredient (API) immediately upon dissolution of the outer enteric coating. No mechanism was intentionally implemented to modify or control the release of drug.[3] Conventional medicines designed in this manner generally exhibit fast absorption, systemic exposure and subsequent onset of the intended pharmaceutical effect. The profile of drug release from a dosage form can be deliberately modified to achieve a variety of objectives, from therapeutic targets to patient convenience. A modified-release drug product is a dosage mechanism that alters the timing, rate or location of release of the active pharmaceutical. These products include extended release, delayed release and targeted release. Modified-release drug products can obtain these drug profiles from a number of strategies including enteric coating and prodrug modification for orally delivered drugs, depot suspensions for parenterally delivered drugs. Selection and design of a modified-release form must take into account the intended route of administration and the physicochemical, pharmacokinetic and pharmacodynamic properties of a drug candidate.[1, 5]

The ultimate goal of an effective drug delivery strategy is to maintain an appropriate therapeutic concentration of an active drug form for the appropriate duration of time and in the appropriate location. For acute maladies requiring fast action, conventional medicines generally deliver drug through a single dose with immediate release to the intended therapeutic location at

concentrations sufficient for therapeutic effect while avoiding drug-induced toxicity. The area between an ineffective concentration and toxic concentration is known as the therapeutic window (Figure 1.1).[6] In contrast, chronic conditions often require a sustained period of therapeutic efficacy to avoid relapse of symptoms. Multi-dose regimens can sustain the desired pharmacological effect. This strategy can lead to wide variations in drug levels during treatment and requires strict patient compliance for the desired pharmacotherapeutic outcome. Modified-release drug strategies are used to avoid pharmacokinetic and compliance complexities associated with frequent dose regimens. These strategies incorporate the required multiple doses for treatment into a drug sustaining those concentrations within the therapeutic window for the desired duration (Figure 1.2).[6]

Spansule[4] was the first sustained-release formulation technology to maintain the therapeutic drug concentration for 12 hours by incorporating coated and uncoated drug beads within a capsule. This approach allowed differential dissolution of drug and thus exposure by altering access to GI fluids.[7] Since its release, the field of drug delivery has expanded exponentially, substantially impacting the pharmaceutical industry. Early research successfully developed many models of oral sustained release systems still used today. More recently, efforts to design novel DDS which can overcome biological barriers has become an area of heightened focus.[8] Today, delivery systems such as transdermal patches, microparticles, nanoparticles, inhalers and antibody-drug conjugate products have cumulative annual revenues greater than $100 billion[9] and most importantly have improved countless lives.

It is the task of a drug delivery scientist to evaluate the proper route of administration and dosage form of a medicine based on the desired therapeutic target and the physicochemical properties of the drug. This chapter covers the challenges and opportunities presented by the

delivery of protein therapeutics, including advances in the development and examination of novel drug delivery platforms to control their release profiles. Particular attention is given to the use of nanogel systems for protein delivery and their characterization.

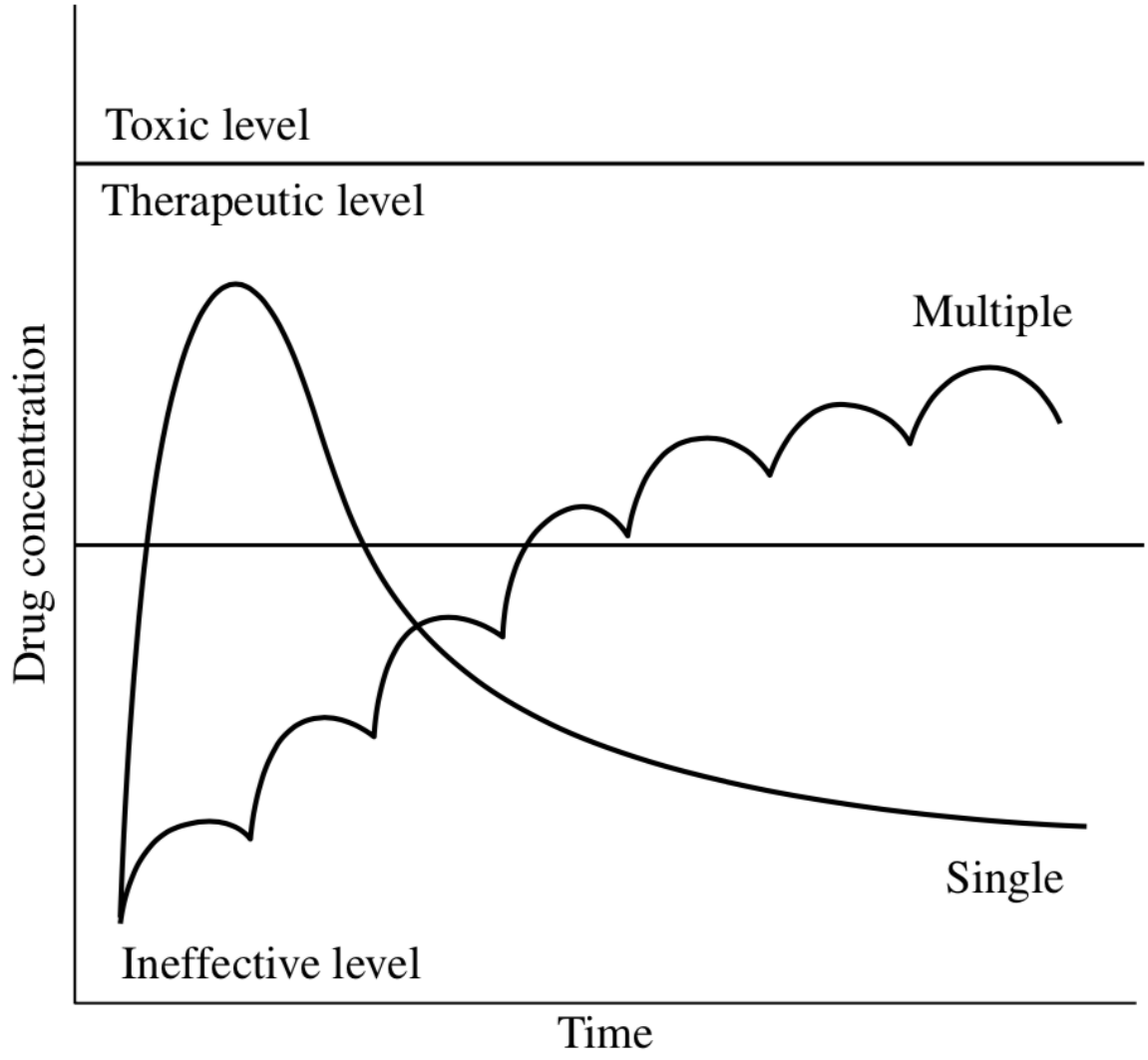

Figure 1.1: Single dose absorption and elimination vs. multi-dose regimen. © 2016 John Wiley & Sons, Inc. Used with permission without changes from Barich, D. H.; Zell, M. T.; Munson, E. J., Physicochemical Properties, Formulation, and Drug Delivery. *Drug Delivery: Principles and Applications*, Second Edition. Edited by Binghe Wang, Longqin Hu, and Teruna J. Siahaan. **2016**. Published 2016 by John Wiley & Sons, Inc.

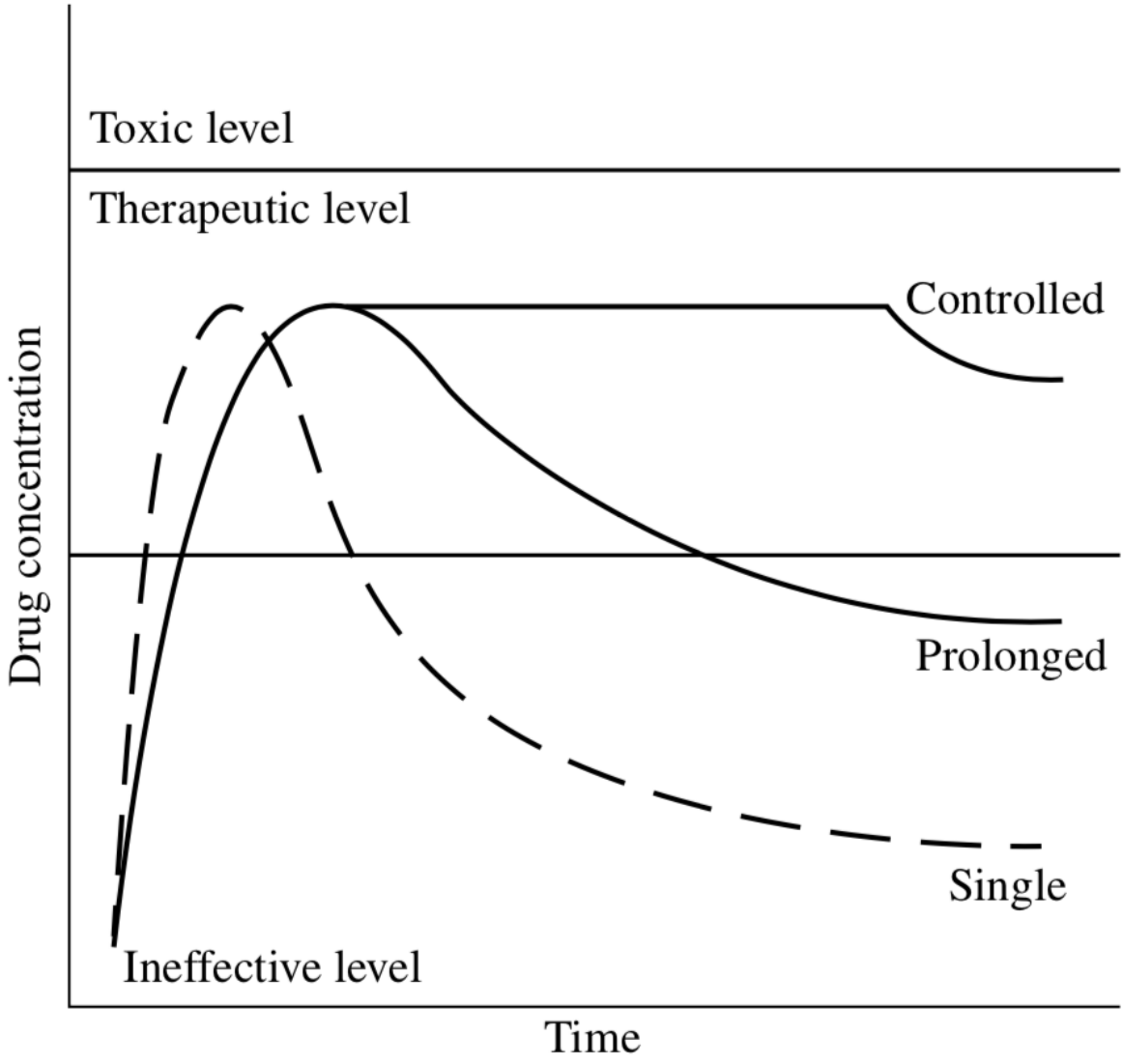

Figure 1.2: Modified-release drug delivery strategies to alter drug exposure profiles. © 2016 John Wiley & Sons, Inc. Used with permission without changes from Barich, D. H.; Zell, M. T.; Munson, E. J., Physicochemical Properties, Formulation, and Drug Delivery. *Drug Delivery: Principles and Applications*, Second Edition. Edited by Binghe Wang, Longqin Hu, and Teruna J. Siahaan. **2016**. Published 2016 by John Wiley & Sons, Inc.

1.2 High Prevalence of Biologics

Over the past four decades, macromolecule drugs known as biologics have become a significant portion of the medicines approved each year within the pharmaceutical industry. These biopharmaceutical drugs can include peptides, recombinant proteins, enzymes, antibodies, antibody drug conjugates and many more. To date, over 260 novel biological therapeutics have been approved for human use for over 230 indications.[10] In 2018, 59 new medical entities (NMEs) were approved by the FDA, and 17 of the approved NMEs were biological license applications (BLAs). Since 2010, 24% of all NMEs approved by the FDA have been biologics (Figure 1.3) with total sales of biopharmaceuticals reaching $188 billion globally in 2017.[11, 12] Developmental pipelines have been similarly affected, with biologics encompassing nearly 20% of all drugs developed in 2013.[13]

1.3 Challenges to the formulation and delivery of protein therapeutics

The increasing development of biopharmaceuticals is largely due to their inherent advantage in specificity and potency compared to small molecule drugs arising from their increased structural complexity. However, these complexities have led to recognizable challenges in their formulation and deliverability.[13] Significant physicochemical differences exist between proteins and small molecule therapeutics particularly with respect to their molecular weight, functional group diversity including ionization and hydrophilic/lipophilic balance and their general chemical and physical structure.[14]

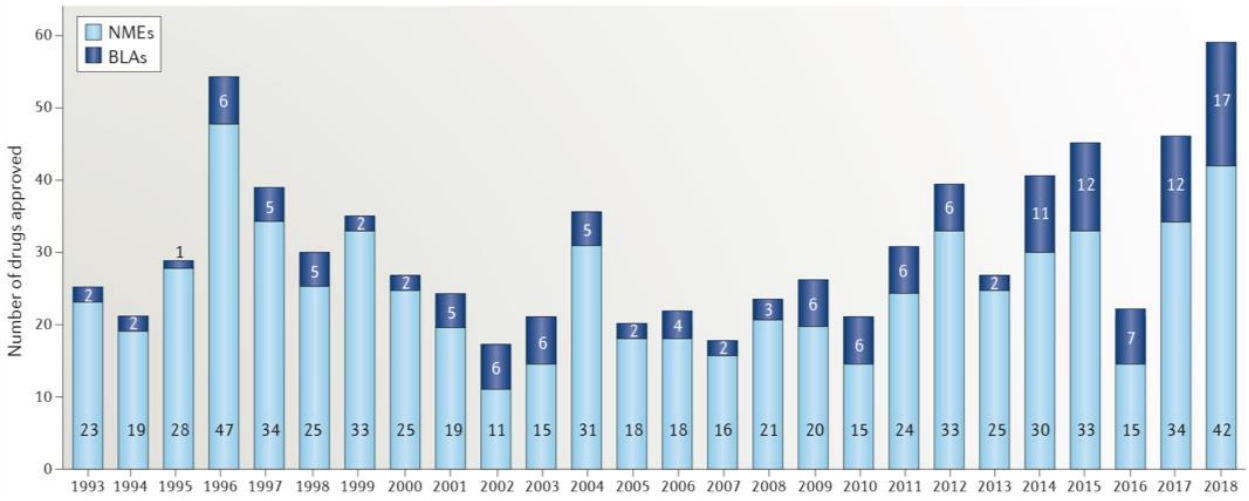

Figure 1.3: FDA approvals of novel molecular entities (NMEs) and biological drug applications (BLAs) since 1993.[12] © 2019 Springer Nature Publishing AG. Used with permission without changes from Mullard, A., 2018 FDA drug approvals. *Nat Rev Drug Discov* **2019,** *18* (2), 85-89.

1.3.1 Protein Structure

Proteins are composed primarily of 20 common amino acids linearly polymerized by peptide (amide) bonds. This linear sequence of amino acids is known as a polypeptide. Wide variability exists within the physicochemical properties of individual amino acid side chains. Variabilities include charge, hydrophobic character, hydrogen-bonding capacity, molecular weight and flexibility which significantly contribute to the higher ordered structure and dynamics of the protein.[15] Proteins form four higher ordered levels of structure: primary, secondary, tertiary and quaternary. The protein primary structure is defined by the linear arrangement of amino acids forming the polypeptide backbone. Secondary structures describe local conformations due to hydrogen bonding initiated between carboxyl oxygens and amide nitrogens of spatially neighboring amino acids backbones. Secondary structure spatial arrangements like the α-helix, β-sheet and β-turn are commonplace in structurally elucidated proteins.[16] Tertiary structural arrangements are a result of the cumulative coalescence of interactions from secondary structures, side chain hydrophobicity, hydrogen bonding, electrostatic interactions, van der Waals forces and disulfide bridging, ultimately determining the protein's three dimensional form. Hydrophobic interactions are substantially impactful during the development of tertiary structure due to hydrophobic side chain water exclusion through the formation of a hydrophobic protein core.[17, 18] The highest ordered structure, quaternary structures, describe the intermolecular interactions between tertiary domains of two or more proteins, which can lead to an array of multimers forming in solution.[17]

The inherent higher ordered structures of proteins and their critical contribution to the heightened specificity of protein therapeutics over small molecules increases the importance of developing a formulation preserving these structures. Chemical degradation of the amino acid

backbone and sides chains through mechanisms such as deamidation and oxidation can lead to decreased potency and/or increased immunogenicity.[19] Significant attention is also paid to the physical aspects of formulations which may lead to the loss of protein function such as moisture or temperature driven protein aggregation and conformational alterations.[20]

1.3.2 Physiological barriers to protein delivery

The degree of physiological barriers impeding the effective delivery of proteins depends on both the method of delivery and site of action. Passage of drugs across cellular barriers generally occurs through four pathways: paracellular, transcellular, active transport or endocytosis. The route in which drugs are able to permeate these biological barriers is highly influenced by its polarity, ionization, physical size and conformation. Paracellular transport is largely restricted to small molecular weight solutes and peptides of less than 8 Å in diameter (ca. 180 Da or 1-2 amino acids).[21] This is due to the presence of tight junctions and is therefore not suitable for the permeation of normally high molecular weight proteins.[22] In order for drugs to passively transverse the membrane lipid bilayer, they must possess a similarly small size, but also significant lipophilic character. The lipophilic characteristics and size exclude a majority of protein therapeutics. Proteins which generally are restrained by their high molecular weight and hydrophilic/charged surfaces are therefore limited to active, facilitative or endocytic transport mechanisms in order to cross cellular barriers. These transportation processes occur through interaction with transmembrane proteins which assist in the traversing of the lipid bilayer down concentration gradients (facilitative) or against concentration gradients through input of energy (active).[23]

1.3.3 Oral delivery of proteins

Orally delivered medicines comprise the majority (62.02%)[24] of currently marketed pharmaceutical products (Figure 1.4) within the US due to their ease of administration and sustained delivery which lead to higher patient compliance.[25] Oral dosage forms are generally less expensive to produce without required sterile manufacturing condtions.[26] Although viewed as the most sought-after route of delivery, oral administration of biopharmaceuticals has been historically challenging.[27, 28] The oral bioavailability of proteins is limited, typically less than 1-2%. It is limited for many reasons, including chemical degradation in the shifting pH of the gastrointestinal tract, proteolytic degradation and limited permeation through mucosal layers and across the intestinal endothelium due to their inherent charge and size.[25, 29, 30] Outside of live-attenuated vaccine products, to date only two peptide-based drugs have been approved for oral delivery. The approved drugs are desmopressin and cyclosporin, each with bioavailabilities of less than 30% despite their relatively small sizes, 1069 Da and 1203 Da, respectively.[31] Other delivery routes such as nasal[32], pulmonary[33], buccal and vaginal have been explored for protein therapeutics with varying success, but are not usually considered in a majority of approaches.[34]

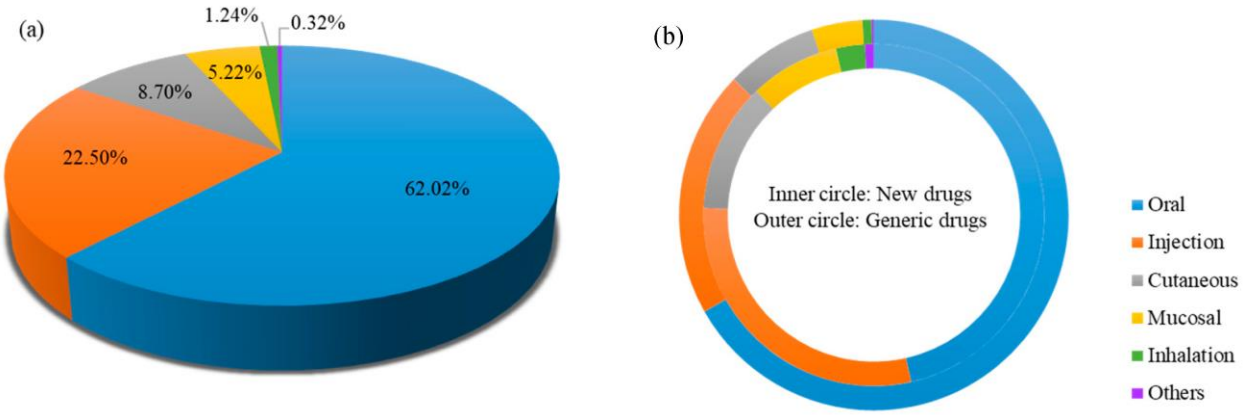

Figure 1.4: (a) Distribution of administration route for currently approved FDA pharmaceutical products. (b) Comparison of new (inner circle) and generic (outer circle) drug administration route distributions. © 1996-2019 MDPI. Used with permission without changes from Zhong, H.; Chan, G.; Hu, Y.; Hu, H.; Ouyang, D. A Comprehensive Map of FDA-Approved Pharmaceutical Products. *Pharmaceutics* **2018**, *10*, 263.

1.3.4 Parenteral delivery of proteins

Due to the challenges presented by the oral delivery of protein therapeutics, the vast majority of approved biologics are parenterally delivered through intravenous, subcutaneous or intramuscular injection. Direct injection avoids many of the barriers associated with oral delivery leading to higher bioavailability and lower manufacturing costs. Unlike orally delivered therapeutics, parenteral injections are able to avoid first-pass hepatic and gastrointestinal metabolism leading to longer circulating half-lives and subsequent effector functions.[35, 36] Although improvements in bioavailability of biologics through parenteral delivery makes their development feasible, many disadvantages still exist.

1.3.5 Burden of parenteral administration on patients and the medical system

Half of the adults worldwide and about 8% of children are estimated to have a chronic condition requiring medical treatment.[37] An estimated 50% of patients requiring long-term therapy for a chronic illness exhibit some form of non-adherence to their prescribed medication regimen.[38, 39] Traditionally, parenterally delivered biologics require the use of needles to administer, which many patients find painful leading to poor patient compliance.[40, 41] Estimated costs of medication non-adherence within the US range from $100 to $290 billion annually.[38] Parenteral administration, particularly intravenous, requires a trained professional to safely administer which can create barriers to compliance. [42] In addition, many proteins have relatively short half-lives in circulation which leads to multiple visits to a medical professional for administration increasing the overall cost to the patient, decreases compliance and stress on the medical system.

1.3.6 Benefits of at-home or self-administration programs on patient compliance and the overall healthcare market

Health care spending in the United States grew 3.9% to $3.5 trillion or $10,739 per person in 2017, reaching 17.9% of the gross domestic product (GDP).[43] Compared to the top ten GDP nations, the US spends nearly twice as much on health care with the cost of labor and products as a significant contributing factors.[44] Treatment of chronic conditions, which can require regular hospital visits, accounts for nearly 75% of total health care spending.[45] In addition to legislative efforts such as the adoption of the Affordable Care Act (ACA) to reduce overall healthcare spending and increase focus and funding on disease prevention efforts, many hospital systems have proposed and implemented home-based care programs. These programs facilitate clinicians administering treatment to acutely ill patients within their own home.[46, 47] These programs drastically reduce the capital resources required for patient treatment when compared to in-hospital care. However, these programs place burden on clinicians, who are unable to see as many patients and are often not reimbursed for travel time. A similar program analyzing the cost savings of an at home medical professional injection compared to clinical-setting administration of the chemotherapeutic bortezomib resulted in a 16.5% cost savings.[48] In continuation of these efforts to reduce the medical costs associated with clinical-setting administration of drugs, educating patients on disease self-management, including drug administration, has been proposed.[45] This type of self-care has been shown to be effective in multiple chronic diseases, most notably the treatment of type 1 diabetes. Patients are trained to monitor their own blood sugar levels and on proper administer insulin injections subcutaneously when needed.[49] At home, self-administration of biotherapeutics is also common practice for chronic diseases like rheumatoid arthritis, primary

immunodeficiency and multiple sclerosis.[50] Many subcutaneous oncology therapies are also currently under consideration.[51, 52]

1.3.7 Subcutaneous injections as a desirable alternative to other parenteral delivery routes

Clinical settings required for safe and effective injections of many biologics have been shown to add to overall treatment costs and are a resource burden on the healthcare system, healthcare providers and patients.[50] A study of overall administration time of trastuzumab when delivered subcutaneously instead of through intravenous (i.v.) infusion showed a decrease in duration of injection from 90 minutes to 5 minutes on average.[53] In addition, use of subcutaneous injections in place of i.v. administration may reduce the risk of systemic infections.[54] Intramuscular (i.m.) injections have been implemented to some degree for the administration of many biopharmaceuticals. However, the depth of skeletal muscle a 1 to 2 inch needle is required leads to an increased potential for pain due to muscle damage or nerve contact. The risk factors associated with the depth required for i.m. injections also makes administration by trained professionals in a clinical setting a requirement.[55]

As a viable alternative to traditional intravenous or intramuscular delivery of biologics, subcutaneously delivered drugs have presented several advantages including improved patient compliance, stronger potential for self-administration and subsequently reduced healthcare costs.[56-58] For these reasons, the global market of subcutaneously delivered biologics is projected to continue grow over the coming years.[56] Overall, increased approvals of biopharmaceuticals coupled with the inherent physicochemical properties which limit their oral bioavailability has led

the biotechnology industry to explore subcutaneous delivery as a viable, convenient and cost-effective means to parenterally administer these unique medicinal products.

1.4 Subcutaneous anatomy and physiology

Subcutaneous injections deliver drug product into the interstitial space located below the dermis known as the hypodermis (Figure 1.5).[59] The main structural components of the hypodermis extracellular matrix (ECM) include collagen and glycosaminoglycans like hyaluronan (hyaluronic acid, HA).[60] Collagen, the most abundant protein in the body of mammals, forms a fibrous network critical for mechanical stability of the ECM.[61] HA is a lineaer anionic polysaccharide of generally high molecular weight (up to 2000 kDa)[62] and concentrations (1g per 100g wet tissue)[63] in the subcutaneous tissues. HA has been proposed to serve as a viscosity modified lubricant and is readily enzymatically degraded with a tissue half-life of 0.5 to 3 days.[62] The structure and physiology of the subcutaneous tissue can vary greatly between species and locations within the body which likely contributes to differences in absorption profiles and pharmacokinetic variance.[64, 65]

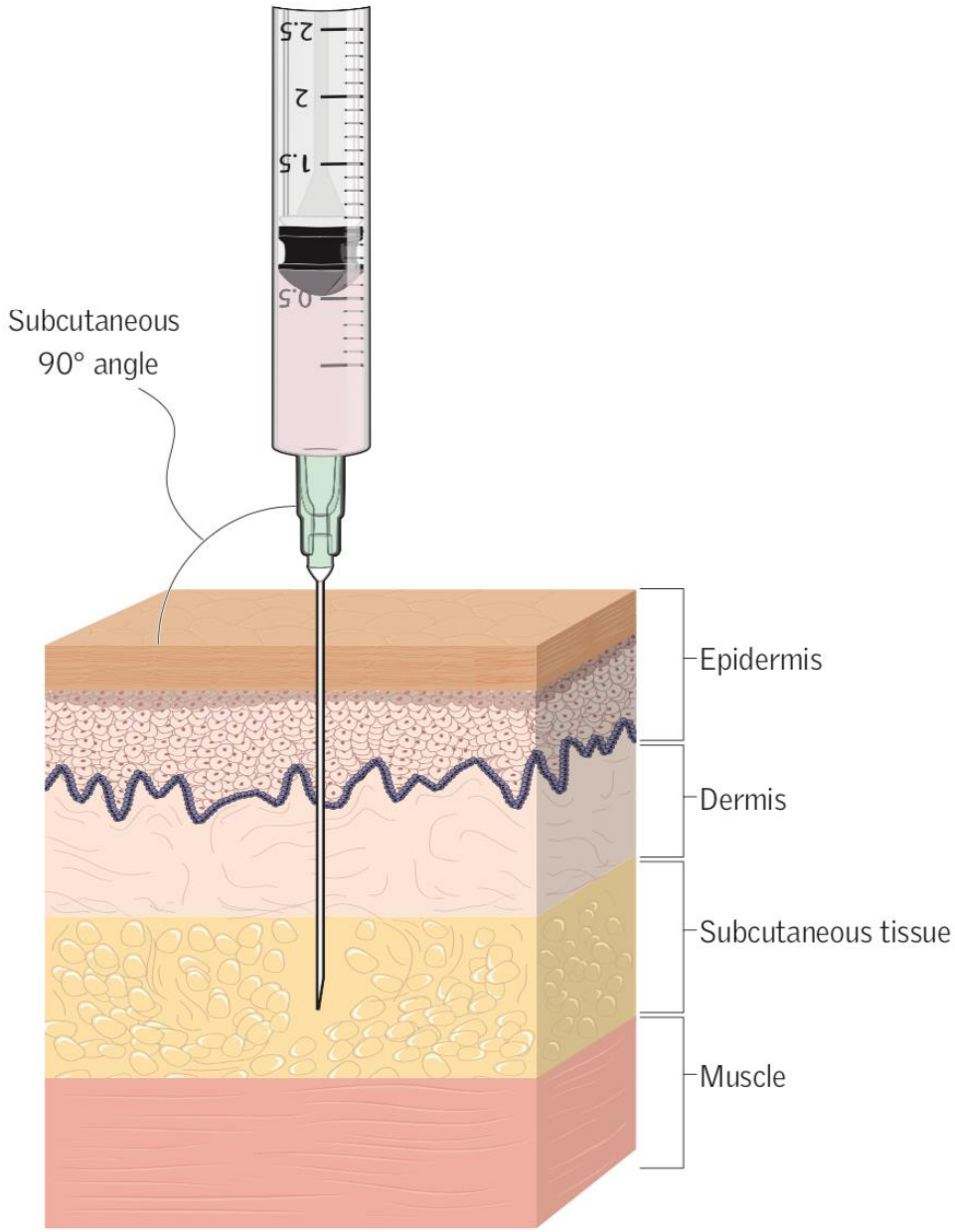

Figure 1.5: Subcutaneous injection with anatomy of skin. © 2015 RCN Publishing Ltd. Used with permission without changes from Ogston-Tuck, S., Subcutaneous injection technique: an evidence-based approach. *Nurs Stand* **2014,** *29* (3), 53-8.

1.5 Pharmacokinetics of subcutaneously delivered biologics

One of the most pressing challenges to the sustained delivery of biologics via intraveneous administration are the short biological half-lives ranging from minutes to hours which are often exacerbated by fast enzymatic degradation or renal clearance.[34] Subcutaneously delivered proteins can exhibit a range of bioavailabilities and release profiles depending on their physicochemical properties and the given formulation.[60, 64, 66] The bioavailability of monoclonal antibodies (mAbs) injected subcutaneously in the clinical-setting ranges from 50-85%.[31] Following subcutaneous injection, protein therapeutics reach systemic circulation either through continuous blood capillaries or through lymphatic vessels if greater than 16-20 kDa.[67, 68] The determinants of absorption for biotherapeutics following subcutaneous delivery is unclear. Absoroption kinetics are believed to be governed by diffusion rates of the biotherapeutic from the injection site and the convective interstitial flow to the site of absorption.[31] Protein therapeutics, like all drugs, are not delivered solely as the active ingredient, but often with a complex formulation of buffers, excipients and stabilizers. These act to enhance the shelf-stability of a pharmaceutical and enable a more efficient delivery to the intended target. Upon injection, proteins transition from conditions in which they are formulated to those of the native interstitial environment.[66] Low bioavailability conditions may form due to interactions with components of the ECM, uptake within circulating immunological cells or foreign bodies like granulomas developing in response to non-native polymeric formulations.[31, 69-71] Effects on biopharmaceutic stability, activity and transportive properties to changes in ionic composition, pH, temperature and osmotic pressure must be considered for proper formulation and delivery prior to subcutaneous injections.[66] Injection volume is limited (< 1.5 mL)[72] within the subcutaneous space due to the high concentration of

structural proteins and polymers used to insulate underlying musculoskeletal tissue from thermal and mechanical stressors.[73]

1.6 Controlled release strategies for parenterally delivered biologics

General objectives of a quality biotherapeutic formulation are: protect the protein from degradation, increase the therapeutic half-life, increase efficacy, reduce side effects, reduce dose frequency, reduce dose amount, alleviate pain associated with injection and reduce the cost of treatment. Strategies to enhance therapeutic half-life, stability and efficacy of a protein therapeutic can be divided into two approaches: chemical modification and colloidal incorporation.[34]

1.6.1 Chemical modifications

Delivery strategies which chemically modify protein therapeutics in order to control their release have been generally shown to improve biologic stability and slow clearance.[34] These strategies include PEGylation, acylation, and hyperglycosylation. Specific studies including the protein therapeutic, route of administration and fold increase in half-life over controls are compiled in Table 1.

1.6.1.1 PEGylation

The discovery of PEGylation of protein therapeutics and the effect on increasing circulation half-life was a monumental advance in the modified pharmacokinetics of protein therapeutics.[74] This advancement enabled the approval of a number of protein therapeutics which were initially limited by short circulating half-lives not practical for dosing regimens or initiated adverse immunological responses.[75] PEGylation entails the covalent conjugation of polyethylene

glycol (PEG) to the biotherapeutic of interest. PEG addition improves stability, half-life and activity of many biological products. This is due to the altering effects on molecular weight, physical size, solubility and the steric hindrance of enzymatic and chemical degradants.[76] The increased water required for solvation of ethylene glycol repeating units provides a 5-10-fold increase in hydrodynamic radius compared to unmodified proteins of similar molecular weight leading to decreased renal clearance and subsequent increased systemic circulation.[77] PEG modification of therapeutic proteins has been found to increase half-life 4.5 to 70-fold.[34].

Covalent addition of PEG functionalized with a bioconjugate reactive handle like N-hydroxysucccinimide esters or maleimides for semi-specific residue addition may partially inhibit the active site of the protein, further impacting the therapeutic effect depending on the amino acid target selected.[34] The balance between biological activity and improved pharmacokinetics inherent in the use of PEG is shown in the case of PEGylated IFN α-2a. PEGylated IFN α-2a exhibited a a 93% decrease in antiviral activity. The therapeutic function of IFN α-2a, was observed following PEG modification, but with a 70-fold increase in serum half-life.[78] PEG is not biologically degradable and must be cleared intact by the kidneys. This is one disadvantage of utilizing PEG derivatives to increase sustain therapeutic half-lives. However, toxicological studies have shown that at the doses generally administered for PEGylated biologics a 600-fold window exist before toxicity has been observed in humans.[79]

1.6.1.2 Acylation

Another approach to the sustained parenteral delivery of proteins is to increase their lipophilicity through covalent acylation with long fatty alkyl chains.[80] This strategy has been shown in some cases to increase the affinity for serum albumin in the blood and thereby increasing

the circulation half-life.[81] Fatty acid conjugation to human insulin led to a 24 hour duration of therapeutic effect for insulin detemir (Levemir) following subcutaneous injection.[82] Similarly, derivatization of the glucagon-like peptide-1 with a range of fatty acids was shown to reduce dosing frequency to a once daily administration. SAR analysis of these conjugates indicated increases in alkyl chain length generally led to decreases in potency, but potency was generally unaffected by the location of substitution near the C-terminal.[83]

1.6.1.3 Hyperglycosylation

Hyperglycosylation of proteins occurs through enzymatic addition of polysaccharides to residues through *in situ* chemical ligation or site-directed mutagenesis to form a glycoconjugate.[84] Similar to PEGylation in its impact on physical properties, hyperglycosylation of protein therapeutics extends pharmacokinetic profiles through reduction in clearance[85], but also through modulation of receptor-facilitated cellular uptake.[86] Unlike PEG, polysaccharide additions resulting from hyperglycosylation are known to be biologically degradable and generally non-toxic.[87]

Subcutaneous injections of various N-glycosylated IFN-α2 showed up to a 25-fold increase in half-life compared to unmodified cytokine, but with variable *in vitro* antiviral and antiproliferative activity.[88] Effect of the selected site of glycosylation on the biological activity of a therapeutic protein can vary widely simply by a the difference of a few amino acids in location. This has been shown in the enhancement of binding versus complete inhibition of an anti-dextran mAb glycosylated in its variable-region.[89, 90]

1.6.2 Colloidal modification

Colloidal incorporation of protein therapeutics offers multiple advantages as a delivery platform including protection of protein from degradation, prolonged release, reduced dosing frequency, increased patient compliance and tailorable plasma concentration profiles.[34] Aspects of colloidal systems and forms which are included in this analysis include the use of biodegradable polymers, microparticle and nanoparticle systems, lipid based nanoparticles and micelles with case study details compiled in Table 2.

1.6.2.1 Use of biodegradable and biocompatible polymers

Implantable polymeric systems for the controlled release of peptide therapeutics was first described by Davis[91] in 1972 using polyacrylamide to deliver of insulin. However, many early applications struggled to reduce inflammation in response to the polymeric implants. To overcome these negative responses while maintaining controllable release, Langer *et al.*[92] employed the first biocompatible polymeric systems to sustain release of bioactive protein for up to 100 days with little to no inflammation. Since that time biocompatible polymers such alginate, collagen, poly (lactide-co-glycolide) (PLGA) and polycaprolactones (PCL) have been some of the most extensively studied.[34]

1.6.2.2 Microparticles and Nanoparticles

Biocompatible polymers are commonly employed as colloidal systems in the form of micro and nano-sized particulates. These strategies generally provide high protein loading, loading efficiency and release in a biologically active form.[93] PLGA microparticles have been extensively studied for a variety systems due to its well-accepted safety profile.[94] PLGA-based systems have

been found to provide sustained delivery of encapsulated protein therapeutics from a depot formation for days up to months.[94] The rate and extent of drug release from particles can depend on both manufacturing technique and the polymers selected.[34, 95] A degarelix-loaded PLGA microparticle study screened three different fabrication techniques; spray drying, extrusion and double emulsion for their duration of release and biological inhibition of secreted hormone following a subcutaneous injection. Duration of inhibition was found to range from 14 days for emulsified drug, 36 days for spray-dried product and 29 days for unformulated drug.[96, 97] In this study, the emulsion based systems were also found to be severely less potent in an *in vitro* examination suggesting destabilization of the protein and thus a likely cause for its reduced *in vivo* efficacy.

The short *in vivo* half-life of IFNα-2b following i.v. infusions, which was responsible for frequent inconvenient and painful injections, drove researchers to develop a microparticle drug delivery system. The microparticle was composed of a gelatin core encapsulating the protein drug followed by a PLGA:Poly(ethylene glycal/butylene terephthalate) shell which when injected subcutaneously, sustained plasma levels of biologically active drug for 13 days compared to less than 12 hours when injected as a simple solution.[98]

Although considerable improvements were achieved in reducing the dose frequency, monthly versus every 2 days[99], of Genentech's Nutropin® (Somatropin, recombinant human growth hormone) when formulated into a depot injection system using Alkermes ProLease® extended release platform, commercialization was discontinued after 5 years due to the "significant resources required" to manufacture the product.[100] Nutropin is now delivered in a multi-dose prefilled-syringe with daily subcutaneous injections.[101] These results further support the required assessment on the net benefits of using fabricated microparticles for protein delivery systems

considering their variability in manufacturing complexity weighed against their therapeutic benefits.

Like microparticles, nanoparticles can be fabricated out of a range of materials including lipids and polymers, but are generally defined as particles of a diameter less than 1000 nm.[102, 103] The reduced size of nanoparticles compared to micro-sized particles has been shown to have effects on cellular uptake, drug release due to surface area to volume differences and injection site duration.[104] Nanoparticles have been utilized to effectively control delivery of both small molecules as well as peptide and protein therapeutics.[105] In one study encapsulating the protein therapeutic salmon calcitonin (sCT) into a mixed Eudragit:PLGA nanoparticle through a double emulsion technique, only modest gains (1.3-fold) in the extension of release were seen over protein solution controls.[106]

1.6.2.3 Lipid vesicles

Lipid vesicles including solid lipid nanoparticles (SLNs) and liposomes are another colloidal delivery system designed to sustain the release of a myriad of drug products. SLNs are generally composed of a solid lipid matrix (e.g. triglycerides, fatty acids, steroids or waxes) stabilized by emulsifiers in an aqueous phase by high pressure homogenization.[107, 108] SLNs have been shown to significantly extend release profiles of biologically active drug in vivo.[108] These lipid vesicles are capable of incorporating both hydrophobic and hydrophilic proteins and peptides through internalization or surface adsorption been shown to significantly extend release profiles of biologically active drug *in vivo*.[108]

Liposomes are composed of a lipid bilayer surrounding an aqueous core preferentially formed by the natural exclusion of water by phospholipid hydrophobic lipid domains.[109] Diameters

of liposomes can range from the 20nm to microns in size depending on the manufacturing process which may include high-energy sonication, extrusion or filtration.[110] Known issues persist with the intrinsic instability of liposomes following injection leading to burst release of loaded drug. To combat unwanted burst release and to avoid macrophage endocytosis, some researchers have stabilized liposomes by encapsulation into polymeric shells or PEGylated their aqueous exposed polar head group.[111] Yatuv *et al.* developed a sustained liposomal delivery system in order to reduce the injection frequency required for coagulation factor VIII (FVIII) replacement therapy for hemophilia A patients. The platform technology utilizes PEG stabilized liposomes (PEGLip) which can adhere to specific amino acid sequences inserted into a protein therapeutic.[112] Following intravenous infusion, standard FVIII treatment provided a mean number of days without bleed of 7.2 days while PEGLip FVIII provided 13.3 days of sustained biological activity.[113] One downside to liposomal formulations is that they generally require lyophilization for enhanced storage colloidal stability.[109]

1.6.2.4 Micelles

Similar to liposomal drug delivery systems, micelles are colloids formed from hydrophobic water exclusion, but in the form of a monolayer of amphipathic surfactants surrounding a hydrophobic core. Micellar formulations of macromolecules have been particularly studied for their ability to preferentially accumulate within tumors due to the enhanced permeability and retention effect (EPR) brought on by compromised vasculature surrounding fast-growing tumors.[114] Micelles and/or nanoparticles have been shown to be effective in delivering to such areas due to their extended circulation time which is required for adequate accumulation within the growing tumor.[115]

1.6.3 Hydrogels

Hydrogels have been traditionally defined as cross-linked polymeric networks capable of retaining large amounts of water without dissolving in order to maintain their three dimensional form.[116] Since their discovery in the early 1960s[117], hydrogels have been employed for a number of biomedical applications[118] outside of drug delivery such as tissue engineering[119, 120], biomedical coatings[121, 122] and diagnostic applications.[123, 124] Generally regarded as biocompatible due to their hydrophilicity and malleability, hydrogels have the ability to load large amounts of water-soluble therapeutics and therefore are well-suited for protein drugs. In addition, unlike the colloidal delivery systems described up to this point, hydrogels generally don't require fabrication processes which could negatively affect protein stability such as exposure to organic solvents, sonication, extreme shear forces or temperatures. These attractive properties have led researchers to develop numerous designs which can enable sustained release of protein therapeutics generally through two broad methods: chemically or physically cross-linked polymers (Table 3).[116]

1.6.3.1 Chemically cross-linked

Radical induced polymerization through UV or visible light is a commonly utilized means of chemical cross-linking in hydrogel systems.[125] In general, the chemical reaction between polymers is performed in situ in the presence of a photoinitiator which is decomposed when exposed to light forming a free radical. When these light-induced radicals are in the vicinity of polymers bearing addtional polymerizable groups such a methacrylates or acrylates, a gel is formed.[126] The ability to crosslink a gel *in vivo* in a minimally invasive manner is one of the major advantages of light induced hydrogels in addition to the fast-pace of the reaction, body temperature compatibility and the spatial and temporal control of initiation. Leech et. al demonstrated the *in*

vitro sustained release of the model protein bovine serum albumin (BSA) through encapsulation within a hyaluronic acid-glycidyl methacrylate (GMHA) and PEG-acrylate hydrogel, crosslinked with UV light.[127, 128] Alone the GMHA-PEG acrylate hydrogel was shown to provide release over a 6 hour period in which 60% of the BSA loaded was released, however when the hydrogel was seeded with BSA loaded PLGA microspheres release was extended to several weeks. BSA in both systems was shown to retain its monomeric structure by GPC retention. The major drawback of hydrogel systems crosslinked by UV-light is the potential for chemical degradation of the protein therapeutic due to the effects of free radical oxidation[129], however multiple reports have indicated preservation of activity of encapsulated enzymes following UV treatment.[130, 131]

1.6.3.2 Physically cross-linked

Non-covalent physical forces which are able to crosslink hydrogel polymer networks and sustain the delivery of proteins include hydrophobic interactions, ionic interactions and hydrogen bonds. Hydrophobic interactions are the most highly explored due to their strength and natural tendency to form in an aqueous environment using amphiphilic polymers. Hydrophobic and electrostatic interactions between polymer-modified cyclodextrin hosts, which are known for their binding pockets, and polymer-modified guest pairing agents have been utilized to form inclusion complexes which trap proteins to modify their release.[132, 133] van de Manakker *et al.* demonstrated the applicability of such a supramolecular structure by complexing an 8-arm PEG, end-modified with β-cyclodextrin or cholesterol in the presence of BSA and lysozyme. In an *in vitro* release model, sustained release of both proteins in occurred for more than nine days at which time the gels were completely dissolved.[134, 135]

1.6.3.3 Nanogels

Nanogels seek to incorporate the same functionalities and advantages of macro hydrogel delivery into a nano-sized vesicle able to circulate systemically for extended periods where they are able to overcome biological barriers due to their smaller dimensions.[136] A study by Hirakura *et al.* reported the development of a nanogel protein delivery system in which the polysaccharide pullulan was derivatized with the hydrophobic molecule cholesteryl and mixed with model peptides to form a spontaneous 20-30 nm assembly. These protein/nanogel complexes were then loaded into an acrylate crosslinked hyaluronan hydrogel and their release monitored *in vivo* following subcutaneous implantation. Mean residence time of the model protein erythropoietin (EPO) increased from 39h to 146h with increasing hydrogel concentration and constant nanogel concentration. EPO associated alone with the nanogel had a mean residence time of 18h. Plasma concentrations were examined using ELISA based techniques which indicate EPO retains some native structure following release from the hybrid gel.[137]

1.6.3.3.1 Mechanical properties

The hydrophobic, electrostatic and hydrogen bond interactions which enable the self-assembly of physically-crosslinked nanogels and their association with biopharmaceutics are dynamic and reversible in the nature. In contrast to chemically crosslinked hydrogels, hydrogels with reversible physical crosslinks can gel at rest, but when shear stress is applied upon injection they exhibit the properties of a low-viscosity fluid.[137] These shear-thinning hydrogels, exhibit this behavior due to the disruption of the equilibrium governing their self-assembly upon applied shear, those favoring assembly (e.g. hydrophobic) and those forces that act against assembly (e.g.

solvation). Together these weak dynamic forces lead to a stable network upon reassembly of equilibrium.[138, 139]

1.6.3.3.2 Protein release mechanisms

The main pathways governing protein release from physically-crosslinked hydrogel systems are dissociation-, diffusion- and degradation-controlled release. In nanogels designed to associate with protein therapeutics to sustain their release, the rate of dissociation can be the rate-limiting factor to the ultimate release of protein from the gel. [140] Diffusion-controlled release systems generally follow Higuchi's kinetics in which the release rate is proportional to the square root of time.[141] Degradation or swelling-controlled release is governed by the alteration of the physical properties of the gel with time due events such as gel erosion. Release of protein from gels due to degradation alone generally follow near zero-order kinetics.[134]

1.7 Experimental methods to model subcutaneous release kinetics *in vitro*

Reliable *in vitro* methods which accurately predict the *in vivo* performance of a subcutaneously administered biologic have been historically difficult. Wide variability can exist in the stressors and interactions a protein experiences in the early stages following injection. Systems such as the recently described subcutaneous injection site simulator, Scissor[142], seek to model these events through the thorough adaptation of the physiological conditions and ECM components of the hypodermis hypothesized to be primary factors in the ultimate bioavailability of a protein. These physiological conditions include pH, ionic composition, interstitial pressure and temperature as well as concentrated hyaluronic acid within a semipermeable dialysis membrane. Initial examination of the Scissor system using four model proteins provided critical

insight into the fate of a biopharmaceutical upon injection including excipient release, protein precipitation and resolubilization and the modifying effects of ECM elements.

1.8 Protein stability assessment

The release of biologically active protein from experimental drug delivery systems is paramount to its clinical viability.[80] Evaluation of the effects of delivery systems on a protein's native structure including chemical, colloidal and conformational stability provide insights which guide further development. A number of techniques are regularly employed to evaluate the structural stability of a protein drug candidate including liquid chromatography, mass spectrometry, Fourier transform infrared spectroscopy (FTIR), circular dichroism (CD), fluorescence spectroscopy and differential scanning calorimetry (DSC). When combined these techniques enable the proper selection of a formulation which minimizes loss of therapeutic function.[143]

1.9 Conclusion

Development of novel drug delivery systems which enable the controlled release and therapeutic performance of critical drugs is an area of continued focus in the research community. A comprehensive understanding of the determinants which govern delivery of drugs with a range of physical and chemical properties is required for the design and selection of an effective dosage form. Chemical and colloidal strategies have been effectively used to overcome the significant challenges to the delivery of protein therapeutics. Overall, the chemical and physical properties of hydrogels, coupled with their usually mild fabrication make them an attractive platform for the

design of a tailorable reservoir system. Further research is required to develop hydrogel systems suitable for the expanding biopharmaceutical market.

Table 1. Recent chemical modification strategies for the sustained parenteral delivery of proteins therapeutics.

Broad Strategy	Material	Protein	Route of Admin.	$t_{1/2}$ - Fold Increase over Control	Remarks	Ref
PEGylation	mPEG	rhTIMP-1	i.p.	25	Mono- and di-lysine substitution with 20kDa mPEG chain. Retained partial inhibitory activity.	[34, 144]
PEGylation	mPEG	rhGH	i.v.	4.5	Mono-substituted N-term or transglutaminase mediated. Native secondary structure retained.	[34, 145]
PEGylation	mPEG	rhTSH	i.m.	~1.5	Mono- cysteine substitution with 40kDa PEG. PEG MW dependent decreased receptor affinity.	[34, 146]
PEGylation	mPEG	IFN-α2a	s.c.	70	Mono-lysine substitution with 40kDa branched PEG. Retained only 7% of antiviral activity of control.	[34, 78]
Hyperglycosylation	PSA; Colominic acid	Asparaginase	i.v.	4	86% enzymatic activity of the native form.	[34, 147]
Hyperglycosylation	PSA; Colominic acid	Insulin	s.c.	3	39kDa and 22kDa N-term substitution.	[34, 148]
Hyperglycosylation	Genetically expressed, N-glycosylation	IFN-α2b	s.c.	25	10-fold reduction in in vitro antiviral activity.	[34, 88]

i.p.: intraperitoneal; i.v.: intraveneous; i.m.: intramuscular; s.c.: subcutaneous;
PEG: Polyethylene glycol; PSA: polysialic acid

Table 2. Recent colloidal modification strategies for the sustained parenteral delivery of proteins therapeutics.

Broad Strategy	Material	Protein	Route of Admin.	$t_{1/2}$ - Fold Increase over Control	Remarks	Ref
Microparticle	PLGA	Degarelix	s.c.	1.25 to (-2)	Spray dried formulation was only formulation that extended inhibition over control, while others hampered.	[34, 96, 97]
Microparticle	Gelatin, $ZnSO_4$; PLGA: PEGT/ PBT	IFN-α2b	s.c.	26	S/O/W emulsion method with 86% EE.	[34, 98]
Microparticle	PLGA (Prolease®)	rhGH	s.c.	13	Nonaqueous, cryogenic fabrication with retainment of nearly all biological activity	[99, 101]
PEGylation/ Microparticle	mPEG; PLGA	Insulin	s.c.	9	O/W emulsion method. Intact secondary structure post release.	[34, 149]
Nanoparticle	Eudragit® RS:PLGA	Salmon Calcitonin (sCT)	s.c.	1.3	Double emulsion method with 69-83% EE. 400-700 nm diameter particles.	[34, 106]
PEGylation/ Liposome	POPC: DSPE-PEG 2000; 97:3 mol%	rFVIII	i.v.	1.8	Thin-lipid film hydration/extrusion. PEG binds to conserved 8 amino acid sequence.	[112, 113]

i.p.: intraperitoneal; i.v.: intraveneous; i.m.: intramuscular; s.c.: subcutaneous;
PEG: Polyethylene glycol; PLGA: poly(lactic-co-glycolic acid)
POPC: 1-palmitoyl-2-oleoyl-glycero-3-phosphocoholine;
PEGT/PBT: polyethylene glycol terephthalate/polybutylene terephthalate

Table 3. Recent hydrogel modification strategies for the sustained parenteral delivery of proteins therapeutics.

Broad Strategy	Material	Protein	Route of Admin.	$t_{1/2}$ - Fold Increase over Control	Remarks	Ref
CC-Hydrogel/ Microparticle	GMHA:PEG-Acrylate, PLGA	BSA	In vitro only	n/a (6h, hydrogel; 700h, hydrogel +microparticle)	Seeded acrylate photocrosslinked hydrogel with protein loaded microparticle	[127, 128]
PC-Hydrogel	β-cyclodextrin: PEG/ Cholesterol:PEG	BSA, Lysozyme	In vitro only	n/a (9 d, inclusion complex)	Supramolecular hydrogel with entrapped protein	[134]
CC-Hydrogel/ PC-Nanogel	AEMA-HA/ Pullulan-Cholesteryl	GLP-1, Insulin, EPO	s.c.	8 (MRT) 18h, Nanogel 146h, Nanogel + Hydrogel	Release quantified by ELISA suggesting some retainment of biological activity	[137]

i.p.: intraperitoneal; i.v.: intraveneous; i.m.: intramuscular; s.c.: subcutaneous;
CC: chemically-crosslinked; PC: physically-crosslinked
PEG: Polyethylene glycol; PLGA: poly(lactic-co-glycolic acid)
GMHA: glycidyl methacrylate hyaluronic acid
AEMA-HA: Aminoethyl methacrylated hyaluronic acid

1.10 References

1. Aulton, M. E.; Taylor, K., *Aulton's pharmaceutics : the design and manufacture of medicines*. 4th ed.; Churchill Livingstone/Elsevier: Edinburgh, 2013; p xiii, 894 p.
2. Lee, P. I.; Li, J.-X., Evolution of Oral Controlled Release Dosage Forms. *Oral Controlled Release Formulation Design and Drug Delivery* **2010**, 21-31.
3. Yun, Y. H.; Lee, B. K.; Park, K., Controlled Drug Delivery: Historical perspective for the next generation. *Journal of Controlled Release* **2015,** *219*, 2-7.
4. Blythe, R. H. Sympathomimetic preparation. US2738303A, 1952.
5. Shargel, L.; Wu-Pong, S.; Yu, A. B. C., Chapter 17. Modified-Release Drug Products. In *Applied Biopharmaceutics & Pharmacokinetics, 6e*, The McGraw-Hill Companies: New York, NY, 2012.
6. Barich, D. H.; Zell, M. T.; Munson, E. J., Physicochemical Properties, Formulation, and Drug Delivery. *Drug Delivery* **2016**.
7. Fassihi, R., Modified-Release Delivery Systems, Extended-Release Capsule Platform. In *Pharmaceutical Dosage Forms: Capsules*, Larry L. Augsburger, S. W. H., Ed. CRC Press: 2017.
8. Park, K., Controlled drug delivery systems: Past forward and future back. *Journal of Controlled Release* **2014,** *190*, 3-8.
9. Anselmo, A. C.; Mitragotri, S., An overview of clinical and commercial impact of drug delivery systems. *Journal of Controlled Release* **2014,** *190*, 15-28.
10. Evens, R.; Kaitin, K., The Evolution Of Biotechnology And Its Impact On Health Care. *Health Affairs* **2015,** *34* (2), 210-219.
11. Walsh, G., Biopharmaceutical benchmarks 2018. *Nature Biotechnology* **2018,** *36*, 1136.

12. Mullard, A., 2018 FDA drug approvals. *Nat Rev Drug Discov* **2019,** *18* (2), 85-89.

13. Mitragotri, S.; Burke, P. A.; Langer, R., Overcoming the challenges in administering biopharmaceuticals: formulation and delivery strategies. *Nature Reviews Drug Discovery* **2014,** *13*, 655.

14. Kulczar, C.; Roth, W.; Carl, S.; Gudmundsson, O.; Knipp, G., Peptide and Protein Drug Delivery. In *Drug delivery*, 2015.

15. Creighton, T. E., *Proteins: Structures and Molecular Properties*. W. H. Freeman: 1993.

16. Berg, J. M.; Tymoczko, J. L.; Stryer, L.; Stryer, L., *Biochemistry*. 5th ed.; W.H. Freeman: New York, 2002.

17. Pelley, J. W., 3 - Protein Structure and Function. In *Elsevier's Integrated Biochemistry*, Pelley, J. W., Ed. Mosby: Philadelphia, 2007; pp 19-28.

18. Nicolau Jr, D. V.; Paszek, E.; Fulga, F.; Nicolau, D. V., Mapping Hydrophobicity on the Protein Molecular Surface at Atom-Level Resolution. *PLoS ONE* **2014,** *9* (12), e114042.

19. Bummer, P. M., Chemical considerations in protein and peptide stability. In *Protein Formulation and Delivery*, 2007; pp 7-42.

20. Koppenol, S., Physical considerations in protein and peptide stability. In *Protein Formulation and Delivery*, 2007; pp 43-72.

21. Karasov, W. H., Integrative physiology of transcellular and paracellular intestinal absorption. *The Journal of Experimental Biology* **2017,** *220* (14), 2495-2501.

22. Anderson, J. M.; Van Itallie, C. M., Physiology and function of the tight junction. *Cold Spring Harb Perspect Biol* **2009,** *1* (2), a002584-a002584.

23. Hillery, A.; Lloyd, A.; Swarbrick, J., *Drug Delivery and Targeting For Pharmacists and Pharmaceutical Scientists*. 2001.

24. Zhong, H.; Chan, G.; Hu, Y.; Hu, H.; Ouyang, D., A Comprehensive Map of FDA-Approved Pharmaceutical Products. *Pharmaceutics* **2018,** *10* (4).

25. Homayun, B.; Lin, X.; Choi, H. A.-O., Challenges and Recent Progress in Oral Drug Delivery Systems for Biopharmaceuticals. LID - E129 [pii] LID - 10.3390/pharmaceutics11030129 [doi]. (1999-4923 (Print)).

26. Fasano, A., Novel Approaches for Oral Delivery of Macromolecules. **1998,** *87* (11), 1351-1356.

27. Goldberg, M.; Gomez-Orellana, I., Challenges for the oral delivery of macromolecules. *Nature Reviews Drug Discovery* **2003,** *2* (4), 289-295.

28. Janapareddi, K.; Jasti, B. R.; Li, X., Evolution of Controlled Drug Delivery Systems. *Drug Delivery* **2016**, 336-352.

29. Philippart, M.; Schmidt, J.; Bittner, B., Oral Delivery of Therapeutic Proteins and Peptides: An Overview of Current Technologies and Recommendations for Bridging from Approved Intravenous or Subcutaneous Administration to Novel Oral Regimens. *Drug Res (Stuttg)* **2016,** *66* (3), 113-20.

30. Renukuntla, J.; Vadlapudi, A. D.; Patel, A.; Boddu, S. H. S.; Mitra, A. K., Approaches for enhancing oral bioavailability of peptides and proteins. **2013,** *447* (1-2), 75-93.

31. Anselmo, A. C.; Gokarn, Y.; Mitragotri, S., Non-invasive delivery strategies for biologics. *Nature Reviews Drug Discovery* **2018,** *18* (1), 19-40.

32. Rohrer, J.; Lupo, N.; Bernkop-Schnürch, A., Advanced formulations for intranasal delivery of biologics. *International Journal of Pharmaceutics* **2018,** *553* (1), 8-20.

33. Depreter, F.; Pilcer, G.; Amighi, K., Inhaled proteins: Challenges and perspectives. *International Journal of Pharmaceutics* **2013,** *447* (1), 251-280.

34. Patel, A.; Cholkar, K.; Mitra, A. K., Recent developments in protein and peptide parenteral delivery approaches. *Therapeutic Delivery* **2014,** *5* (3), 337-365.

35. Kolars, J. C.; Watkins, P. B.; Merion, R. M.; Awni, W. M., First-pass metabolism of cyclosporin by the gut. **1991,** *338* (8781), 1488-1490.

36. Pond Sm Fau - Tozer, T. N.; Tozer, T. N., First-pass elimination. Basic concepts and clinical consequences. (0312-5963 (Print)).

37. Schmidt, H., Chronic Disease Prevention and Health Promotion. In *Public Health Ethics: Cases Spanning the Globe*, D, H. B.; L, W. O.; Dawson, A.; Saenz, C.; Reis, A.; Bolan, G., Eds. Cham (CH), 2016; pp 137-176.

38. Cutler, R. L.; Fernandez-Llimos, F.; Frommer, M.; Benrimoj, C.; Garcia-Cardenas, V., Economic impact of medication non-adherence by disease groups: a systematic review. *BMJ Open* **2018,** *8* (1), e016982-e016982.

39. World Health Organization.; Sabaté, E., *Adherence to long-term therapies : evidence for action*. World Health Organization: Geneva, 2003; p xv, 198 p.

40. McMurtry, C. M.; Noel, M.; Taddio, A.; Antony, M. M.; Asmundson, G. J. G.; Riddell, R. P.; Chambers, C. T.; Shah, V.; HelpinKids; Adults, T., Interventions for Individuals With High Levels of Needle Fear: Systematic Review of Randomized Controlled Trials and Quasi-Randomized Controlled Trials. *Clin J Pain* **2015,** *31* (10 Suppl), S109-S123.

41. Orenius, T.; LicPsych; Säilä, H.; Mikola, K.; Ristolainen, L., Fear of Injections and Needle Phobia Among Children and Adolescents: An Overview of Psychological, Behavioral, and Contextual Factors. *SAGE Open Nursing* **2018,** *4*, 2377960818759442.

42. Agrawal, H.; Thacker, N.; Misra, A., 11 - Parenteral Delivery of Peptides and Proteins. In *Challenges in Delivery of Therapeutic Genomics and Proteomics*, Misra, A., Ed. Elsevier: London, 2011; pp 531-622.

43. National Health Expenditures 2017. CMS, Ed. 2018.

44. Papanicolas, I.; Woskie, L. R.; Jha, A. K., Health Care Spending in the United States and Other High-Income Countries. *JAMA* **2018,** *319* (10), 1024.

45. Demonaco, H. J.; Von Hippel, E., Reducing Medical Costs and Improving Quality via Self-Management Tools. *PLoS Medicine* **2007,** *4* (4), e104.

46. Leff, B., Hospital at Home: Feasibility and Outcomes of a Program To Provide Hospital-Level Care at Home for Acutely Ill Older Patients. *Annals of Internal Medicine* **2005,** *143* (11), 798.

47. Montalto, M., The 500-bed hospital that isn't there: the Victorian Department of Health review of the Hospital in the Home program. (0025-729X (Print)).

48. Touati, M.; Lamarsalle, L.; Moreau, S.; Vergnenegre, F.; Lefort, S.; Brillat, C.; Jeannet, L.; Lagarde, A.; Daulange, A.; Jaccard, A.; Vergnenegre, A.; Bordessoule, D., Cost savings of home bortezomib injection in patients with multiple myeloma treated by a combination care in Outpatient Hospital and Hospital care at Home. *Support Care Cancer* **2016,** *24* (12), 5007-5014.

49. Iannotti, R. J.; Schneider, S.; Nansel, T. R.; Haynie, D. L.; Plotnick, L. P.; Clark, L. M.; Sobel, D. O.; Simons-Morton, B., Self-efficacy, outcome expectations, and diabetes self-management in adolescents with type 1 diabetes. *J Dev Behav Pediatr* **2006,** *27* (2), 98-105.

50. Bittner, B.; Richter, W.; Schmidt, J., Subcutaneous Administration of Biotherapeutics: An Overview of Current Challenges and Opportunities. *BioDrugs* **2018,** *32* (5), 425-440.

51. Tjalma, W.; Huizing, M. T.; Papadimitriou, K., The smooth and bumpy road of trastuzumab administration: from intravenous (IV) in a hospital to subcutaneous (SC) at home. *Facts Views Vis Obgyn* **2017,** *9* (1), 51-55.

52. Tetteh, E. K.; Morris, S., Evaluating the administration costs of biologic drugs: development of a cost algorithm. *Health Econ Rev* **2014,** *4* (1), 26.

53. Jackisch, C.; Muller, V.; Dall, P.; Neumeister, R.; Park-Simon, T. W.; Ruf-Dordelmann, A.; Seiler, S.; Tesch, H.; Ataseven, B., Subcutaneous Trastuzumab for HER2-positive Breast Cancer - Evidence and Practical Experience in 7 German Centers. *Geburtshilfe Frauenheilkd* **2015,** *75* (6), 566-573.

54. Fathallah, A. M.; Balu-Iyer, S. V., Anatomical, Physiological, and Experimental Factors Affecting the Bioavailability of sc-Administered Large Biotherapeutics. *Journal of Pharmaceutical Sciences* **2015,** *104* (2), 301-306.

55. Bergeson, P. S.; Singer, S. A.; Kaplan, A. M., Intramuscular injections in children. *Pediatrics* **1982,** *70* (6), 944-8.

56. *Subcutaneous Biologics, Technologies and Drug Delivery Systems, 2018-2030*; Roots Analysis: 2018; p 401.

57. Dychter, S. S.; Gold, D. A.; Haller, M. F., Subcutaneous drug delivery: a route to increased safety, patient satisfaction, and reduced costs. *J Infus Nurs* **2012,** *35* (3), 154-60.

58. Jones, G. B.; Collins, D. S.; Harrison, M. W.; Thyagarajapuram, N. R.; Wright, J. M., Subcutaneous drug delivery: An evolving enterprise. *Sci Transl Med* **2017,** *9* (405).

59. Ogston-Tuck, S., Subcutaneous injection technique: an evidence-based approach. *Nurs Stand* **2014,** *29* (3), 53-8.

60. Kagan, L., Pharmacokinetic Modeling of the Subcutaneous Absorption of Therapeutic Proteins. *Drug Metabolism and Disposition* **2014,** *42* (11), 1890-1905.

61. Kadler, K. E.; Baldock, C.; Bella, J.; Boot-Handford, R. P., Collagens at a glance. *Journal of Cell Science* **2007,** *120* (12), 1955-1958.

62. Fraser, J. R. E.; Laurent, T. C.; Laurent, U. B. G., Hyaluronan: its nature, distribution, functions and turnover. *Journal of Internal Medicine* **1997,** *242* (1), 27-33.

63. Swabb Ea Fau - Wei, J.; Wei J Fau - Gullino, P. M.; Gullino, P. M., Diffusion and convection in normal and neoplastic tissues. (0008-5472 (Print)).

64. Richter, W. F.; Bhansali, S. G.; Morris, M. E., Mechanistic Determinants of Biotherapeutics Absorption Following SC Administration. *The AAPS Journal* **2012,** *14* (3), 559-570.

65. Kagan, L.; Turner, M. R.; Balu-Iyer, S. V.; Mager, D. E., Subcutaneous absorption of monoclonal antibodies: role of dose, site of injection, and injection volume on rituximab pharmacokinetics in rats. *Pharm Res* **2012,** *29* (2), 490-9.

66. Kinnunen, H. M.; Mrsny, R. J., Improving the outcomes of biopharmaceutical delivery via the subcutaneous route by understanding the chemical, physical and physiological properties of the subcutaneous injection site. *J Control Release* **2014,** *182*, 22-32.

67. Porter, C. J. H.; Charman, S. A., Lymphatic Transport of Proteins After Subcutaneous Administration. *Journal of Pharmaceutical Sciences* **2000,** *89* (3), 297-310.

68. Supersaxo, A.; Hein, W. R.; Steffen, H., Effect of molecular weight on the lymphatic absorption of water-soluble compounds following subcutaneous administration. *Pharm Res* **1990,** *7* (2), 167-9.

69. Turner, M. R.; Balu-Iyer, S. V., Challenges and Opportunities for the Subcutaneous Delivery of Therapeutic Proteins. *J Pharm Sci* **2018,** *107* (5), 1247-1260.

70. Hamuro, L.; Kijanka, G.; Kinderman, F.; Kropshofer, H.; Bu, D. X.; Zepeda, M.; Jawa, V., Perspectives on Subcutaneous Route of Administration as an Immunogenicity Risk Factor for Therapeutic Proteins. *J Pharm Sci* **2017,** *106* (10), 2946-2954.

71. Yasukawa, K.; Sawamura, D.; Sugawara, H.; Kato, N., Leuprorelin acetate granulomas: case reports and review of the literature. *Br J Dermatol* **2005,** *152* (5), 1045-7.

72. Mathaes, R.; Koulov, A.; Joerg, S.; Mahler, H. C., Subcutaneous Injection Volume of Biopharmaceuticals-Pushing the Boundaries. *J Pharm Sci* **2016,** *105* (8), 2255-9.

73. Alkhouli, N.; Mansfield, J.; Green, E.; Bell, J.; Knight, B.; Liversedge, N.; Tham, J. C.; Welbourn, R.; Shore, A. C.; Kos, K.; Winlove, C. P., The mechanical properties of human adipose tissues and their relationships to the structure and composition of the extracellular matrix. *Am J Physiol Endocrinol Metab* **2013,** *305* (12), E1427-35.

74. Abuchowski, A.; McCoy, J. R.; Palczuk, N. C.; van Es, T.; Davis, F. F., Effect of covalent attachment of polyethylene glycol on immunogenicity and circulating life of bovine liver catalase. *J Biol Chem* **1977,** *252* (11), 3582-6.

75. Davis, F. F., The origin of pegnology. *Adv Drug Deliv Rev* **2002,** *54* (4), 457-8.

76. Fishburn, C. S., The pharmacology of PEGylation: balancing PD with PK to generate novel therapeutics. *J Pharm Sci* **2008,** *97* (10), 4167-83.

77. Parveen, S.; Sahoo, S. K., Nanomedicine: clinical applications of polyethylene glycol conjugated proteins and drugs. *Clin Pharmacokinet* **2006,** *45* (10), 965-88.

78. Bailon, P.; Palleroni, A.; Schaffer, C. A.; Spence, C. L.; Fung, W.-J.; Porter, J. E.; Ehrlich, G. K.; Pan, W.; Xu, Z.-X.; Modi, M. W.; Farid, A.; Berthold, W.; Graves, M., Rational Design of a Potent, Long-Lasting Form of Interferon: A 40 kDa Branched Polyethylene Glycol-Conjugated Interferon α-2a for the Treatment of Hepatitis C. *Bioconjugate Chemistry* **2001,** *12* (2), 195-202.

79. Webster, R.; Elliott, V.; Park, B. K.; Walker, D.; Hankin, M.; Taupin, P., PEG and PEG conjugates toxicity: towards an understanding of the toxicity of PEG and its relevance to PEGylated biologicals. In *PEGylated Protein Drugs: Basic Science and Clinical Applications*, Veronese, F. M., Ed. Birkhäuser Basel: Basel, 2009; pp 127-146.

80. Frøkjaer, S.; Otzen, D., *Protein drug stability: a formulation challenge. Nat Rev Drug Discov 4:298-306*. 2005; Vol. 4, p 298-306.

81. Kurtzhals, P.; Havelund, S.; Jonassen, I.; Kiehr, B.; Larsen, U. D.; Ribel, U.; Markussen, J., Albumin binding of insulins acylated with fatty acids: characterization of the ligand-protein interaction and correlation between binding affinity and timing of the insulin effect in vivo. **1995,** *312* (3), 725-731.

82. P.V, J.; Nair, S. V.; Kamalasanan, K., Current trend in drug delivery considerations for subcutaneous insulin depots to treat diabetes. *Colloids and Surfaces B: Biointerfaces* **2017,** *153*, 123-131.

83. Knudsen, L. B.; Nielsen, P. F.; Huusfeldt, P. O.; Johansen, N. L.; Madsen, K.; Pedersen, F. Z.; Thøgersen, H.; Wilken, M.; Agersø, H., Potent Derivatives of

Glucagon-like Peptide-1 with Pharmacokinetic Properties Suitable for Once Daily Administration. *Journal of Medicinal Chemistry* **2000,** *43* (9), 1664-1669.

84. Pisal, D. S.; Kosloski, M. P.; Balu-Iyer, S. V., Delivery of Therapeutic Proteins. *Journal of Pharmaceutical Sciences* **2010,** *99* (6), 2557-2575.

85. Varki, A., Biological roles of glycans. *Glycobiology* **2017,** *27* (1), 3-49.

86. Solá, R. J.; Griebenow, K., Glycosylation of Therapeutic Proteins: An Effective Strategy to Optimize Efficacy. *BioDrugs* **2010,** *24* (1), 9-21.

87. Jain, K.; Kesharwani, P.; Gupta, U.; Jain, N., *A review of glycosylated carriers for drug delivery*. 2012; Vol. 33, p 4166-86.

88. Ceaglio, N.; Etcheverrigaray, M.; Kratje, R.; Oggero, M., Novel long-lasting interferon alpha derivatives designed by glycoengineering. *Biochimie* **2008,** *90* (3), 437-49.

89. Zhang, P.; Woen, S.; Wang, T.; Liau, B.; Zhao, S.; Chen, C.; Yang, Y.; Song, Z.; Wormald, M. R.; Yu, C.; Rudd, P. M., Challenges of glycosylation analysis and control: an integrated approach to producing optimal and consistent therapeutic drugs. **2016**.

90. Wright, A.; Tao, M. H.; Kabat, E. A.; Morrison, S. L., Antibody variable region glycosylation: position effects on antigen binding and carbohydrate structure. *EMBO J* **1991,** *10* (10), 2717-2723.

91. Davis, B. K., Control of diabetes with polyacrylamide implants containing insulin. **1972,** *28* (3), 348-348.

92. Langer, R.; Folkman, J., Polymers for the sustained release of proteins and other macromolecules. *Nature* **1976,** *263* (5580), 797-800.

93. Ye, M.; Kim, S.; Park, K., Issues in long-term protein delivery using biodegradable microparticles. *J Control Release* **2010,** *146* (2), 241-60.

94. Shi, Y.; Li, L. C., Current advances in sustained-release systems for parenteral drug delivery. *Expert Opin Drug Deliv* **2005,** *2* (6), 1039-58.

95. Freiberg, S.; Zhu, X. X., Polymer microspheres for controlled drug release. *International Journal of Pharmaceutics* **2004,** *282* (1), 1-18.

96. Schwach, G.; Oudry, N.; Giliberto, J. P.; Broqua, P.; Luck, M.; Lindner, H.; Gurny, R., Biodegradable PLGA microparticles for sustained release of a new GnRH antagonist: part II. In vivo performance. *Eur J Pharm Biopharm* **2004,** *57* (3), 441-6.

97. Schwach, G.; Oudry, N.; Delhomme, S.; Lück, M.; Lindner, H.; Gurny, R., Biodegradable microparticles for sustained release of a new GnRH antagonist – part I: screening commercial PLGA and formulation technologies. *European Journal of Pharmaceutics and Biopharmaceutics* **2003,** *56* (3), 327-336.

98. Li, Z.; Li, L.; Liu, Y.; Zhang, H.; Li, X.; Luo, F.; Mei, X., Development of interferon alpha-2b microspheres with constant release. *International Journal of Pharmaceutics* **2011,** *410* (1-2), 48-53.

99. Tracy, M. A., Development and Scale-up of a Microsphere Protein Delivery System. *Biotechnology Progress* **1998,** *14* (1), 108-115.

100. Genentech and Alkermes Announce Decision to Discontinue Commercialization of Nutropin Depot. Genentech, Inc.; Alkermes, Inc.: 2004.

101. Yuen, K.; Amin, R., Developments in administration of growth hormone treatment: focus on Norditropin® Flexpro&reg. *Patient Preference and Adherence* **2011**, 117.

102. Christian, P.; von der Kammer, F.; Baalousha, M.; Hofmann, T., *Nanoparticles: Structure, Properties, Preparation and Behaviour in Environmental Media*. 2008; Vol. 17, p 326-43.

103. Singh, R.; Lillard, J. W., Nanoparticle-based targeted drug delivery. *Experimental and Molecular Pathology* **2009,** *86* (3), 215-223.

104. Kohane, D. S., Microparticles and nanoparticles for drug delivery. (0006-3592 (Print)).

105. Rizvi, S. A. A.; Saleh, A. M., Applications of nanoparticle systems in drug delivery technology. *Saudi Pharmaceutical Journal* **2018,** *26* (1), 64-70.

106. Glowka, E.; Sapin-Minet, A.; Leroy, P.; Lulek, J.; Maincent, P., Preparation andin vitro–in vivoevaluation of salmon calcitonin-loaded polymeric nanoparticles. *Journal of Microencapsulation* **2010,** *27* (1), 25-36.

107. Kammari, R.; Das, N. G.; Das, S. K., Chapter 6 - Nanoparticulate Systems for Therapeutic and Diagnostic Applications. In *Emerging Nanotechnologies for Diagnostics, Drug Delivery and Medical Devices*, Mitra, A. K.; Cholkar, K.; Mandal, A., Eds. Elsevier: Boston, 2017; pp 105-144.

108. Almeida, A.; Souto, E., Solid lipid nanoparticles as a drug delivery system for peptides and proteins. *Advanced Drug Delivery Reviews* **2007,** *59* (6), 478-490.

109. Swaminathan, J.; Ehrhardt, C., Liposomal delivery of proteins and peptides. *Expert Opin Drug Deliv* **2012,** *9* (12), 1489-503.

110. Walde, P.; Ichikawa, S., Enzymes inside lipid vesicles: preparation, reactivity and applications. *Biomolecular Engineering* **2001,** *18* (4), 143-177.

111. Solaro, R.; Chiellini, F.; Battisti, A., Targeted Delivery of Protein Drugs by Nanocarriers. *Materials* **2010,** *3* (3), 1928-1980.

112. Baru, M., The use of PEGylated liposomes in the development of drug delivery applications for the treatment of hemophilia. *International Journal of Nanomedicine* **2010**, 581.

113. Spira, J.; Plyushch, O. P.; Andreeva, T. A.; Andreev, Y., Prolonged bleeding-free period following prophylactic infusion of recombinant factor VIII reconstituted with pegylated liposomes. *Blood* **2006,** *108* (12), 3668-3673.

114. Torchilin, V., Tumor delivery of macromolecular drugs based on the EPR effect. *Adv Drug Deliv Rev* **2011,** *63* (3), 131-5.

115. Torchilin, V. P., Micellar Nanocarriers: Pharmaceutical Perspectives. *Pharmaceutical Research* **2006,** *24* (1), 1-16.

116. Vermonden, T.; Censi, R.; Hennink, W. E., Hydrogels for Protein Delivery. **2012,** *112* (5), 2853-2888.

117. Wichterle, O.; LÍM, D., Hydrophilic Gels for Biological Use. *Nature* **1960,** *185* (4706), 117-118.

118. Caló, E.; Khutoryanskiy, V. V., Biomedical applications of hydrogels: A review of patents and commercial products. *European Polymer Journal* **2015,** *65*, 252-267.

119. Hunt, J. A.; Chen, R.; Van Veen, T.; Bryan, N., Hydrogels for tissue engineering and regenerative medicine. **2014,** *2* (33), 5319.

120. Lee, J.-H.; Kim, H.-W., Emerging properties of hydrogels in tissue engineering. *Journal of Tissue Engineering* **2018,** *9*, 204173141876828.

121. Kim, C.-L.; Kim, D.-E., Durability and Self-healing Effects of Hydrogel Coatings with respect to Contact Condition. *Scientific Reports* **2017,** *7* (1).

122. Liu, G.; Ding, Z.; Yuan, Q.; Xie, H.; Gu, Z., Multi-Layered Hydrogels for Biomedical Applications. *Frontiers in Chemistry* **2018,** *6*.

123. Mao, X.; Chen, G.; Wang, Z.; Zhang, Y.; Zhu, X.; Li, G., Surface-immobilized and self-shaped DNA hydrogels and their application in biosensing. *Chemical Science* **2018**.

124. Tavakoli, J.; Tang, Y., Hydrogel Based Sensors for Biomedical Applications: An Updated Review. *Polymers* **2017,** *9* (12), 364.

125. Nguyen, K. T.; West, J. L., Photopolymerizable hydrogels for tissue engineering applications. *Biomaterials* **2002,** *23* (22), 4307-4314.

126. Karaca, N.; Temel, G.; Karaca Balta, D.; Aydin, M.; Arsu, N., Preparation of hydrogels by photopolymerization of acrylates in the presence of Type I and one-component Type II photoinitiators. *Journal of Photochemistry and Photobiology A: Chemistry* **2010,** *209* (1), 1-6.

127. Leach, J. B.; Schmidt, C. E., Characterization of protein release from photocrosslinkable hyaluronic acid-polyethylene glycol hydrogel tissue engineering scaffolds. *Biomaterials* **2005,** *26* (2), 125-135.

128. Van Tomme, S. R.; Storm G Fau - Hennink, W. E.; Hennink, W. E., In situ gelling hydrogels for pharmaceutical and biomedical applications. (0378-5173 (Print)).

129. Davies, M. J., Protein oxidation and peroxidation. *Biochemical Journal* **2016,** *473* (7), 805-825.

130. Pescosolido, L.; Miatto, S.; Di Meo, C.; Cencetti, C.; Coviello, T.; Alhaique, F.; Matricardi, P., Injectable and in situ gelling hydrogels for modified protein release. **2010,** *39* (6), 903-909.

131. Censi, R.; Vermonden T Fau - van Steenbergen, M. J.; van Steenbergen Mj Fau - Deschout, H.; Deschout H Fau - Braeckmans, K.; Braeckmans K Fau - De Smedt, S. C.; De Smedt Sc Fau - van Nostrum, C. F.; van Nostrum Cf Fau - di Martino, P.; di Martino P Fau - Hennink, W. E.; Hennink, W. E., Photopolymerized thermosensitive hydrogels for tailorable diffusion-controlled protein delivery. (1873-4995 (Electronic)).

132. Choi, H. S.; Yui, N., Design of rapidly assembling supramolecular systems responsive to synchronized stimuli. *Progress in Polymer Science* **2006,** *31* (2), 121-144.

133. Szente, L.; Puskás, I.; Csabai, K.; Fenyvesi, É., Supramolecular Proteoglycan Aggregate Mimics: Cyclodextrin-Assisted Biodegradable Polymer Assemblies for Electrostatic-Driven Drug Delivery. *Chemistry – An Asian Journal* **2014,** *9* (5), 1365-1372.

134. van de Manakker, F.; Braeckmans, K.; Morabit, N. e.; De Smedt, S. C.; van Nostrum, C. F.; Hennink, W. E., Protein-Release Behavior of Self-Assembled PEG–β-Cyclodextrin/PEG–Cholesterol Hydrogels. *Advanced Functional Materials* **2009,** *19* (18), 2992-3001.

135. van de Manakker, F.; van der Pot, M.; Vermonden, T.; van Nostrum, C. F.; Hennink, W. E., Self-Assembling Hydrogels Based on β-Cyclodextrin/Cholesterol Inclusion Complexes. *Macromolecules* **2008,** *41* (5), 1766-1773.

136. Hamidi, M.; Azadi, A.; Rafiei, P., Hydrogel nanoparticles in drug delivery. *Advanced Drug Delivery Reviews* **2008,** *60* (15), 1638-1649.

137. Hirakura, T.; Yasugi, K.; Nemoto, T.; Sato, M.; Shimoboji, T.; Aso, Y.; Morimoto, N.; Akiyoshi, K., Hybrid hyaluronan hydrogel encapsulating nanogel as a protein nanocarrier: New system for sustained delivery of protein with a chaperone-like function. *Journal of Controlled Release* **2010,** *142* (3), 483-489.

138. Guvendiren, M.; Lu, H. D.; Burdick, J. A., Shear-thinning hydrogels for biomedical applications. *Soft Matter* **2012,** *8* (2), 260-272.

139. Rajagopal, K.; Schneider, J. P., Self-assembling peptides and proteins for nanotechnological applications. *Current Opinion in Structural Biology* **2004,** *14* (4), 480-486.

140. Li, J.; Mooney, D. J., Designing hydrogels for controlled drug delivery. *Nat Rev Mater* **2016,** *1* (12), 16071.

141. Siepmann, J.; Peppas, N. A., Higuchi equation: derivation, applications, use and misuse. (1873-3476 (Electronic)).

142. Kinnunen, H. M.; Sharma, V.; Contreras-Rojas, L. R.; Yu, Y.; Alleman, C.; Sreedhara, A.; Fischer, S.; Khawli, L.; Yohe, S. T.; Bumbaca, D.; Patapoff, T. W.; Daugherty, A. L.; Mrsny, R. J., A novel in vitro method to model the fate of subcutaneously administered biopharmaceuticals and associated formulation components. *Journal of Controlled Release* **2015,** *214*, 94-102.

143. Middaugh, C. R.; Pearlman, R., Proteins as Drugs: Analysis, Formulation and Delivery. In *Novel Therapeutics from Modern Biotechnology: From Laboratory to Human Testing*, Oxender, D. L.; Post, L. E., Eds. Springer Berlin Heidelberg: Berlin, Heidelberg, 1999; pp 33-58.

144. Batra, J.; Robinson, J.; Mehner, C.; Hockla, A.; Miller, E.; Radisky, D. C.; Radisky, E. S., PEGylation Extends Circulation Half-Life While Preserving In Vitro and In Vivo Activity of Tissue Inhibitor of Metalloproteinases-1 (TIMP-1). *PLoS ONE* **2012,** *7* (11), e50028.

145. Da Silva Freitas, D.; Mero, A.; Pasut, G., Chemical and Enzymatic Site Specific PEGylation of hGH. *Bioconjugate Chemistry* **2013,** *24* (3), 456-463.

146. Qiu, H.; Boudanova, E.; Park, A.; Bird, J. J.; Honey, D. M.; Zarazinski, C.; Greene, B.; Kingsbury, J. S.; Boucher, S.; Pollock, J.; McPherson, J. M.; Pan, C. Q., Site-Specific PEGylation of Human Thyroid Stimulating Hormone to Prolong Duration of Action. *Bioconjugate Chemistry* **2013,** *24* (3), 408-418.

147. Fernandes, A. I.; Gregoriadis, G., The effect of polysialylation on the immunogenicity and antigenicity of asparaginase: implication in its pharmacokinetics. *International Journal of Pharmaceutics* **2001,** *217* (1), 215-224.

148. Jain, S.; Hreczuk-Hirst, D. H.; McCormack, B.; Mital, M.; Epenetos, A.; Laing, P.; Gregoriadis, G., Polysialylated insulin: synthesis, characterization and biological activity in vivo. *Biochimica et Biophysica Acta (BBA) - General Subjects* **2003,** *1622* (1), 42-49.

149. Hinds, K. D.; Campbell, K. M.; Holland, K. M.; Lewis, D. H.; Piché, C. A.; Schmidt, P. G., PEGylated insulin in PLGA microparticles. In vivo and in vitro analysis. *Journal of Controlled Release* **2005,** *104* (3), 447-460.

Chapter II: Physical characterization of a hyaluronan-vitamin E conjugate

2.1 Introduction

New pharmaceutical drugs may be small molecules, peptides or proteins of 10's to 100kDa's in size. There is no single universal delivery system able to encapsulate and sustain the delivery of all molecules, which cover a wide spectrum of biophysical properties. Amphiphilic polymer derivatives composed of hydrophilic and hydrophobic domains are extensively used to encapsulate and control delivery of small molecule therapeutics following self-assembly into micelle-like structures, both currently and historically.[1] These materials are also compatible with large molecules such as D-α-Tocopherol modified poly ethylene glycol 1000 (PEG1000) succinate (TPGS), was first synthesized by the Eastman Kodak Company in the 1950s as a water soluble vitamin E supplement suitable for oral administration. TPGS is now generally recognized as safe (GRAS) and approved for use as a pharmaceutical emulsifier, solubilizer, detergent and permeation enhancer.[2, 3] TPGS has been shown to increase the solubility of multiple poorly soluble drugs through incorporation within its amphiphilic structure in which the lipophilic tocopherol alkyl tail forms the core of the drug encapsulating micelle while the hydrophilic PEG forms the aqueous exposed shell.[4-6] In addition to enhancing drug solubility, TPGS has also been shown to effectively control the release kinetics of small molecule therapeutics[7] and biologics[8] following administration. In a similar amphiphilic platform to TPGS, the polysaccharide dextran was hydrophobically modified with α-tocopherol succinate to enable the formation of a self-assembling micelle, which effectively encapsulated and sustained the *in vitro* release of the chemotherapeutic doxorubicin for 96 h.[9]

Several carrier systems, including tocopherol-modified dextran, are currently under investigation to determine the plausibility of employing polymers which are biologically compatible, biodegradable, with low immunogenicity and toxicity while also providing attractive

biological and physico-chemical functionality.[10] Polysaccharides such as dextran[11], chitosan[12] and hyaluronic acid[13] have been extensively researched in this regard due to their hydrophilicity, large variety in chemical composition and biological functionality, and for their ease of production.[14] Hyaluronic acid has been shown to be a particularly attractive drug carrier due to the following characteristics: its tunability[15], both in physical[13] and in chemical character[16], its CD44 receptor affinity, which is frequently over expressed on tumor surfaces,[17] as well as its potential for intralymphatic delivery following subcutaneous injections.[18]

Hyaluronic acid or hyaluronan (HA) is a linear polysaccharide is ubiquitous within human physiology, particularly as a major component of the extra cellular matrix (ECM).[19] The structure of HA consists of alternating units of the repeating *β*-1,4- D-glucuronic acid-*β*-1,3-*N*-actyl-D-glucosamine disaccharide. HA is an anionic, non-sulfated glycosaminoglycan with endogenous molecular weight from 100 kDa to 8 MDa. HA is readily degraded by a family of endogenous enzymes named hyaluronidase, which are expressed in nearly all human tissues.[13, 20, 21]

Hydrophobic modification of HA through covalent addition of a variety of hydrophobic substituents has been shown to create self-assembled particles.[22, 23] These particles are capable of non-covalently associating with a wide-range of pharmaceutically relevant small molecule payloads including fluorescent dyes,[24, 25] chemotherapeutics[26, 27] and corticosteroids.[28] In these cases, the resulting amphiphilic HA derivatives provided extended drug release kinetics without negatively impacting the desired therapeutic or diagnostic effect. Recently our lab showed that a tocopherol-modified HA conjugate (HAtoco) complexed with a potent toll-like receptor 7/8 agonist sustained local anti-tumor immunomodulatory effects when injected intratumorally.[29] Upon injection, a nano-suspension depot was formed, effectively suppressing tumor growth in

murine synergistic tumors and spontaneous canine cancers with no adverse systemic immunological responses.

The objective of this study is to explore the application of the HAtoco conjugate which includes optimization of its physical attributes, applicability to the delivery of protein therapeutics, characterization of its *in vivo* release kinetics and the assessment of the conjugate's physical, chemical and enzymatic stability.

2.2 Materials and Methods

2.2.1 Materials

Sodium hyaluronate (HA) was obtained from Lifecore Biomedical (Chaska, MN). SnakeSkin™ Dialysis Tubing and N-hydroxysulfosuccinimide (Sulfo-NHS) were obtained from Thermo Fisher Scientific (Waltham, MA). Float-A-Lyzer G2 Dialysis Devices were purchased from Spectrum Labs (Waltham, MA). Cyanine7-amine (Cy7-Amine) was purchased from Lumiprobe (Hunt Valley, MD). Chemical reagents including, Stains-all, hyaluronidase from bovine testes (+)-α-tocopherol, 1-ethyl-3-(e-dimethylaminopropyl)carbodiimide hydrochloride (EDC-HCl), N,N'-dicyclohexylcarbodiimide (DCC), 4-dimethylaminopyridine (DMAP), N-(tert-butoxycarbonyl) glycine (Boc-Gly-OH), trifluoroacetic acid (TFA), tetrabutylammonium hydroxide (TBA-OH), and 1-hydroxybenzotriazole hydrate (HOBT-H_2O) were purchased from Sigma Aldrich (St. Louis, MO). TAE buffer (40X) molecular biology grade was purchased from Promega (Madison, WI). Solvents for flash chromatography, HPLC grade solvents, agarose, and centrifugal filters were purchased from Fisher Scientific (Hampton, NH).

2.2.2 Synthesis of hyaluronan – vitamin E conjugate (HAtoco)

Hyaluronan – tocopherol conjugates were synthesized using a glycine-modified tocopherol.[29] (+)-α-Tocopherol (Vitamin E) was coupled to a Boc-protected glycine through DCC/DMAP mediated esterification in anhydrous CH_2Cl_2 overnight. The reaction mixture then was cooled to -20°C and filtered. The filtrate was purified by silica gel flash chromatography using a hexane-ethyl acetate gradient and dried *in vacuo*. The resulting product oil was treated with 12.5% (v/v) TFA in CH_2Cl_2 for 0.5 h at 0°C and an additional 1 h at 25°C to remove Boc protecting groups, and subsequently dried *in vacuo* to remove solvent and TFA. The gray solid product was purified by silica gel flash chromatography using a hexane-ethyl acetate gradient with elution at 5% ethyl acetate and again dried to yield a white solid product **1**. Sodium hyaluronate (6.7, 33, 100 or 250 kDa) were fully dissolved at 20 mg/ml in deionized water, followed by addition of Dowex AG 50W-X8 resin (10-fold excess to HA by mass) and stirred gently overnight at 20°C. The resin was removed by filtration and filtrate titrated with TBA-OH to pH 8-9, yielding a slightly pink solution. The HA-TBA solution was subsequently frozen and lyophilized to yield a pink-yellow cake **2**. HA-TBA was then dissolved in DMF (16.67 mg/ml, 26.85mM on a disaccharide basis) and subsequently added to a mixture of **1** (amount reacted ranged from 0.268-1.34mM corresponding to a 5-25% disaccharide substitution), EDC-HCl (1.5 molar equivalents to **1**) and HOBT-H_2O (2.5 molar equivalents to **1**) in DMF. The reaction mixture was stirred at 20°C overnight. Product crude was dialyzed (10 kDa MWCO for >6.7kDa HA or 3.5kDa MWCO for <6.7kDa HA) against 50% ethanol (v/v) for 12 h, 150 mM sodium chloride for 12 h and water with three changes over 72 h. The dialyzed HA-tocopherol (HAtoco) product was lyophilized to yield a white fibrous cake **3** (Scheme 1). Tocopherol substitution on a disaccharide molar basis was calculated by ^{1}H NMR acquired on a 400 MHz Bruker AV spectrometer equipped with a X-

channel broadband observe probe. Peak area ratios between the N-acetyl peak of HA (-CH_3, 2 ppm) and methyl groups of the tocopherol chain (12H, 0.8 ppm) were used to calculate the degree of substitution (Equation 1). General naming of HA-tocopherol analogs are as follows: "MW" HAtoco "tocopherol substitution as a percent of conjugated disaccharide units".

(1) $\%\ Degree\ of\ Substition$

$$= \left(\frac{(Tocopherol\ Methyl\ Peak\ Area, 0.8\ ppm)/12\ protons}{(HA, N-acetyl\ Peak\ Area, 2\ ppm)/3\ protons} \right) * 100$$

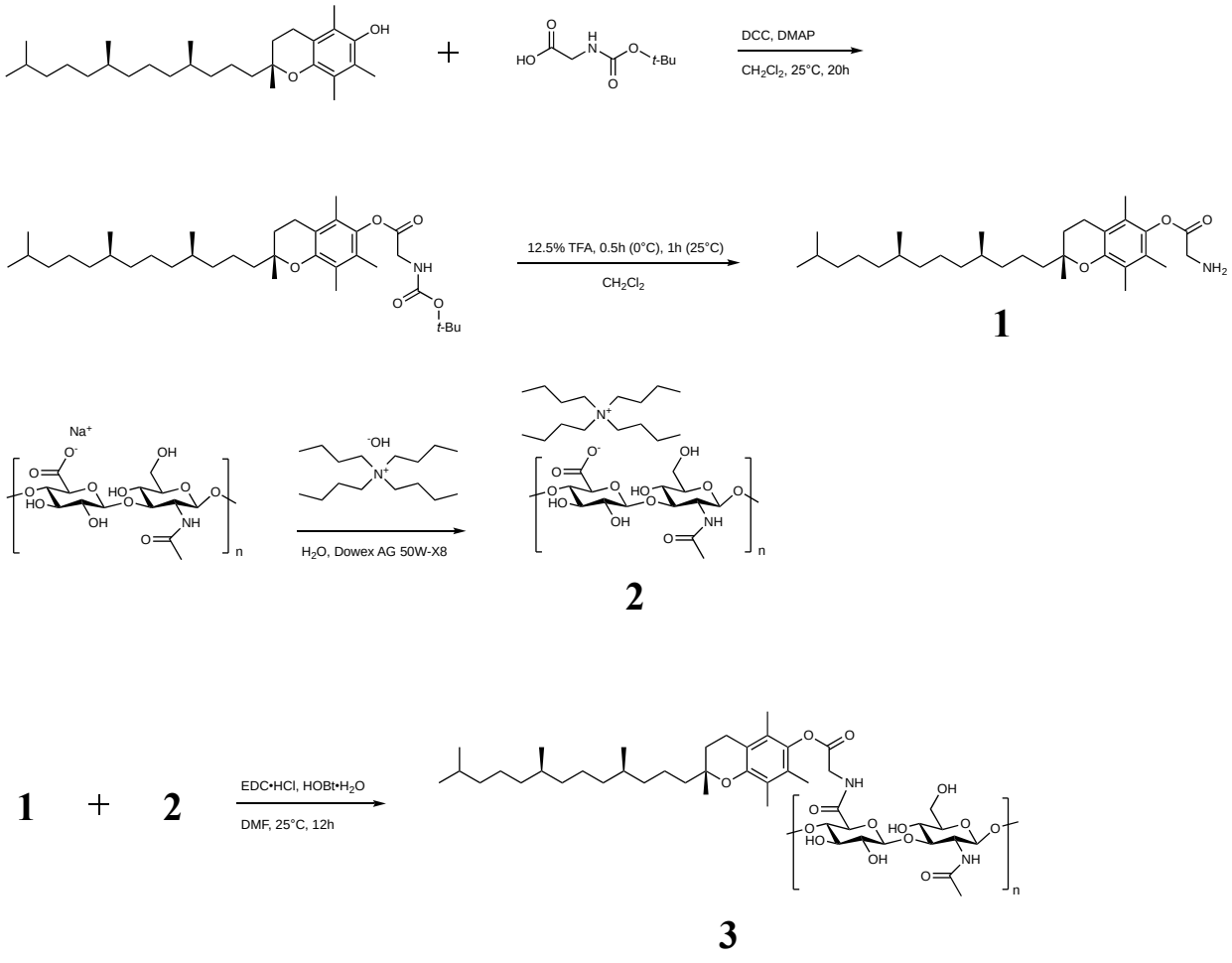

Scheme 1: Synthesis of hyaluronan-Vitamin E (HAtoco).

2.2.3 Assessment of protein binding capacity of HAtoco MW and substitution variants by intrinsic tryptophan fluorescence

The protein binding capacity of various hyaluronan-tocopherol analogs was assessed using the model-protein bovine serum albumin (BSA). BSA steady-state intrinsic tryptophan fluorescence spectra was acquired using a fluorescence plate reader manufactured by Fluorescence Innovations Inc. (Minneapolis, MN). Excitation wavelength was set at 295 nm coupled with a 310 nm long-pass dichroic mirror. Emission spectra were acquired from 300 – 400 nm with integration time of 1000 ms. Spectra were acquired at 25°C. BSA in PBS at 0.1 mg/ml was used to dissolve lyophilized HAtoco derivatives or 33 kDa HA at 7.9, 79, 790 and 7900 μM on a disaccharide basis with MW adjusted based on tocopherol substitution (Equation 2-6) and allowed to mix overnight at 20°C, protected from light. All samples were analyzed on a 384-well plate (*N*=6). Spectra contributions from HAtoco, HA or buffer were subtracted from raw data and processed using Microsoft Excel to derive the spectral moment (Equation 7-9) as described by Wei et al.[30], and plotted against an average disaccharide molecular weight concentration.

(2) $A = \ \#\ of\ Disaccharides\ in\ Base\ Polymer = \dfrac{Polymer\ MW}{Disaccharide\ MW}$

(3) $B = \ Cumulative\ non - subsitituted\ disaccharide\ MW$

$= A * (1 - \ \%\ Tocopherol\ substition) * (non - substituted\ disaccharide\ MW)$

(4) $C = \ Cumulative\ tocopherol\ subsitituted\ disaccharide\ MW$

$= A * (\%\ Tocopherol\ substition) * (tocopherol\ substituted\ disaccharide\ MW)$

(5) $D = \ Cumulative\ modified\ polymer\ MW = B + C$

(6) $Average\ Disaccharide\ MW\ of\ Modified\ Polymer = \dfrac{D}{A}$

(7) $Intensity = \int I(x)dx$

(8) $Moment = \frac{\int I(x)xdx}{\int I(x)dx}$

(9) $I(x) = fluorescent\ signal\ at\ wavelength\ (x)$

2.2.4 *In vitro* release of model proteins formulated with HAtoco

Model proteins BSA, lysozyme and RNAase were dissolved in deionized PBS, pH 7.4 to 10 mg/ml and subsequently added to an equal mass of lyophilized 33 kDa HAtoco10 or 33 kDa HA. The protein/HAtoco solution was mixed overnight at 20°C covered from light. Float-A-Lyzer dialysis cassettes (300 kDa MWCO) were filled with 0.8 ml of 1% (w/v) 622 kDa sodium hyaluronate (HMW HA) in PBS, pH 7.4 with 0.05% (w/v) NaN_3 as an anti-microbial agent. Protein/HAtoco mixtures (0.2 ml) were pipetted into the HMW HA solution within the dialysis cassette and dialyzed against 30 ml of PBS, pH 7.4, 0.05% (w/v) NaN_3, in a 50 ml conical centrifuge tube at 37°C while stirring. All release experiments were performed in triplicate. At predetermined intervals, the entire dialysate volume was replaced with fresh buffer and prior dialysate frozen at -80°C for future analysis. Percent protein released was determined by HPLC peak area against a standard curve. All chromatography was performed on a Shimadzu LC-2010C HT (Kyoto, Japan) with in-line UV detection (280 nm) using an Phenomenex Aeries 3.6 μm Widepore XB-C18 column (250 x 4.5 mm) at 50°C. Gradient mobile phases were A: 9:1, H_2O:Acetonitrile, 0.05% (v/v) TFA and B: 1:9, H_2O:Acetonitrile, 0.05% (v/v) TFA with elution 20-100% B over 6 min at a flow rate of 1.0 ml/min. Formulas for determining percent drug released are as follows:

$$\%DR_t = \frac{Drug\ Concentration\ \left(\frac{mg}{ml}\right) * Dialysate\ Volume\ (ml)}{Drug\ Initially\ Loaded\ (mg)} * 100$$

$$\%CDR_t = \%DR_t + CDR_{t-1}$$

where $\%DR_t$ = percentage of drug released at time (t); $\%CDR_{t-1}$ = cumulative drug released at time point prior to (t); $\%CDR_t$ = cumulative drug released at time (t). Release profiles were fit using a one phase decay nonlinear regression in Prism 6 (Graphpad Software, San Diego, CA).

2.2.5 Viscosity of HAtoco

The viscosity of 33kDa HAtoco10 was measured using a Brookfield DV-III Programmable Rheometer (Middleboro, MA) with a cone spindle and Thermo NESLAB RTE 740 circulating bath (Thermo Scientific) against Brookfield viscosity standards (4.9, 9.5, 49 cP) at 25°C. 33kDa HAtoco10 was dissolved to 10 mg/ml (23.26 mM discaccharide basis) and HA standards of 6.4, 33, 100, 200 and 622 kDa were dissolved to 9.33 mg/ml (23.26 mM discaccharide basis). Measurements were made in triplicate with individual sample torques adjusted as closely as possible to 60%. 33kDa HAtoco10 apparent molecular weight was determined through interpolation of a non-linear regression (one-phase decay) of the known molecular weight HA standards using Graphpad Prism 6.

2.2.6 HAtoco Solution Turbidity

Solution turbidity was analyzed using a Hach 2100N Turbidimeter (Loveland, CO) calibrated using Stablcal Turbidity Standards (7500 – 0.1 NTU). Measurements were made using 33kDa HAtoco10 , 200 kDa and 33 kDa HA at 10 mg/ml in PBS, pH 7.4. Measurements were made in single replicates due to volume requirements.

2.2.7 Characterization of HAtoco by Gel Permeation Chromatography and Agarose gel electrophoresis

Gel permeation chromatography was performed on a Shodex HQ-806M column with 5mM ammonium acetate, pH 5, at a flow rate of 0.8 ml/min within a 40°C oven using a Shimadzu LC-2010C HT. Elution profiles were monitored using an in-line UV/Vis detector at 214 nm and in-line fluorescence detector (295 Ex./330 Em.) using a Waters 2475 Multi λ Fluorescence Detector (Milford, MA). Samples were dissolved initially at 1.5 mg/ml in PBS overnight at 25°C without shaking and then diluted five-fold in mobile phase buffer prior to injection (80μl).

Agarose gel electrophoresis was performed based on the protocol of Cowan et al.[31] on a Fisher Scientific mini-horizontal electrophoresis unit (Hampton, NH). Agarose (500 mg) was first suspended in 50 ml (1% (w/v)) 1X TAE buffer (40mM Tris-acetate, 1 mM EDTA, pH 8.2-8.4). The suspension was heated in a 1100 W microwave for 50 s with stirring ever 10 s until light boiling occurred. The solution was then poured evenly onto a 7 x 10 mm tray with a 10-well comb and allowed to solidify at room temperature for 30 min. Once solidified, gel was oriented to run towards the anode terminal and submerged in 300 ml of 1X TAE buffer. 33kDa HAtoco 10 and HA standards (6.4, 33, 60, 100, 200, 323, 622 and 2000 kDa) were dissolved to 0.5 mg/ml in PBS, 15 μl removed and mixed with 30 μl of water and 9 μl of loading buffer (0.02% (w/v) bromophenol blue, 2M sucrose, 1X TAE buffer). An 18 μl aliquot of each sample (2.5 μg) was loaded into each well and electrophoresis carried out at ambient temperature at a constant voltage of 20V for 30 min and 40V for 2 h. Following the run, gels were submerged in a staining solution of 0.005% (w/v) Stains-all, 50% (v/v) ethanol and incubated at ambient temperature protected from light for 12 h. Gels were destained by submerging in 10% (v/v) ethanol covered from light for one day with

at least one bath change. Final destaining was performed by exposing the gel to laboratory room fluorescent lighting for 10 min before imaging.

2.2.8 HAtoco Particle Characterization by Dynamic Light Scattering and Micro Flow Imaging

The 33kDa HAtoco10 particles were analyzed using a Brookhaven ZetaPALS (Brookhaven Instrument Corporation, Holtsville, NY) and a MFI 5000 Series (ProteinSimple) instruments. Samples were dissolved to 10, 5, 2.5, 1.25 and 0.625 mg/ml for the DLS studies and 1 mg/ml for the MFI experiment in PBS, pH 7.4, overnight at 25°C. Dynamic light scattering was performed using a 653 nm laser placed at 90 degrees with samples measured in five acquisitions at an acquisition time of 30 s each. The viscosities of samples were set at 16.4 cP for 10mg/ml HAtoco based on previous measurements (Sec. 2.2.5) and iteratively decreased with concentration to the viscosity of PBS (0.89 cP) based on published rheological studies on the correlation of concentration and hyaluronan viscosity.[32, 33] Inputted viscosity parameters for each concentration are reported in Figure 2.13. Autocorrelation functions were fit using a NNLS (non-negative least squares) algorithm within the instrument software and reported as number and intensity average diameter and distributions. Polydispersity of the distribution was measured by cumulants analysis of the autocorrelation function within the instrument software. MFI measurements were made in triplicate with a required buffer baseline of <1000 particles/ml and a 3 ml sample flow through volume.

2.2.9 Thermal Dependence of HAtoco Static Light Scattering

Static light scattering of HAtoco was collected using a steady-state fluorometer (Photon Technology International/Horiba, Kyoto, Japan). 33kDa HAtoco10 or 33kDa HA was dissolved to 10 mg/ml in PBS, pH 7.4 overnight at room temperature, protected from light. Samples were measured in quartz cuvettes excited at 405 nm and emission detected at the same wavelength at 180°. Measurements were made from 10 to 90°C in 2.5°C increments with an equilibration time of 2 min.

2.2.10 Synthesis and Characterization of HAtoco and HA Cy7 Conjugates

Fluorescently labeled HA or HAtoco was synthesized (Scheme 2) by first dissolving 5 mg (0.0124 mmol disaccharide) of 33 kDa HA or 33 kDa HAtoco (0.0116 mmol disaccharide) to 10 mg/ml in 0.1 M MES, pH 4.25 overnight at room temperature. Next, 23.7 mg (0.124 mmol) EDC-HCl and 26.9 mg Sulfo-NHS (0.124 mmol) was added to the HA solution sequentially and stirred for 15 min at room temperature. Cy7-Amine (0.25 mg, 0.35 μmol, 0.03 molar equivalents to HA/HAtoco disaccharide) pre-dissolved to 2 mg/ml in DMSO was diluted 4-fold in PBS, pH 7.4, (0.5 ml final volume) and added to stirring HA/EDC/Sulfo-NHS solution. The reaction proceeded for 4 h at ambient temperature protected from light. Unconjugated dye and coupling reagents were removed by exhaustive dialysis using a 10 kDa MWCO membrane against a 2 L bath of PBS, pH 7.4 for 12 h, repeated three times and stored at 4°C until further testing.

2.2.11 In vivo release following subcutaneous injection

All animal studies were approved by the University of Kansas Institutional Animal Care and Use Committee. Female BALB/c mice (16 – 20 g) were purchased from Charles River. Hair

in the hind limbs was removed prior to treatment and imaging to reduce autofluorescence using depilatory cream. Assuming 100% mass recovery, purified HA-Cy7 (7.14 mg/ml) and HAtoco-Cy7 (10 mg/ml) samples were diluted 4-fold and 2-fold respectively with 10 mg/ml matching non-fluorescent samples to a final molar concentration of 23.26 mM on a disaccharide basis. Initial sample fluorescent intensities were visually assessed as comparable. Mice (3 per group) were anesthetized with isoflurane (3%) and injected subcutaneously with 10 μl of HAtoco-Cy7 or HA-Cy7 in the center of the hind footpad. Whole body fluorescent images were acquired at predetermined timepoints using a CRi Maestro In Vivo Imaging System (Cambridge Research & Instrumentation, Inc., Woburn, MA) equipped with a 671 – 705 nm excitation bandpass filter and an 800 nm long pass emission filter. All images acquired at a constant exposure of 2000 ms at 810 nm and equally scaled using the instrument software. Quantification of fluorescent intensity remaining at the injection site was performed by exporting images to ImageJ and adjusting threshold to a pixel intensity greater than 10 for HA-Cy7 images and greater than 200 for HAtoco-Cy7 in an effort to compensate for differences in sample intensities and to adequately distinguish from autofluorescence. Integrated density (mean intensity*area) of the remaining fluorescent signal was measured from the area of the entire foot to the ankle. Signal for intensities for both samples were normalized for comparison, and an elimination phase fit was performed using a non-linear, one-phase decay model in Graphpad Prism 6.

2.2.12 Evaluation of HAtoco conjugate chemical stability by High Performance Liquid Chromatography

Chemical stability of the glycine-ester linkage between hyaluronan and tocopherol at elevated temperatures was assessed by monitoring the free tocopherol within the HAtoco solution

over time through an adapted serum extraction procedure prior to RP-HPLC quantification.[34] 33kDa HAtoco10 was first dissolved to 10 mg/ml in PBS, pH 6 and placed at 37°C in sealed containers for 0h, 1h, 4h, 8h, 24h, 48h and 8 days. Samples were removed at designated time-points and frozen at -20°C until further testing. The general extraction work flow begins with 300 μl of test sample (10mg/ml HAtoco or buffer control) to which 600 μl of absolute ethanol is added and the mixture vortexed for 30 s. Next, 450 μl of hexane is added to the mixture and vortexed again for 30 s. Immiscible layers are allowed to separate (~30 s) and 300 μl of the organic (top) layer carefully removed without disruption of the aqueous layer. Sample is then dried on a rotary evaporator at 170 mbar, 35°C and placed under high vacuum (<4 mbar) for 1 h at room temperature. Dried sample is then dissolved in 200 μl of absolute ethanol and tested for tocopherol content by RP-HPLC. Extraction recovery was examined by suspending a known amount of tocopherol oil in a fresh solution of 10mg/ml HAtoco to a concentration of 500 μg/ml (N=5) and proceeding with extraction of the entire volume as described above. RP-HPLC analysis was performed using a Shimadzu LC-2010C HT with in-line UV detection (280 nm). Chromatography was performed on a ZORBAX Eclipse XDB 80Å C8 column (50 x 2.1 mm, 5μm) at 35°C. Gradient mobile phases were A: H_2O and B: Acetonitrile with elution 10% B over 5 min, ramp to 100% B over 10 min, hold for 3 min and ramp to initial conditions over 3 min. Mobile phase was set at a flow rate of 1.0 ml/min. Tocopherol concentration was determined through peak area correlation of known tocopherol standards serially diluted in absolute ethanol.

2.2.13 Hyaluronidase Degradation of HAtoco

The 33kDa HAtoco10 and 200 kDa HA were dissolved in PBS, pH 6 to 10.526 mg/ml overnight at 25°C without shaking. Hyaluronidase from bovine testes (HAdase) was dissolved separately in PBS, pH 6 to 1 mg/ml overnight at 25°C protected from light. Samples were heated to 37°C in an oil bath and mixed to give a final concentration of 10 mg/ml HAtoco or 200 kDa HA with or without 50 μg/ml HAdase. Mixtures were sampled at 24h, 48h and 8 days and stored at -80°C until further analysis. All samples were thawed to room temperature and analyzed by agarose electrophoresis as described previously with the modification that 10 μg samples were loaded for HAtoco for heightened signal, and the electrophoresis run conditions were extended to a constant voltage of 20V for 30 min and 40V for 3.5 h for improved resolution.

2.3 Results

2.3.1 Synthesis of hyaluronan – tocopherol conjugates

Hyaluronic acid was successfully reacted with glycine-modified α-tocopherol through EDC/HOBt mediated amidation of the D-glucoronic acid carboxylate (Scheme 1) with unreacted tocopherol removed by exhaustive dialysis. Tocopherol substitution onto the backbone of HA was quantified by ^{1}H NMR using the peak area ratio of the HA N-acetyl protons (1.9 ppm) and the tocopherol side chain methyl protons (0.8 ppm) (Figure 2.1). HAtoco conjugates of varying degree of substitution (5-25%, Figure 2.2, 2.3) and molecular weight (6.7-250 kDa, Figure 2.4) were synthesized with actual substitution and reaction efficiency tabulated in Table 1.

Slight increases in the reaction efficiency of 33kDa HAtoco were observed with increasing degree of tocopherol substitution (63-83%), but noticeable differences were seen in

the hydration rate and extent with higher substitutions. Poor dissolution was observed for conjugates with higher than 10 mol% substitution, which is exemplified in the decreasing intensity of the ^{1}H NMR signal. In addition, peak broadening with higher substitution was observed, likely indicative of increasing polydispersity. Similarly, conjugates of varying molecular weight with a constant substitution of 10 mol% had reaction efficiencies ranging from (71-90%), but with no clear correlation to molecular weight. HAtoco conjugates of molecular weight greater than 33kDa struggled to dissolved, similar to conjugates with >10mol% substitutions. ^{1}H NMR signal intensity reductions and peak broadening are again observable with increasing molecular weight. Overall, HA base-polymer molecular weight no greater than 33kDa and tocopherol substitution no greater than 10mol% were observed to exemplify dissolution characteristics most desirable for a product candidate that can be easily handled, characterized and administered.

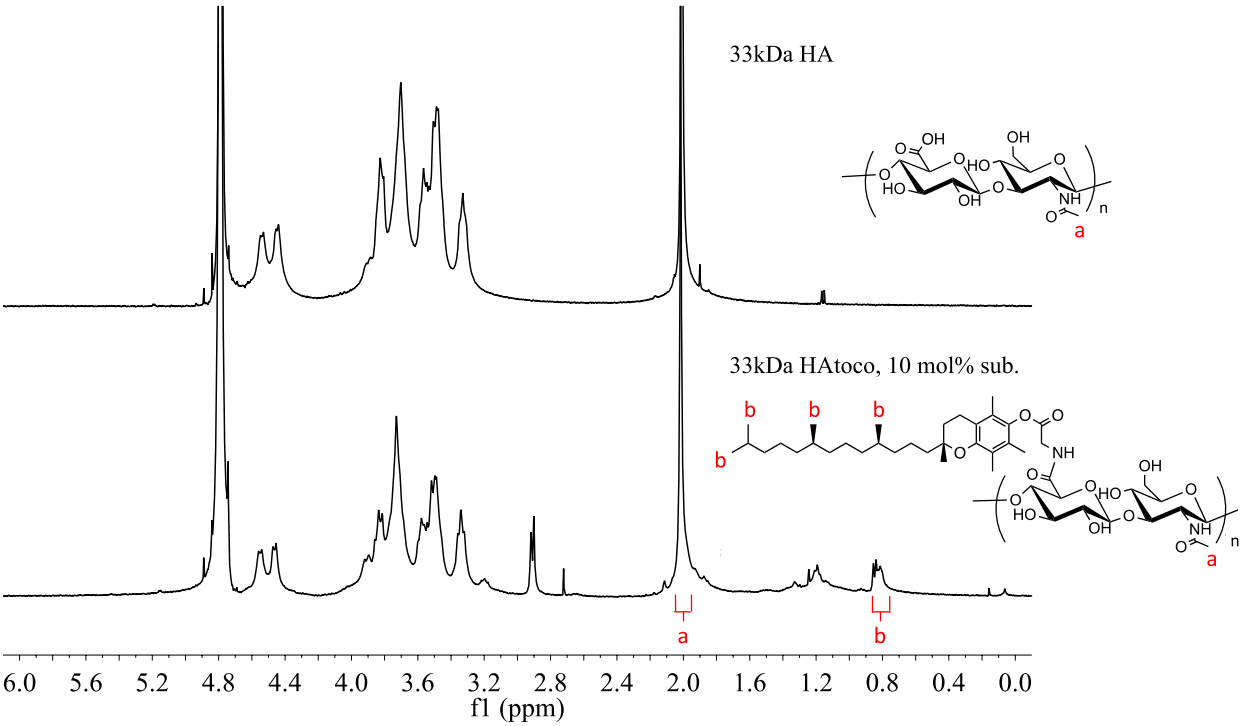

Figure 2.1: ^{1}H NMR spectra of 33 kDa HA (above) and 33 kDa HA tocopherol, 10 mol% subst. (below) with contributions from N-acetyl peak of HA (a, -CH_3, 2.0 ppm) and methyl group of tocopherol chain (b, 0.8 ppm) labeled.

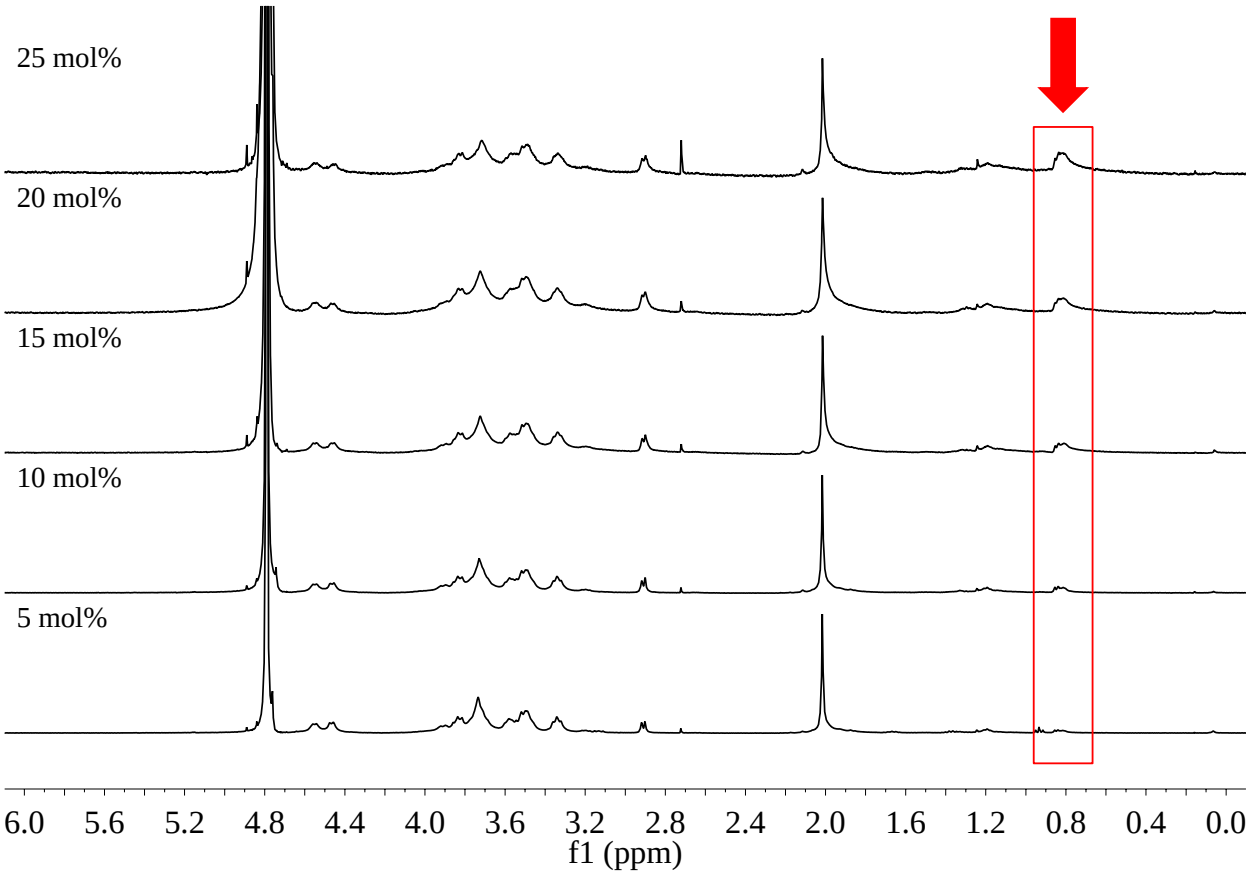

Figure 2.2: Stacked ^{1}H NMR spectra of 33 kDa HA with tocopherol substitutions from 5-25 mol% stoichiometry. Signal intensity of N-acetyl protons (2.0 ppm) normalized for substitution comparison. Increase in tocopherol associated hydrophobic tail methyl protons (0.8 ppm) outlined in red.

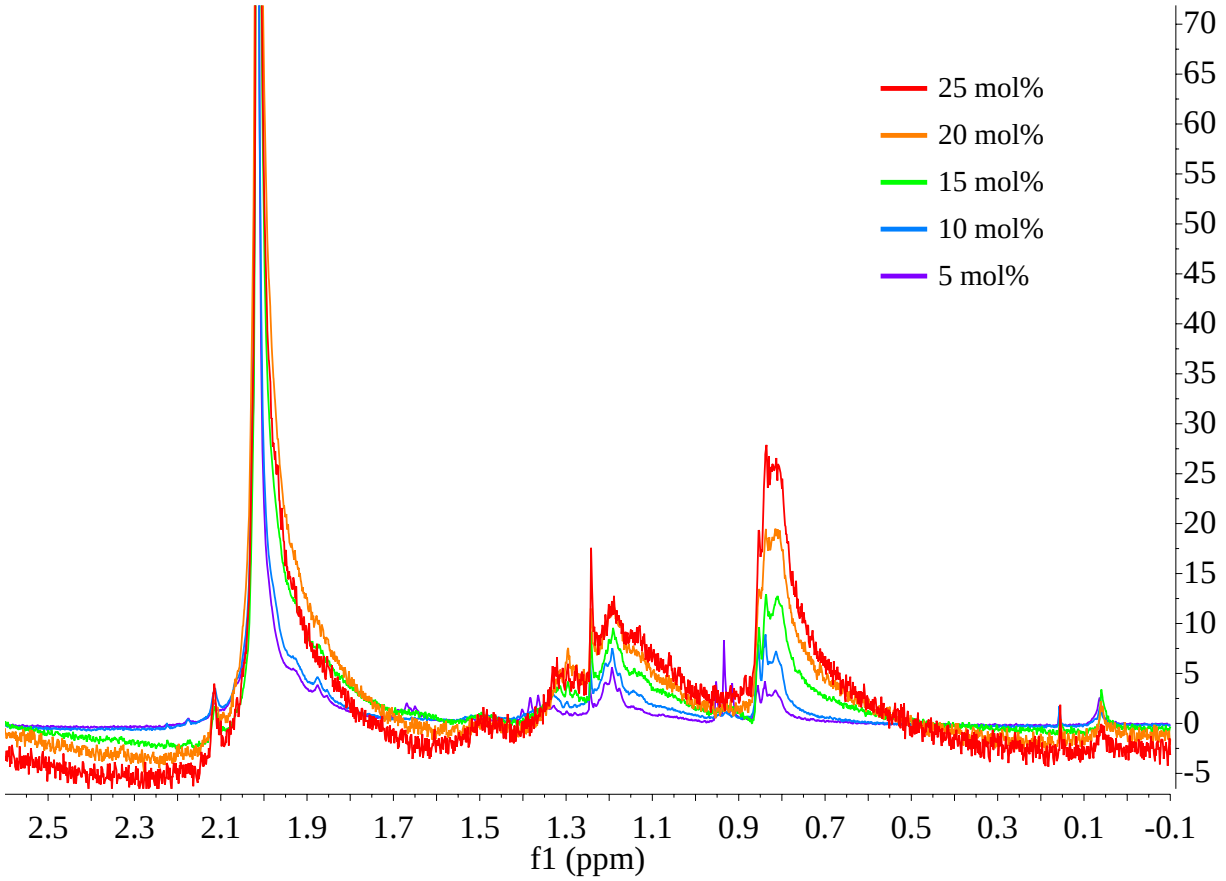

Figure 2.3: Overlayed ^{1}H NMR spectra of 33 kDa HA with tocopherol substitution from 5-25 mol% stoichiometry. Signal intensity of N-acetyl protons (2.0 ppm) normalized for substitution comparison. Increase in tocopherol associated hydrophobic tail methyl protons (0.8 ppm) outlined in red.

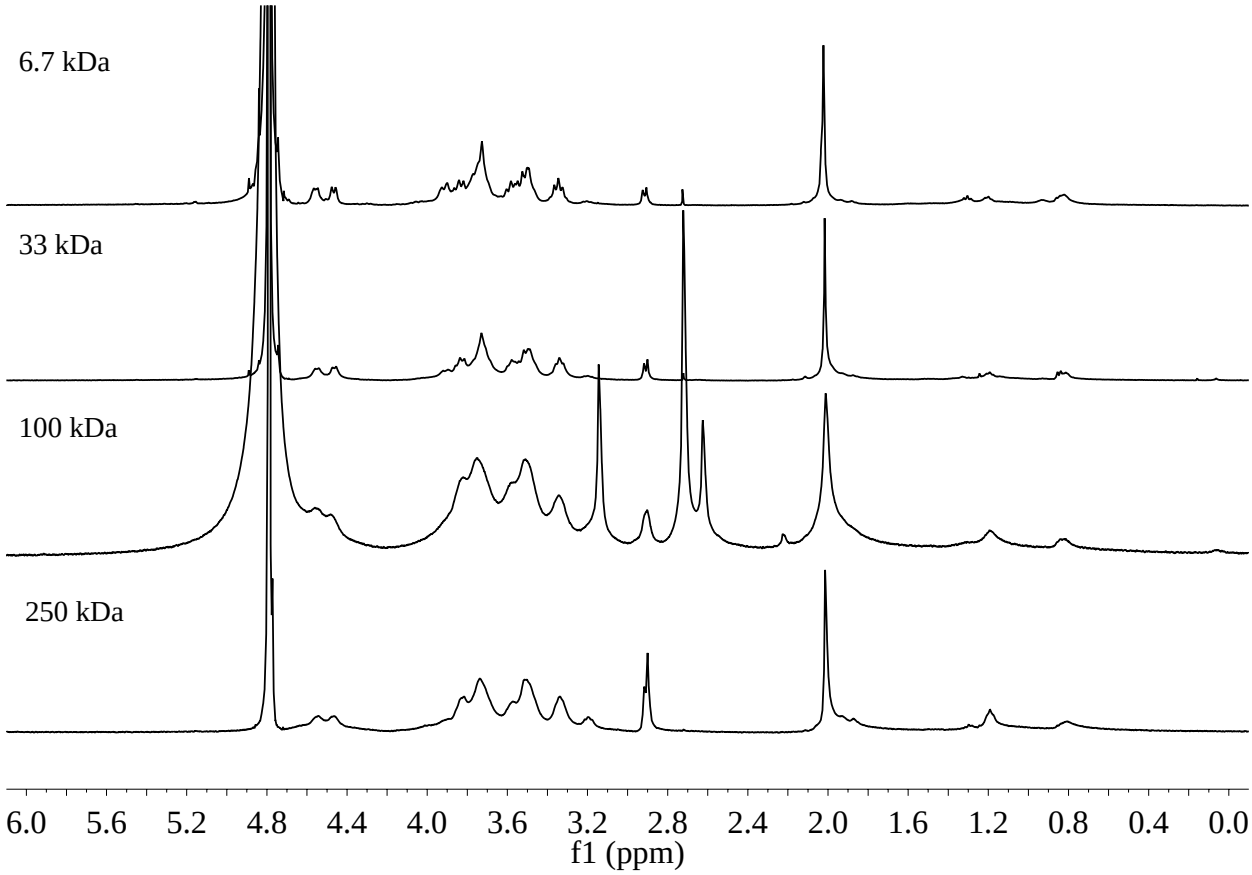

Figure 2.4: Stacked ^{1}H NMR spectra of 6.7, 33, 100 and 250 kDa HA with tocopherol substitution 10 mol% stoichiometry. Signal intensity of N-acetyl protons (2.0 ppm) normalized for substitution comparison.

MW (kDa)	Substitution, Stoichiometry (mol%)	Substitution, Actual (mol%)	Efficiency (%)
33	5	3.1	62.4
33	10	7.1	71.2
33	15	12.8	85.6
33	20	17.1	85.7
33	25	20.6	82.5
6.7	10	8.4	83.8
33	10	7.1	71.2
100	10	7.5	75.3
250	10	9.1	90.9

Table 1: Compiled degree of substitution analysis for all HAtoco variants by ^{1}H NMR peak area analysis (Equation 1) of hyaluronan *N*-acetyl protons (3H, 2.0 ppm) and methyl tocopherol chain protons (12H, 0.8 ppm).

2.3.2 Assessment of protein binding capacity of HAtoco MW and substitution variants by intrinsic tryptophan fluorescence

In a continuation of previous studies[29] where HAtoco was shown to complex with a hydrophobic small molecule TLR agonist in a depot-like manner, HAtoco derivatives were mixed with a model protein (BSA) in increasing concentrations and intrinsic tryptophan fluorescence spectra examined for alterations (Figure 2.5). Blue-shifts in the emission peak of BSA when mixed with increasing amounts of all HAtoco derivatives were observed in addition to clear quenching of overall signal intensity suggesting substantial increases in the apolarity of the tryptophan local environment likely through interaction with the tocopherol moieties. Emission peak moment also known as the mean spectral center of mass (MSM) was plotted against HAtoco disaccharide concentration to assess affinity differences between HAtoco variants and BSA (Figure 2.6). No clear differences were observed between different tocopherol substitution or molecular weight HA derivatives.

2.3.3 *In vitro* release of model proteins formulated with HAtoco

The potential of HAtoco as a protein binding complex was further explored through an in vitro release assay intended to model the release of protein following subcutaneous injection. Due to the poor dissolution characteristics observed with high molecular weight (>33kDa) and high tocopherol substitution (>10mol%) conjugates coupled with no clear differences observed in protein binding by fluorescent moment shifts, 33kDa HA with a 10mol% substitution was selected as the lead conjugate candidate for further characterization.

Model proteins BSA, RNase and lysozyme were mixed with 1% (w/v) 33kDa HAtoco10 in a 1:1 (m/m) ratio and injected within a semi-permeable dialysis bag containing high molecular

weight hyaluronan. Release dialysate was sampled at varying intervals, protein concentration quantified by RP-HPLC and cumulative protein released plotted as a percentage of initial protein loaded (Figure 2.7). Release profiles were fit using a non-linear regression to generally assess release half-life between protein formulated in 33kDa HAtoco10 versus unmodified 33kDa HA. All HAtoco formulated model proteins were found to release with about a 2-fold longer half-life when compared to unmodified HA suggesting HAtoco has the potential to associate with a broader range of protein therapeutics.

2.3.4 Viscosity Determination of HAtoco

Absolute viscosity of 33kDa HAtoco10 and unmodified HA standards was measured using a temperature-controlled rheometer validated with standards of known viscosity. HAtoco at 1% (w/v) was found to have a viscosity of 16.4 ± 0.1 cP at a shear rate of 86.25 sec^{-1}. HAtoco apparent molecular weight was determined by interpolation of the non-liner fit of unmodified HA molecular weight versus viscosity (Figure 2.8). 33kDa HAtoco10 had a viscosity equal to unmodified 187kDa HA at the same molar concentration indicating significant addition of viscosity occurs with hydrophobic modification of the hyaluronan backbone.

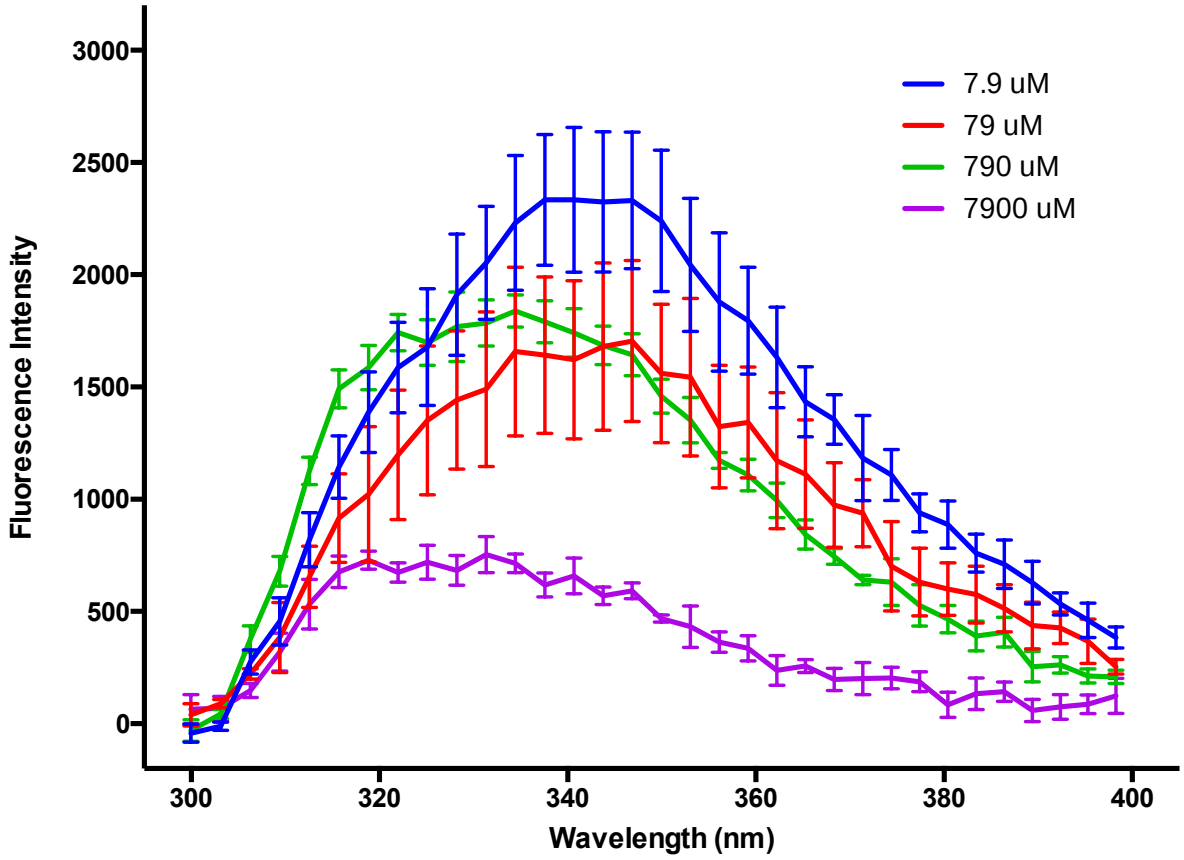

Figure 2.5: BSA (0.1 mg/ml) intrinsic tryptophan fluorescence with increasing 33kDa HAtoco10 concentration (7.9μM to 7900μM disaccharide basis), error bars represent SD (*N*=4).

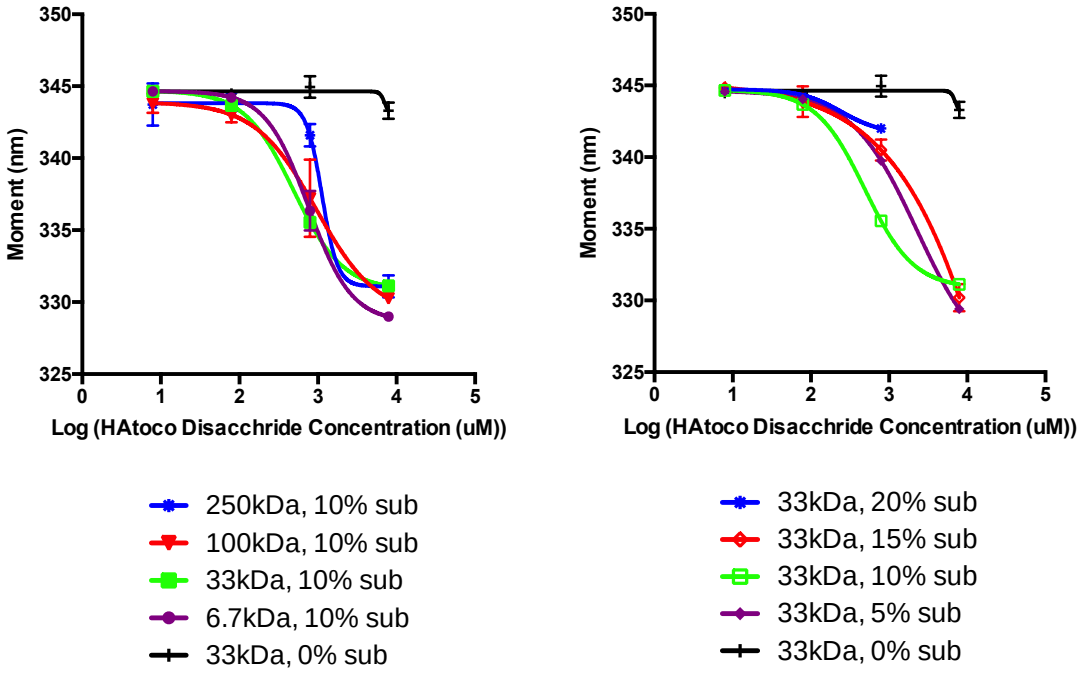

Figure 2.6: BSA (0.1 mg/ml) intrinsic tryptophan fluorescence moment versus HAtoco variant concentration (7.9μM to 7900μM disaccharide basis), data points represent mean ± SD (*N*=4). Data fit using a four-parameter logistic non-linear regression with Graphpad Prism 6. 33kDa HAtoco20 could not be fully solubilized at 7900μM and thus is not reported.

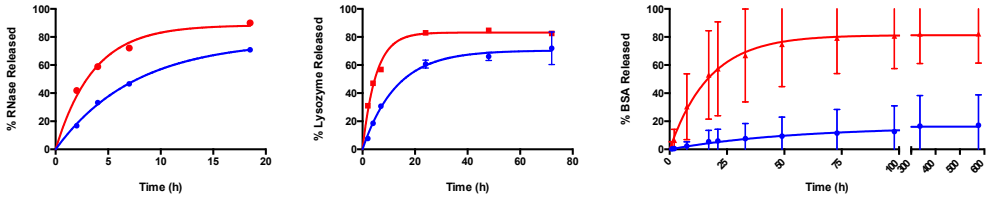

	RNase				Lysozyme				BSA			
Sample	$t_{1/2}$ (h)	95% CI	R^2	*N*	$t_{1/2}$ (h)	95% CI	R^2	*N*	$t_{1/2}$ (h)	95% CI	R^2	*N*
33kDa HAtoco10	5.2	4.1 - 7.2	0.99	1	8.9	7.3 - 11.2	0.99	3	37.7	14.7 - ∞	0.18	3
33kDa HA	2.5	1.6 - 5.6	0.97	1	3.5	2.8 - 4.7	0.97	1	17.3	8.0 - 24.5	0.66	3

Figure 2.7: In vitro release profiles of model protein RNase (left), Lysozyme (center) and BSA (right) formulated with 33kDa HAtoco10 or 33kDa HA. Release profiles were fit with a one-phase decay, non-linear regression with Y0 constrained to zero. Data points represent mean ± SD (when applicable).

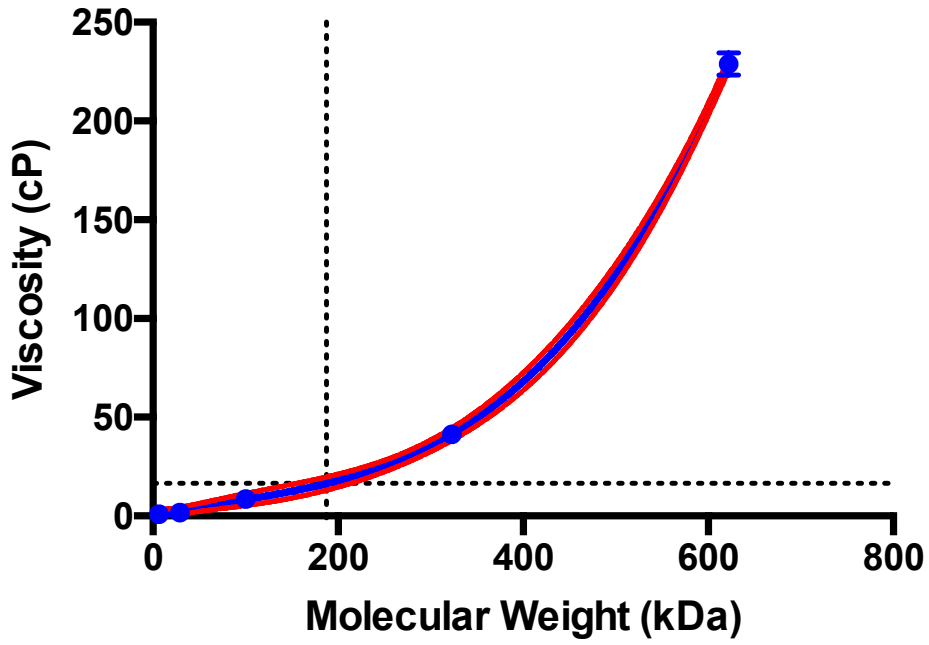

Figure 2.8: Non-linear regression of viscosity vs. molecular weight of HA standards. Red dotted line indicates regression 95% confidence interval. Black dotted line indicates value obtained for 33kDa HAtoco10 (10 mg/ml) and the corresponding apparent molecular weight.

2.3.5 HAtoco solution turbidity

Visual characterization of the solid and solution states of 33kDa HAtoco10 versus unmodified HA are seen in Figure 2.8. Under the current processing conditions, following dialysis purification, HAtoco is freeze dried into a fibrous cake for extended storage stability. In contrast, polydisperse sodium hyaluronan reagents are purchased as a dried powder (Figure 2.8, top). When dissolved in PBS to 1% (w/v), 33kDa HAtoco10 presents as a turbid, but homogenous solution while hyaluronan of equal base polymer molecular weight (33kDa) and viscosity (200kDa) presents as a clear solution (Figure 2.8, bottom). Turbidity differences were quantified against formazin standards of specified turbidity and 1% (w/v) 33kDa HAtoco10 was found to have a turbidity of 102 NTU (nephelometric turbidity units) while all HA standards and buffer were found to have a turbidity of less than 1.3 NTU. These results suggest HAtoco develops into a self-associating particle when dissolved in aqueous buffer.

2.3.6 Characterization of HAtoco by Gel Permeation Chromatography

Assembly of the HAtoco particle complex and its effective size in solution was first assessed by gel permeation chromatography using a Shodex 806-M HQ column equilibrated with 5 mM ammonium acetate, pH 5 mobile phase. 33kDa HAtoco10 and unmodified polydisperse HA standards were prepared at 1.5 mg/ml and diluted 5-fold with mobile phase prior to injection. Chromatography was monitored by UV-absorption at 214 nm (Figure 2.10, top). To assess column performance, retention volumes of HA standards were compared to pullulan polysaccharide standards run under similar aqueous conditions defined in the manufacturer's certificate of analysis (Figure 2.10, bottom). The upper limit of resolution was found to be 100kDa based on minimal change in peak retention at high molecular weights. Interestingly, 33kDa HAtoco 10 had a similar

retention to unmodified 33kDa HA, which was unexpected based on the visual turbid particulate nature of the solution. To further investigate this unexpected result, in-line fluorescence detection was added with excitation and emission set to 295 nm and 330 nm respectively based on observed fluorescence from the conjugate alone during previously described protein binding assays. No fluorescent signal was detected throughout the entire HAtoco chromatogram. When the column was removed from the flow path and sample injection repeated, an immediately eluting sharp peak with increased UV (214nm) peak area and substantial fluorescent intensity was observed (Figure 2.11). These results indicate that 33kDa HAtoco10 forms a large enough effective size where it is unable to pass through the entrance frit of an analytical gel permeation column and that it contains substantial unreacted 33kDa HA.

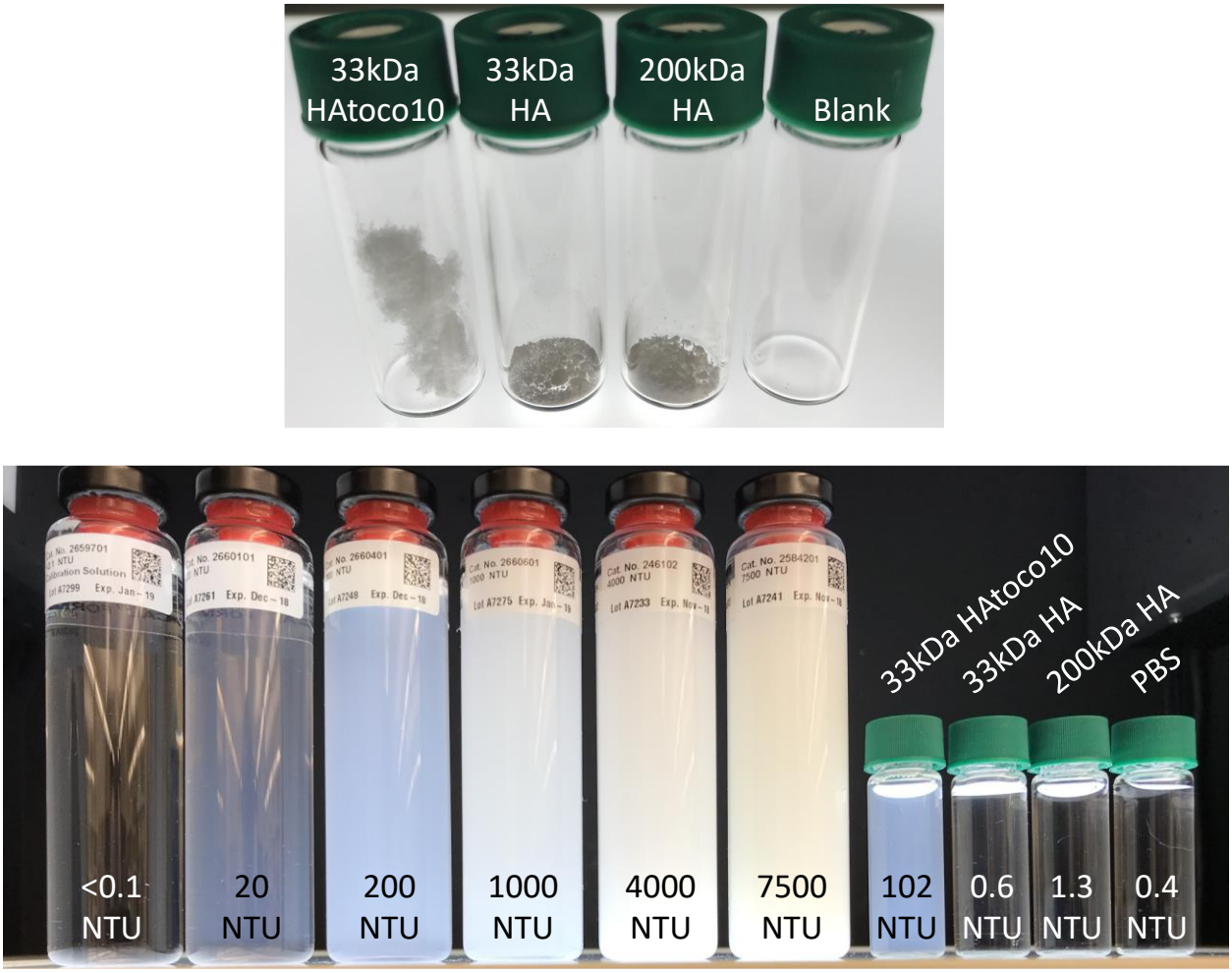

Figure 2.9: (Top) Equal dry mass (10 mg) 33kDa HAtoco10, 33kDa HA and 200kDa HA. (Bottom) 33kDa HAtoco10 (10 mg/ml) visual and measured turbidity compared to 33kDa HA, 200kDa HA, PBS and formazin turbidity standards. NTU = nephelometric turbidity units.

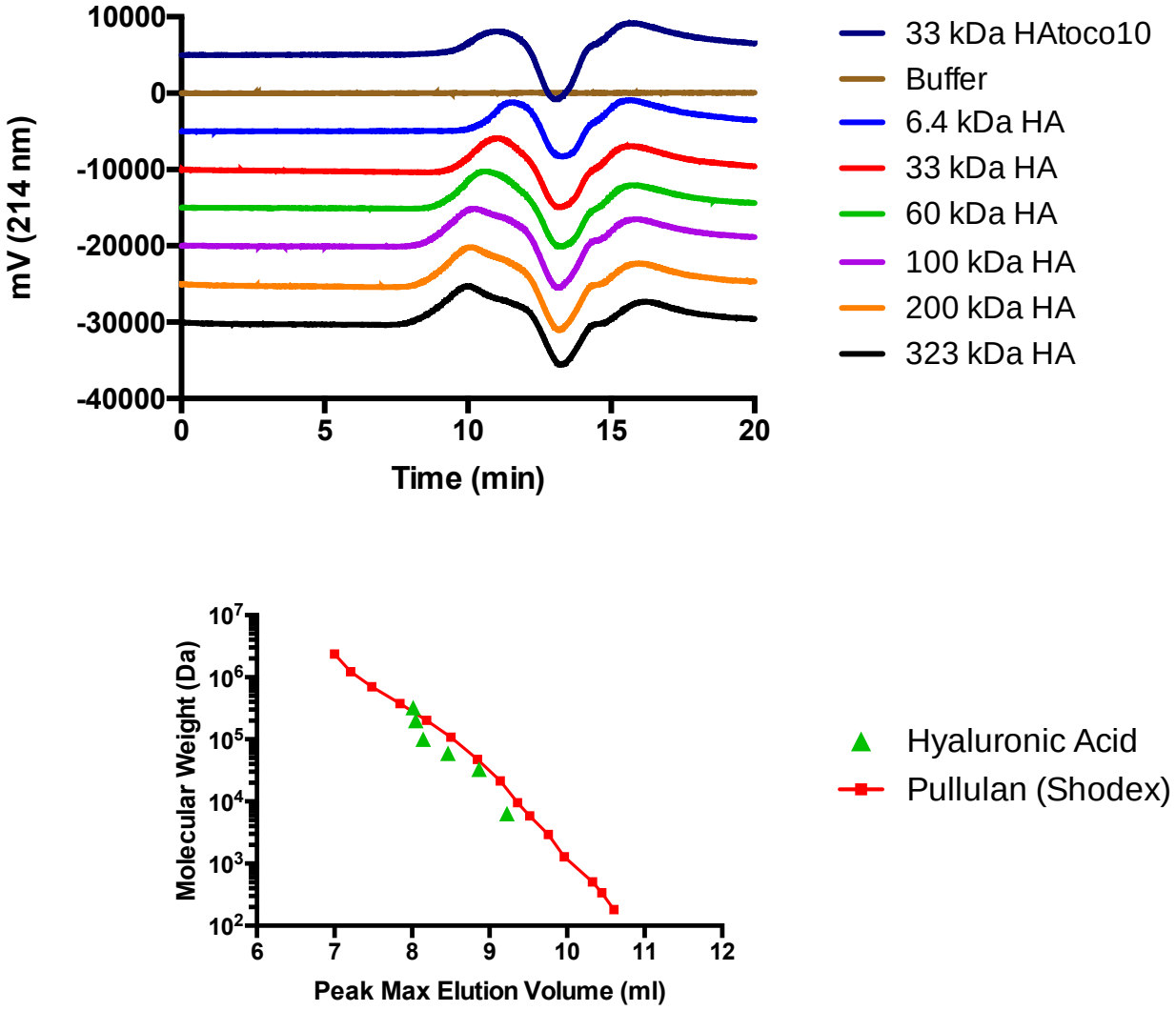

Figure 2.10: (above) Gel permeation chromatograph of 33kDa HAtoco10 and HA molecular weight standards (323, 200, 100, 60, 33 and 6.4 kDa) run on a Shodex 806-M HQ monitored by UV-absorption at 214 nm. (below) Peak elution volume versus HA molecular weight standards compared to column certificate of analysis pullulan polysaccharide molecular weight versus elution correlation.

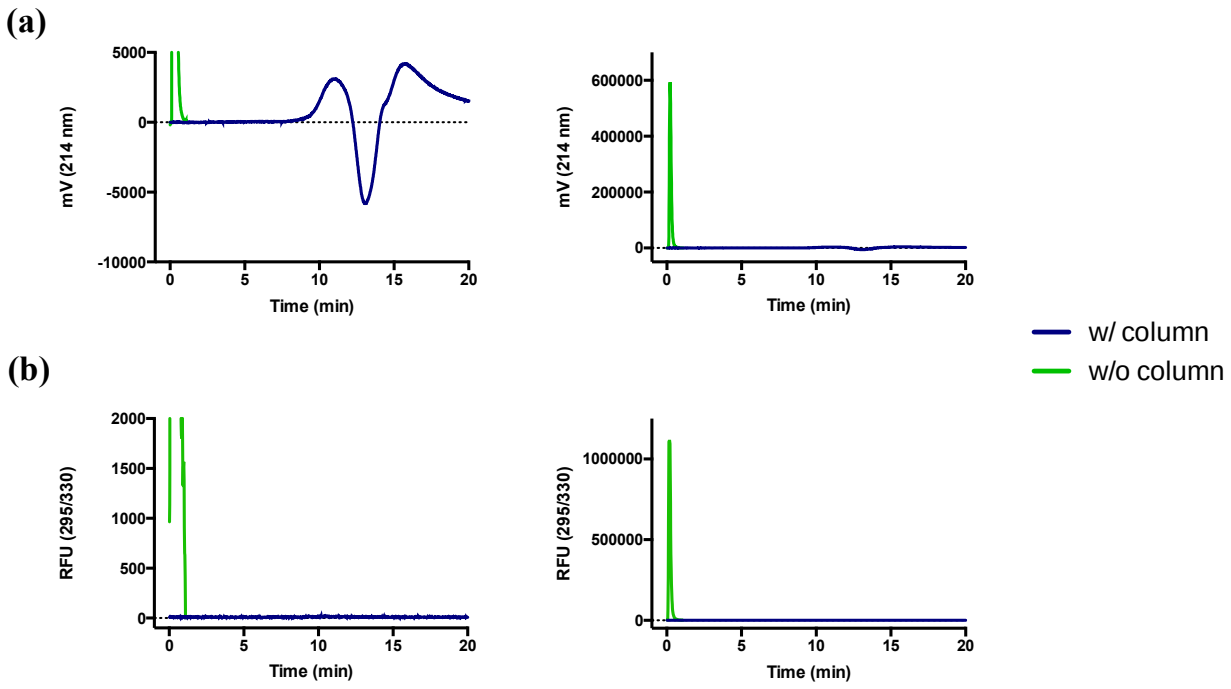

Figure 2.11: (a) Gel permeation chromatograph of 33kDa HAtoco10 monitored by UV-absorption at 214 nm with and without a Shodex 806-M HQ column (left) zoomed and (right) full scale. (b) Gel permeation chromatograph of 33kDa HAtoco10 monitored by fluorescence (295 Ex/330 Em) with and without a Shodex 806-M HQ column (left) zoomed and (right) full scale.

2.3.7 Characterization of HAtoco by agarose electrophoresis

Effective size analysis of HAtoco in solution was next assessed by running samples on a 1% (w/v) agarose gel with TAE, pH 8.3 running buffer and visualized using Stains-all. 33kDa HAtoco10 and unmodified polydisperse HA standards of increasing molecular weight (6.4, 33, 60, 100, 200, 323, 622 and 2000 kDa) were equally loaded (2.5 μg) onto the gel and ran with gel-oriented for the negatively charge polymers to distribute towards the anode (Figure 2.12). HA standards were found to visualize and resolve well between 33 and 2000 kDa with retention of only 6.4 kDa HA undetermined. Electrophoresis of 33kDa HAtoco10 resulted in two distinct polydisperse populations, one at a similar retention to 33kDa HA and the other of a similar retention to 2000 kDa HA. These results support previous observations from visual and GPC experiments indicating 33kDa HAtoco10 forms a large particulate complex in solution similar in effective size to 2000 kDa HA and that significant unreacted base-polymer (33kDa) remains within the sample mixture. No polymer with visualized within the well or gel entrance suggesting electrophoresis within a 1% (w/v) agarose gel is sufficient to assess all sub-populations contained within the HAtoco sample.

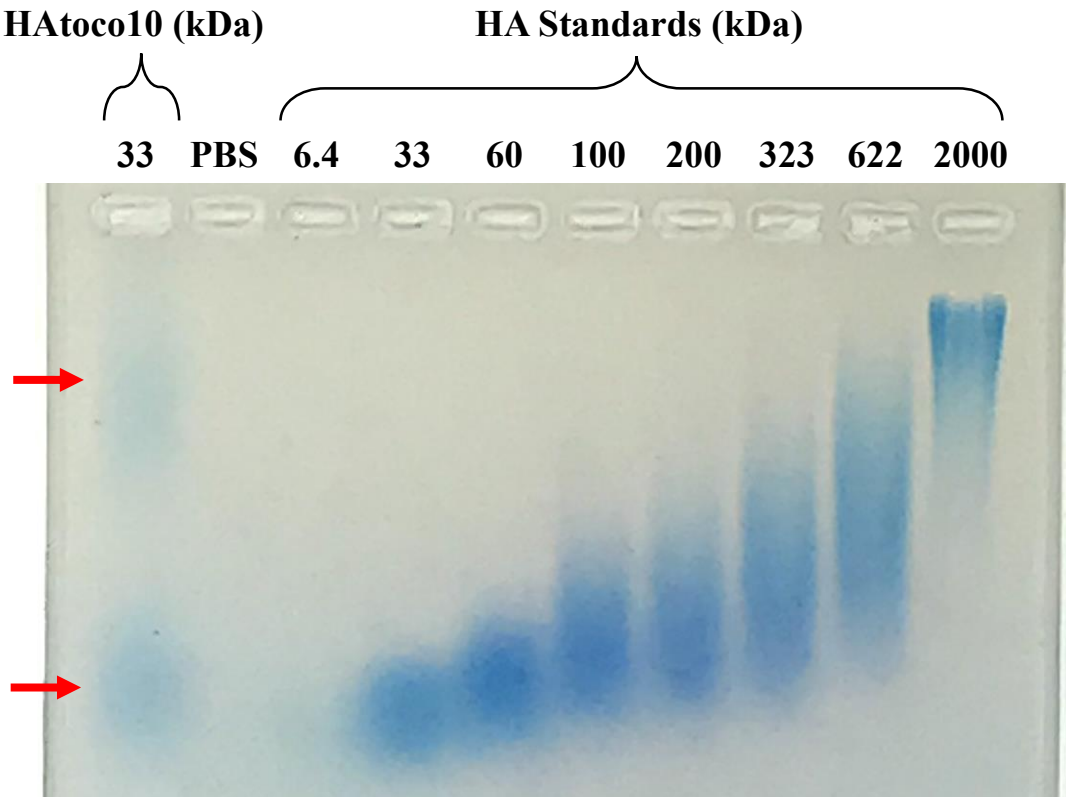

Figure 2.12: Agarose electrophoresis of 33kDa HAtoco10 (far left) against HA molecular weight standards (left to right; 6.4, 33, 60, 100, 200, 323, 622 and 2000 kDa) visualized with Stains-all. Separated fractions of 33kDa HAtoco10 sample at ~33kDa and ~2000 kDa indicated by red arrows.

2.3.8 HAtoco particle characterization by DLS and MFI

The distribution of HAtoco particle size was further investigated by DLS and MFI. DLS samples of 33kDa HAtoco10 dissolved in PBS, pH 7.4 to 10, 5, 2.5, 1.25 and 0.625 mg/ml and measured in five, 30 s acquisitions. The autocorrelation function was found to decay more rapidly with decreasing amounts of HAtoco suggesting a decrease in the particle size distribution upon dilution (Figure 2.13a). Relationship of the viscosity of HAtoco with concentration was estimated based on published rheology studies[33] of the concentration effects on the viscosity of 2200 kDa HA at a shear rate of 91 ± 7 sec^{-1} (Figure 2.13b, left). Upper bound viscosity was set as the measured absolute viscosity reported in Figure 2.8 for 10 mg/ml HAtoco (16.4 ± 0.1 cP) at a similar shear rate, while lower bound was set as 0.89 cP, the reported viscosity of PBS within the DLS software. Following adjustment of viscosity parameters, both number and intensity averaged diameters of the multimodal distribution analysis were found to decrease with increasing HAtoco concentration, opposite of the initial observations of the autocorrelation function alone. Intensity averaged diameter decreased exponentially from ~900nm at 0.625mg/ml to 150nm at 10mg/ml. Number averaged diameter decreased exponentially from ~20nm at 0.625 mg/ml to 4.5nm at 10 mg/ml with the exception of the 2.5 mg/ml sample. Polydispersity was found to increase with HAtoco concentration indicating the development of a wider distribution of particle size at higher concentrations (Figure 2.13b, right). Similar results were seen when the intensity and number multimodal distributions are viewed versus concentration of HAtoco (Figure 2.13c). Both distributions were seen to decrease in diameter with increasing concentration. When distributions were combined, three populations of particles were resolved for the three highest concentrations (10, 5 and 2.5 mg/ml), one of high concentration and low particle size and two of lower concentration and higher particle size. Upon further dilution (1.25 and 0.625 mg/ml), the high

particle size populations were merged into one. These observations mirror the results seen following agarose electrophoresis of HAtoco where a low molecular weight population (small particle size) of heightened intensity (high quantity) and a high molecular weight population (large particle size) of lower intensity (low quantity) were resolved.

MFI analysis of 33kDa HAtoco10 at 1 mg/ml compared to unmodified 33kDa HA and 200kDa HA at equal concentrations showed an order of magnitude increase in the quantities of >1 μm particles (Figure 2.14). This trend continued in subsequent bins of increasing particle size, but with an exponentially decreasing overall particle concentration. These results indicate a greater quantity of particles bordering the visible range (>100 μm) exist following tocopherol substitution of HA.

2.3.9 Thermal dependence of HAtoco colloidal stability

HAtoco colloidal stability was analyzed by monitoring static light scattering as a function of temperature. 33kDa HAtoco10 and 33kDa HA samples dissolved in PBS to 10 mg/ml were measured in triplicate in sealed quartz cuvettes from 10°C to 90°C (Figure 2.15). Unmodified HA exhibited no appreciable scattering throughout the temperature range tested and no visible difference in clarity post-heating indicating no aggregation of the polymer occurred. Heating of HAtoco resulted in a linear decrease in scattering from 25,000 kcps to 15,000 kcps which correlates to a reduction in particle size. Visual inspection of HAtoco solution post-heating showed no discernable difference in turbidity suggesting particles are resistant to temperature induced irreversible aggregation and particle size alterations may be reversible.

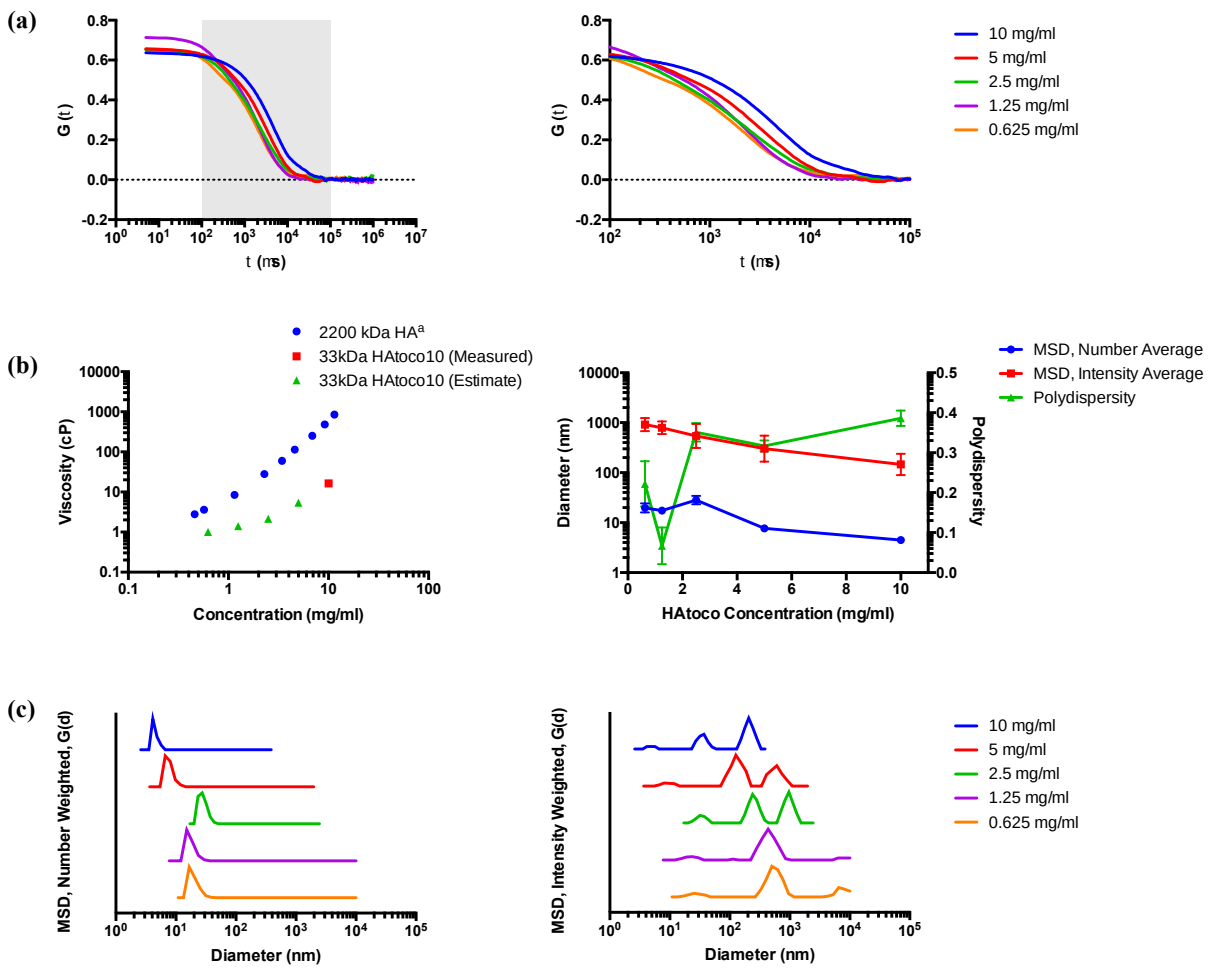

Figure 2.13: Dynamic light scattering of 33kDa HAtoco10 (10, 5, 2.5, 1.25 and 0.625 mg/ml) in PBS pH, 7.4. (a) Auto correlation function unzoomed (left) and zoomed (right) showing variance in decay with concentration. (b) (left) Measured and estimated viscosity of serially diluted 33kDa HAtoco10 (10 mg/ml = 16.4 cP (measured at a shear rate of 86.25 sec^{-1}), 5 mg/ml = 5.37 cP, 2.5 mg/ml = 2.148 cP, 1.25 mg/ml = 1.4 cP and 0.625 mg/ml = 1 cP) and published[a,33] viscosity versus concentration of 2200 kDa HA at a shear rate of 91 ± 7 sec^{-1}. (right) Viscosity adjusted MSD (multimodal size distribution) diameter and polydispersity with increasing HAtoco concentration. All samples measured in five acquisitions of 30 s each at room temperature with data represented

as mean ± SD. (c) Viscosity adjusted number (left) and intensity (right) weighted differential distribution (G(d)) versus diameter of varying concentrations of HAtoco. Distributions staggered for visual clarity.

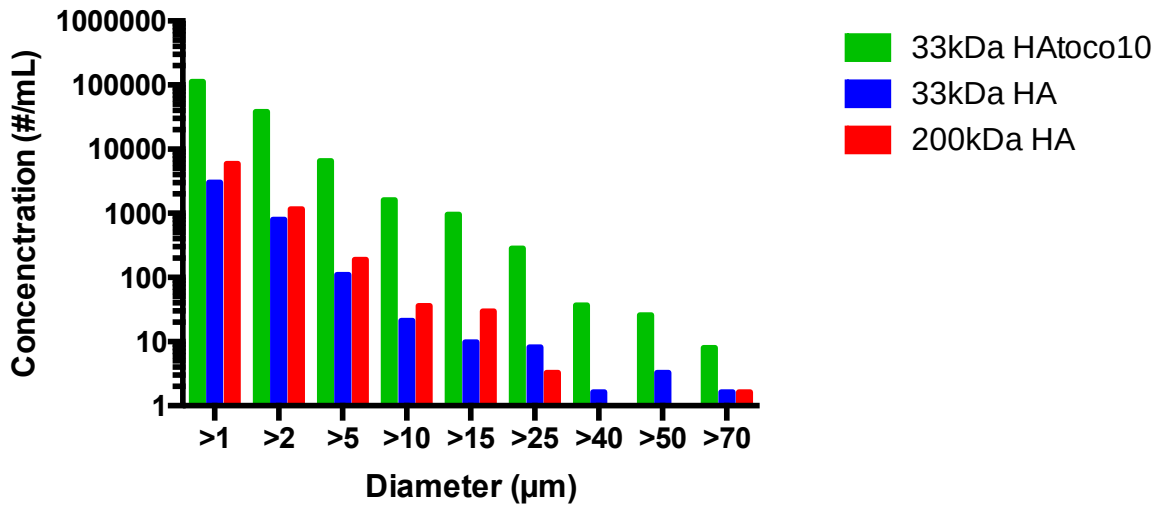

Figure 2.14: MFI sizing of 33kDa HAtoco10, 33kDa HA and 200kDa HA at 1 mg/ml in PBS, pH 7.4. Diameters represent binned count between current size cut-off and succeeding size cut-off.

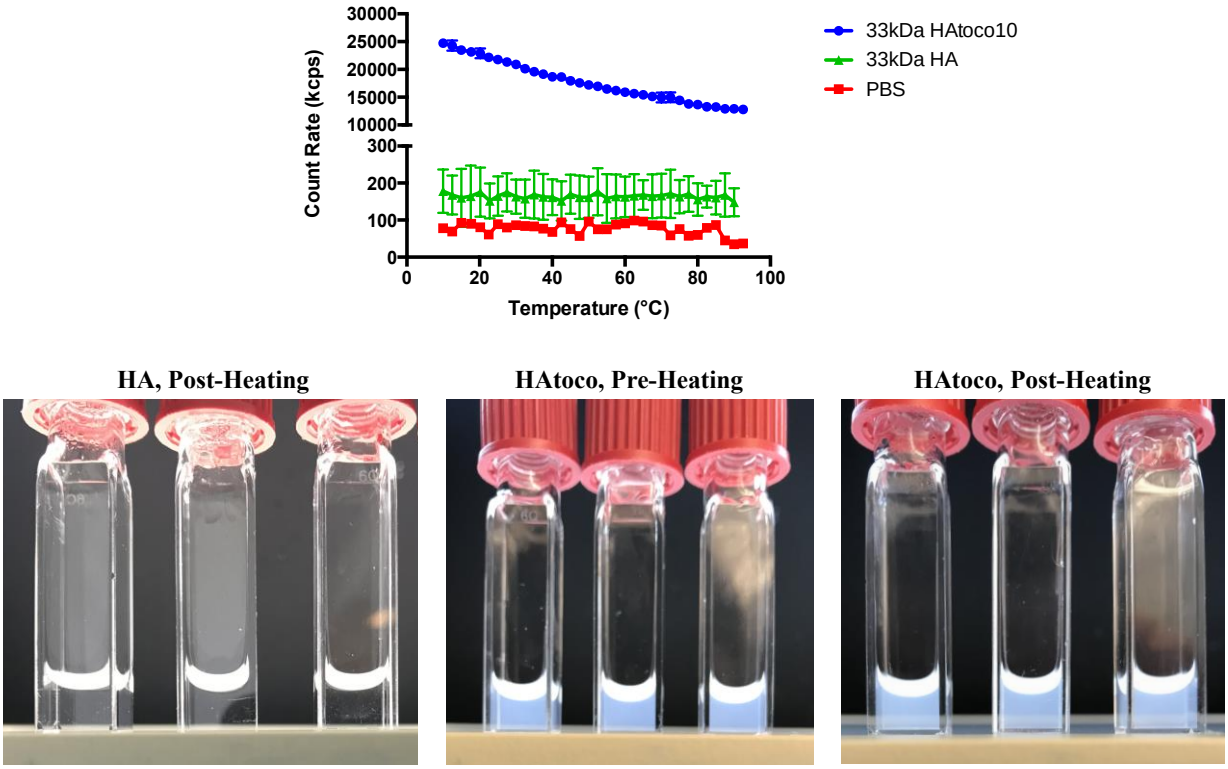

Figure 2.15: Colloidal stability of 33kDa HAtoco10, 1% (w/v) in PBS, pH 7.4 monitored by static light scattering with temperature ramped from 10 to 90°C. HAtoco samples were measured in triplicate with data represented as mean ± SD. (Top) static light scattering count rate versus temperature for HAtoco and PBS samples. (Bottom) Images of triplicate quartz screw top cuvettes with fresh HAtoco and following temperature ramp and cooling.

2.3.10 In vivo release following subcutaneous injection

In order to assess the potential of HAtoco as a depot forming platform following subcutaneous injections, fluorescently labelled derivatives of both 33kDa HAtoco10 and 33kDa HA were synthesized and injected into the footpad of a BALB/c mouse and monitored for injection-site fluorescence for 60 days (Figure 2.16). Fluorescent intensity following injection for both derivatives was found to initially increase to a maximum around 4 days post injection for HAtoco and 1 day for HA suggesting a potential self-quenching mechanism upon initial injection. This had been observed in previous studies of fluorescent HA's.[35] Following the period of quenched fluorescent signal intensity, an exponential decay of fluorescent signal from both samples occurred with HAtoco signal significantly extended. Fluorescent intensity over background autofluorescence was measured, normalized and reported as integrated density (mean intensity x area) of the entire injected foot (Figure 2.17). Elimination phase of both release profiles were fitted using a one-phase decay non-linear regression with shared plateaus. HA fluorescent conjugate was found to release from the injection site with a half-life of 5 days while HAtoco conjugate was found to release with a half-life of 25 days.

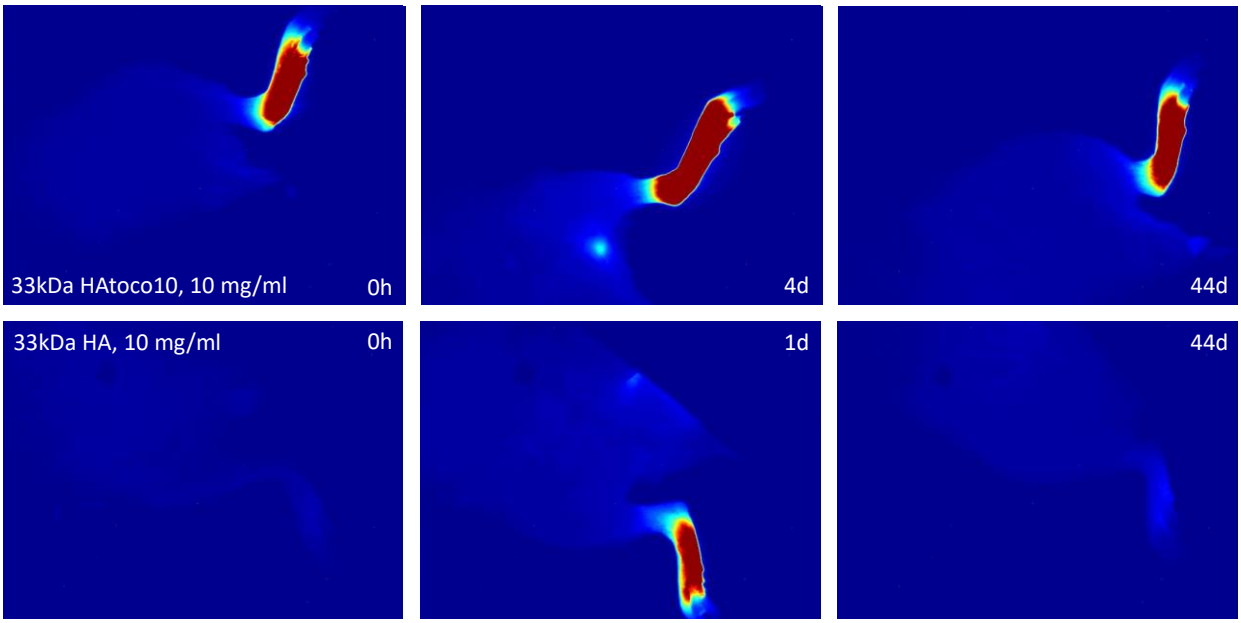

Figure 2.16: *In vivo* release of 33kDa HA-Cy7 or 33kDa HAtoco10-Cy7 fluorescent conjugates following subcutaneous injection to the footpad of a BALB/c mouse.

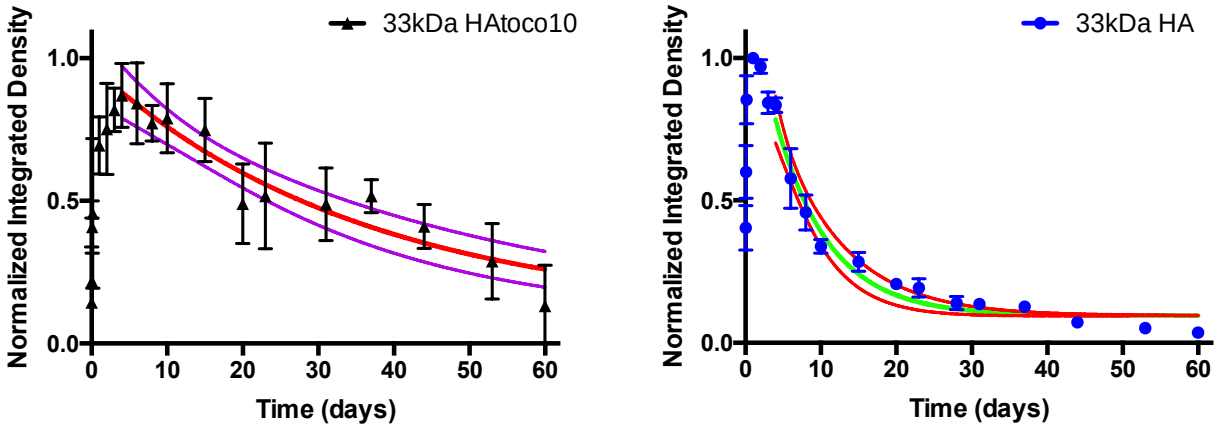

Sample	$t_{1/2}$ (days)	95% CI	R^2
33kDa HAtoco10	24.8	19.3 to 34.7	0.9676
33kDa HA	4.9	3.9 to 6.5	0.9119

Figure 2.17: *In vivo* release profiles of 33kDa HA-Cy7 and 33kDa HAtoco10-Cy7 conjugates remaining at the site of injection. Elimination phase fit using a one phase decay, non-linear regression with both plateaus constrained to equal values. Dotted-lines represent 95% confidence interval of regression, data represented as mean ± SD (N = 3).

2.3.11 Chemical stability of HAtoco lysine linker at elevated temperatures

Chemical stability of the lysine linkage between HA and tocopherol within the 33kDa HAtoco10 conjugate was examined at 37°C in PBS, pH 6 at 1% (w/v). Samples were stored up to 8 days before free tocopherol analysis using an adapted ethanol/hexane extraction followed by RP-HPLC quantification. Potential to recover free tocopherol within the HAtoco matrix was validated by suspending known amounts of tocopherol to 500 μg/ml in HAtoco, extracted and percent recovery assessed against a calibration curve of known tocopherol standards in ethanol (Figure 2.18a and b). Percent recovery of five independently tested samples was found to be 84 ± 14% (Figure 2.18c). Fresh HAtoco was found to contain 17 μg/ml of free tocopherol and samples exposed to elevated temperature for up to 8 days did not show increases in free tocopherol content (Figure 2.18d). These results suggest the lysine linkage used to conjugate HA to tocopherol is not susceptible to chemical degradation/hydrolysis under the conditions tested. However, measurable free tocopherol content is present within the freshly dissolved HAtoco sample suggesting sequestered tocopherol not removed by dialysis purification exists at levels equal to ~2.4% of measured tocopherol content within 33kDa HAtoco10 by ^{1}H NMR.

2.3.12 Hyaluronidase Degradation of HAtoco

Enzymatic degradation of HAtoco by its natural endogenous enzyme hyaluronidase was analyzed by assessing size alterations with digestion time (up to 8 days) at elevated temperature (37°C). Size was monitored by agarose electrophoresis with visualization by Stains-all (Figure 2.19). Unmodified 200kDa HA control was observed to degrade to a significantly lower molecular within 24 h when exposed to 50 μg/ml of HAdase with no visible change in retention or band intensity without enzyme. In contrast, HAtoco was found to enzymatically degrade at a slower rate

with observable changes in size occurring between 2 and 8 days. HAtoco did not exhibit this extent of degradation without enzyme present at elevated temperature. No development of low molecular weight bands were seen upon apparent enzymatic degradation of HAtoco over 8 days suggesting development of molecular weights <33kDa which were not observable in previous agarose gels (Figure 2.12). In addition, with the extension of electrophoresis and higher polymer loading, 33kDa HAtoco10 separated into three distinct sub populations, one >33kDa, another >200kDa and a large effective size species >2000 kDa. This pattern mirrors in distribution the three particle sub populations observed in the combined number and intensity multimodal distributions measured by DLS (Figure 2.13c).

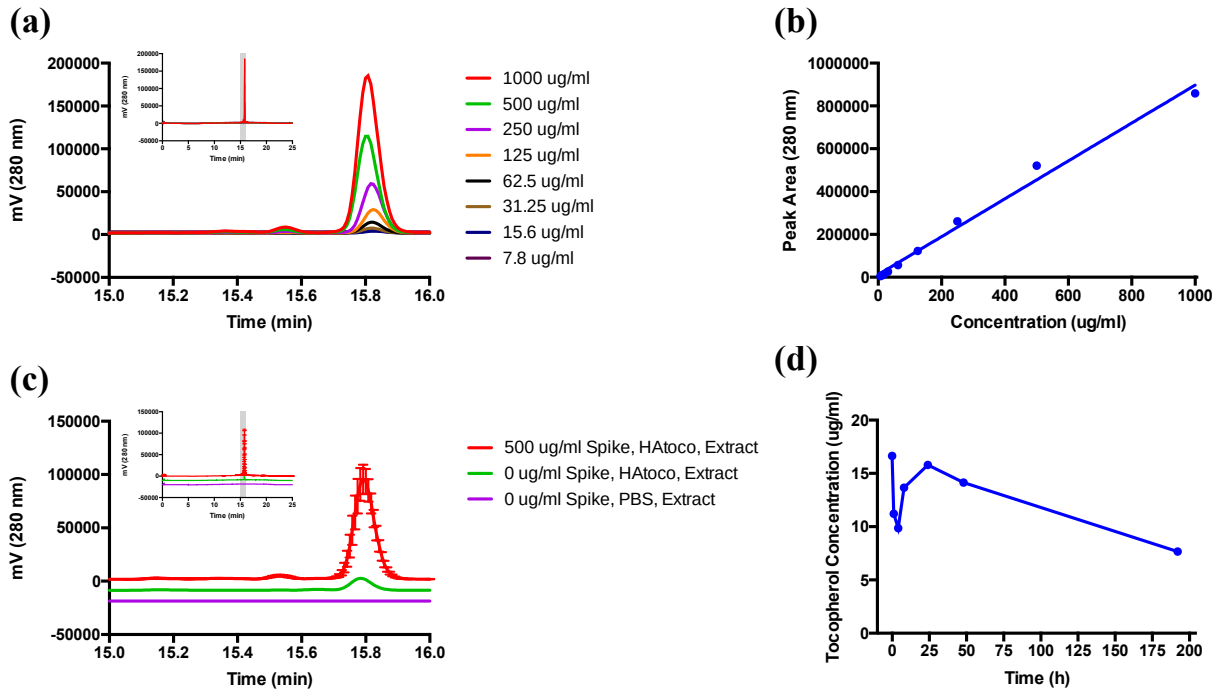

Figure 2.18: RP-HPLC analysis of free tocopherol following EtOH/Hexane extraction of thermally stressed 33kDa HAtoco10. (a) RP-HPLC chromatogram of tocopherol standards in absolute ethanol (1000 - 7.8 μg/ml) monitored by UV-absorption at 280 nm. (b) Peak area of tocopherol standards versus concentration with linear regression. (c) RP-HPLC chromatogram of 500 μg/ml tocopherol spiked 33kDa HAtoco10, 1% (w/v), (*N*=5) with error bars equal to ± SD, unspiked 33kDa HAtoco10, 1% (w/v) and unspiked PBS. (d) Measured free tocopherol within samples of 33kDa HAtoco10, 1% (w/v) in PBS, pH 6 following storage at 37°C for 0h, 1h, 4h, 8h, 24h, 48h and 8 days (*N* = 1).

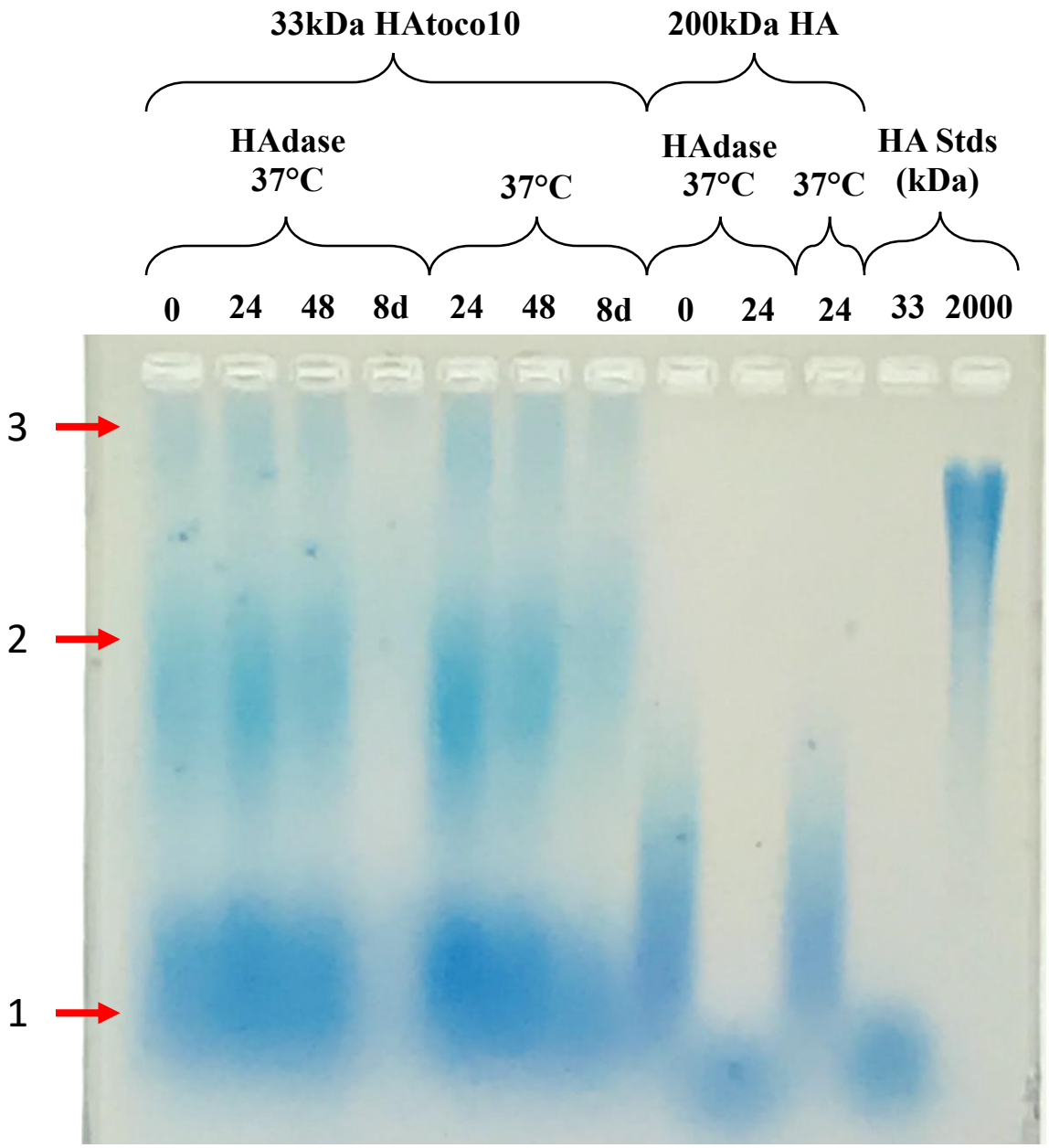

Figure 2.19: Agarose electrophoresis analysis of 33kDa HAtoco10 and 200kDa HA with or without 50 ug/ml hyaluronidase (HAdase) for 0h, 24h, 48h and 8 days at 37°C. (Far right) HA molecular weight standards (33, 2000 kDa). All samples visualized with Stains-all. Red arrows highlight three sub populations of HAtoco (1 = >33kDa, 2 = >200 kDa and 3 = >2000 kDa).

2.4 Discussion

Novel drug delivery platforms which effectively bind therapeutics with a range of physicochemical properties in addition to controlling the release upon administration are in development and of high interest. The flexibility of chemical and physical attributes of natural polysaccharides like hyaluronic acid make these molecules ideal candidates for novel, targeted-delivery and tailorable drug carriers. A hyaluronic acid conjugate, hydrophobically modified with α-tocopherol (HAtoco), was recently shown by our lab to effectively associate with a small molecule immunological agonist in a depot-like formation and sustain its immunotherapeutic effect locally upon subcutaneous administration.[29] In this study, the development of the HAtoco platform is continued by further characterization of the physical and chemical properties and the capacity to deliver protein therapeutics in a controlled manner.

First, effects of altering the hyaluronic acid backbone molecular weight were explored by synthesizing HAtoco conjugates of 6.7, 33, 100 and 250kDa with a constant tocopherol substitution of 10 mol%. Similarly, the effects of altering the degree of tocopherol substitution were explored by synthesizing conjugates of 5, 10, 15, 20 and 25 mol% with a constant molecular weight of 33kDa. There are challenges associated with quantitative ^{1}H NMR analysis of chemical substitutions onto high molecular weight. For example, HA, including poor chemical shift dispersion leads to significant spectral overlap particularly within the backbone region 4.0ppm – 3.1ppm. Additionally, as a result of erent high viscosity and associated concentrations required for adequate signal intensity, increasing polymer molecular weight leads to longer correlation (tumbling) times which gives rise to peak broadening and reduced spectral resolution.[36] These are issues routinely associated with spectroscopy of high molecular weight polymers due to the back bone flexibility and dynamic motion. This can be partially overcome by conducting NMR at

elevated temperatures, however, HA is subject to rapid thermal degradation. Thus, this was not a viable option. Assuming complete removal of unreacted tocopherol within the dialysis purified conjugate, the degree of tocopherol substitution was assessed by ^{1}H NMR using the peak area ratio of the commonly referenced[16] -CH_3 protons of the HA *N*-acetyl group and the -CH_3 protons of the tocopherol phytyl side chain. Clear broadening and weakening of the NMR spectrum was observed for both increases in tocopherol content and polymer molecular weight. This is likely due to the observed increases in solution viscosity upon tocopherol conjugation and incomplete dissolution. Reaction efficiencies increased from 62% to 85% with increasing tocopherol substitution and between 70% to-90% for increasing molecular weight polymer. Calculated substitutions at higher substitution degrees and molecular weights at which substantial peak broadening occurs likely suffer from low precision due to poor peak resolution. Overall, tocopherol substitutions above 10mol% and molecular weights above 33kDa were found to exhibit poor to incomplete dissolution, limiting accurate ^{1}H NMR analysis. .

Analysis of the binding capacity of HAtoco to protein therapeutics was assessed using the model protein BSA and binding isotherms created by monitoring the moment of the intrinsic tryptophan fluorescence. For a more representative comparison of HAtoco variants, disaccharide molar concentrations adjusted for average molecular weight of the disaccharide post-tocopherol substitution were plotted against fluorescent moment. No significant difference was observed in the binding capacity of the HAtoco variants to BSA, likely due to its known hydrophobicity.[37] This hydrophobicity is beneficial when BSA is used as a blocking reagent within ELISA protocols or other assays requiring minimal non-specific binding.[38] Unmodified HA did not produce any alteration of the BSA spectral moment, suggesting binding is specific to tocopherol moieties. Complete dissolution of 33kDa HAtoco10 at high concentrations coupled with its higher molecular

weight and thus potential to form a particle large enough (>100 nm)[39, 40] to sustain delivery from an injection site without immediate clearance made it the best candidate for development moving forward.

The *in vitro* release of three model proteins (BSA, lysozyme and RNase) were assessed when mixed with the lead HAtoco candidate, 33kDa HAtoco10, compared to unmodified 33kDa HA. HAtoco was found to release protein at a 2-fold higher release half-life when fit to a one-phase decay regression compared to HA for all model proteins tested. Large variability in the release half-life between model proteins in both formulations was apparent with BSA being much greater than lysozyme followed by RNase (BSA >> Lysozyme > RNase). A possible reason for this clear discrepancy is again likely due to the overall heightened surface hydrophobicity of BSA followed by lysozyme than the more polar RNase.[41, 42]

Another possible difference in release between lysozyme and RNase, although small based on the 95% confidence intervals of the regression fit, could be explained by differences in their isoelectric points. Both proteins have a similar molecular weight, RNase at 13.7 kDa and lysozyme at 14.3 kDa, but lysozyme is significantly more basic with a pI of 11.35[43] compared to a pI of 9.6[44] for RNase. Release assays were examined in PBS at pH 7.4 with samples injected into concentrated (1% (w/v)) high molecular weight hyaluronan to simulate conditions found in the ECM of subcutaneous tissue. Neutral to slightly acidic conditions, due to the contributions of hyaluronic acid, would induce a net positive overall charge for both proteins with lysozyme exhibiting a higher charge magnitude. Thus, differences in release could be due to the interaction of the more positively charged lysozyme dispersed into a hydrogel of anionic polymer compared to the slightly more neutral RNase. The extension of BSA release through an electrostatic interaction as opposed

to a hydrophobic one is less likely as BSA has an acidic pI (4.7)[45] and would exhibit a net negative charge in the environment examined.

Increases in the release of BSA with unmodified HA alone as well as the wide-error in release profiles for both HA and HAtoco samples could be a result of non-specific hydrophobic binding to surfaces within the release system such as the dialysis bag or plastic container, leading to skewed and variable measurements of released BSA concentration. In all release systems tested, except for BSA mixed with HAtoco, release plateaued at ~80% of the total protein initially loaded. Possibly explanations for this observation include again poor recovery due to non-specific binding, but also could be a result of protein degradation during the time-course of the assay. These results suggest HAtoco can effectively bind and release a range of protein therapeutics in a sustained manner following simulated injections.

The absolute viscosity and turbidity of 33kDa HAtoco10 were found to be significantly higher than the 33 kDa base polymer when measured using a cone plate rheometer and light scattering turbidimeter. Enhanced intramolecular and intermolecular chain interactions through the hydrophobic effect are likely responsible for increases in both viscosity and particle assembly.[15]

Agarose gel electrophoresis was found to be the most robust means of assessing the effective size of the hydrophobically modified HAtoco conjugate due to HPLC column inlet limitations that precluded GPC. Upon increased loading of HAtoco, agarose gels were able to resolve three distinct yet polydisperse populations within the purified conjugates. One lower molecular weight band associated with unreacted 33kDa HA and two higher molecular weight bands above 200 and 2000 kDa were observed. Development of multiple distinct sub populations of modified hyaluronan was an unexpected result. One theory explaining how this could have

developed is that during the reaction of hyaluronan and tocopherol, modified polymers began assembling into subvisible particles shielding themselves from further tocopherol conjugation except for surface exposed polymers, which continued to react. Upon particle relaxation under the initial ethanolic dialysis step and reformation upon exposure to fully aqueous systems, distinct populations of varying tocopherol substitutions were made, populations not distinguishable by ^{1}H NMR substitution analysis. To reduce system complexity in future reactions, extended reactions times coupled with an increased dialysis cut-off (100 kDa) need to be employed.

Particle sizing experiments using DLS were in good agreement with the results from the agarose gel experiments in that three distinct populations of about 10, 70 and 200 nm diameter particles were resolved in samples of HAtoco dissolved at 10 mg/ml. The highest number of particles (~10 nm) corresponding to the expected size range of unreacted 33kDa HA.[46] High molecular weight hyaluronic acid in the range of the HAtoco bands observed by agarose electrophoresis, >200 kDa and >2000 kDa, have been measured by DLS to have radii of hydration of ~35nm and ~125nm respectively.[47] These corresponding sizes are in good agreement to those measured by DLS for HAtoco.

HAtoco particle size for all sub populations were observed to decrease with additional HAtoco in solution. In the most dilute solutions tested (1.25 and 0.625 mg/ml), the two largest sub populations merged into one. The effects of multiple scattering in such an uncorrected system can explain the trend toward smaller particle size with increasing turbidity of the sample.[48] The fusion of populations however, cannot be explained by multiple scattering effects, but may be a result of concentration dependent equilibrium shift in which differentially substituted sub populations are driven to form new particles due to the low concentrations of HAtoco.

MFI analysis of particles nearing the visible range showed HAtoco increased the concentration of particles an order of magnitude for all sizes examined (up to 100 μm). The overall decreasing concentration of particles with increasing particle size was consistent between HAtoco and unmodified HA. These results suggest that if used in the future for clinical applications, HAtoco may need to be properly filtered to eliminate larger size particles which may partially occlude fine injection needles (27-30 gauge).

The *in vivo* release of fluorescently labelled HAtoco showed a clear depot development mirroring that seen in previously published studies where HAtoco was reported to manifest a local depot formation in the delivery of an immunological agonist.[29] HAtoco-Cy7 conjugates persisted at the subcutaneous injection site for over 60 days, while HA-Cy7 lasted for almost 30. The persistence of unmodified HA was longer than previously published findings of fluorescently labelled HA subcutaneously injected (<18 days),[49] leading to the possibility that the degree of substitution of the unmodified HA was such that a self-assembling particle was made prolonging its release. Increasing fluorescence intensity seen in both systems upon injection suggest some form of self-quenching, perhaps due to self-assembled particles, was initially occurring, but upon relaxation and release of the polymer from the site of injection quench was decreased. These results suggest that if association with a small molecule or protein therapeutic is strong enough to withstand *in vivo* conditions, release from the injection site may be extended for over two months. The extended residence time of the HAtoco conjugate is in line with the duration of cosmetic hyaluronic acid based dermal fillers (4-12 months) and much longer than the 24 h turnover of unmodified HA.[50]

Colloidal stability analysis of HAtoco through static light scattering with ramping temperature ramps up to 90°C indicated that the HAtoco particle linearly decreases in size with

temperature suggesting collapsing of the hydrophobic core. The increase in hydrophobic interactions with temperature is well documented[51] and thus can explain the increase in strength of the hydrophobic core reducing the HAtoco particle size. Visual inspection of HAtoco after cooling indicated no apparent degradation of the colloid had occurred. Similarly, the covalent ester glycine linkage between HA and tocopherol was assessed at elevated temperatures (37°C) using an organic solvent extraction method coupled with RP-HPLC. No observable increase in free tocopherol content within the HAtoco system was observed over 8 days of incubation indicating limited to no hydrolysis of the ester linkage. Lastly, the stability of HAtoco was analyzed in the presence of the endogenous enzyme hyaluronidase. HAtoco was found to degrade to molecular weights unobservable on a 1% agarose gel within 8 days at 37°C compared to less than 24 h for unmodified HA. The decrease in hyaluronidase activity may be due to poor enzyme accessibility brought on by HAtoco particle formation or substitution of tocopherol to the HA backbone.

2.5 Conclusions

Novel formulation platforms capable of modifying the release kinetics of a multitude of drug classes will continue to be a focus of pharmaceutical technical development. The recent description of an HA-tocopherol conjugate has shown its potential as a novel amphiphilic carrier capable of sustaining release of small molecule therapeutics following subcutaneous injection. In this study, the potential of HAtoco as a drug delivery platform was expanded to include the sustained delivery of protein therapeutics. In addition, the backbone molecular weight and tocopherol substitution were optimized, *in vivo* release kinetics determined with extensive chemical and physical characterization. Overall, these results show HAtoco can extend the release

of several model proteins particularly those of hydrophobic surface character such as BSA and is thermally and chemically stable with extended *in vivo* residence time.

2.6 References

1. Martin, C.; Aibani, N.; Callan, J. F.; Callan, B., Recent advances in amphiphilic polymers for simultaneous delivery of hydrophobic and hydrophilic drugs. *Therapeutic Delivery* **2015,** *7* (1), 15-31.
2. Cawley, J.; Stern, M. Water-soluble tocopherol derivatives. US2680749A, 1951.
3. Strickley, R. G.; Oliyai, R., Solubilizing Vehicles for Oral Formulation Development. In *Solvent Systems and Their Selection in Pharmaceutics and Biopharmaceutics*, Augustijns, P.; Brewster, M. E., Eds. Springer New York: New York, NY, 2007; pp 257-308.
4. Fan, Z.; Chen, C.; Pang, X.; Yu, Z.; Qi, Y.; Chen, X.; Liang, H.; Fang, X.; Sha, X., Adding Vitamin E-TPGS to the Formulation of Genexol-PM: Specially Mixed Micelles Improve Drug-Loading Ability and Cytotoxicity against Multidrug-Resistant Tumors Significantly. **2015,** *10* (4), e0120129.
5. Lu, J.; Huang, Y.; Zhao, W.; Chen, Y.; Li, J.; Gao, X.; Venkataramanan, R.; Li, S., Design and Characterization of PEG-Derivatized Vitamin E as a Nanomicellar Formulation for Delivery of Paclitaxel. **2013,** *10* (8), 2880-2890.
6. Guo, Y.; Luo, J.; Tan, S.; Otieno, B. O.; Zhang, Z., The applications of Vitamin E TPGS in drug delivery. **2013,** *49* (2), 175-186.

7. Mu, L.; Feng, S. S., A novel controlled release formulation for the anticancer drug paclitaxel (Taxol®): PLGA nanoparticles containing vitamin E TPGS. *Journal of Controlled Release* **2003,** *86* (1), 33-48.

8. Meng, X.; Liu, J.; Yu, X.; Li, J.; Lu, X.; Shen, T., Pluronic F127 and D-alpha-Tocopheryl Polyethylene Glycol Succinate (TPGS) Mixed Micelles for Targeting Drug Delivery across The Blood Brain Barrier. *Sci Rep* **2017,** *7* (1), 2964.

9. Yu, J.; Zhou, Y.; Chen, W.; Ren, J.; Zhang, L.; Lu, L.; Luo, G.; Huang, H., Preparation, Characterization and Evaluation of α-Tocopherol Succinate-Modified Dextran Micelles as Potential Drug Carriers. **2015,** *8* (10), 6685-6696.

10. Yadav, P.; Yadav, H.; Shah, V. G.; Shah, G.; Dhaka, G., Biomedical Biopolymers, their Origin and Evolution in Biomedical Sciences: A Systematic Review. *J Clin Diagn Res* **2015,** *9* (9), ZE21-ZE25.

11. Van Tomme, S. R.; Hennink, W. E., Biodegradable dextran hydrogels for protein delivery applications. *Expert Review of Medical Devices* **2007,** *4* (2), 147-164.

12. Bhattarai, N.; Gunn, J.; Zhang, M., Chitosan-based hydrogels for controlled, localized drug delivery. *Advanced Drug Delivery Reviews* **2010,** *62* (1), 83-99.

13. Burdick, J. A.; Prestwich, G. D., Hyaluronic Acid Hydrogels for Biomedical Applications. *Advanced Materials* **2011,** *23* (12), H41-H56.

14. Coviello, T.; Matricardi, P.; Marianecci, C.; Alhaique, F., Polysaccharide hydrogels for modified release formulations. *Journal of Controlled Release* **2007,** *119* (1), 5-24.

15. Tiwari, S.; Bahadur, P., Modified hyaluronic acid based materials for biomedical applications. *International Journal of Biological Macromolecules* **2019,** *121*, 556-571.

16. Schanté, C. E.; Zuber, G.; Herlin, C.; Vandamme, T. F., Chemical modifications of hyaluronic acid for the synthesis of derivatives for a broad range of biomedical applications. **2011,** *85* (3), 469-489.

17. Misra, S.; Heldin, P.; Hascall, V. C.; Karamanos, N. K.; Skandalis, S. S.; Markwald, R. R.; Ghatak, S., Hyaluronan-CD44 interactions as potential targets for cancer therapy. **2011,** *278* (9), 1429-1443.

18. Bagby, T. R.; Cai, S.; Duan, S.; Thati, S.; Aires, D. J.; Forrest, L., Impact of Molecular Weight on Lymphatic Drainage of a Biopolymer-Based Imaging Agent. **2012,** *4* (4), 276-295.

19. Fraser, J. R. E.; Laurent, T. C.; Laurent, U. B. G., Hyaluronan: its nature, distribution, functions and turnover. *Journal of Internal Medicine* **1997,** *242* (1), 27-33.

20. Laurent, U. B. G.; Reed, R. K., Turnover of hyaluronan in the tissues. *Advanced Drug Delivery Reviews* **1991,** *7* (2), 237-256.

21. Lepperdinger, G.; Strobl, B.; Kreil, G., HYAL2, a Human Gene Expressed in Many Cells, Encodes a Lysosomal Hyaluronidase with a Novel Type of Specificity. **1998,** *273* (35), 22466-22470.

22. Payne, W. M.; Svechkarev, D.; Kyrychenko, A.; Mohs, A. M., The role of hydrophobic modification on hyaluronic acid dynamics and self-assembly. *Carbohydrate Polymers* **2018,** *182*, 132-141.

23. Choi, K. Y.; Chung, H.; Min, K. H.; Yoon, H. Y.; Kim, K.; Park, J. H.; Kwon, I. C.; Jeong, S. Y., Self-assembled hyaluronic acid nanoparticles for active tumor targeting. *Biomaterials* **2010,** *31* (1), 106-114.

24. Hill, T. K.; Abdulahad, A.; Kelkar, S. S.; Marini, F. C.; Long, T. E.; Provenzale, J. M.; Mohs, A. M., Indocyanine Green-Loaded Nanoparticles for Image-Guided Tumor Surgery. *Bioconjugate Chemistry* **2015,** *26* (2), 294-303.

25. Wang, X.; Gu, X.; Wang, H.; Sun, Y.; Wu, H.; Mao, S., Synthesis, characterization and liver targeting evaluation of self-assembled hyaluronic acid nanoparticles functionalized with glycyrrhetinic acid. **2017,** *96*, 255-262.

26. Tian, G.; Sun, X.; Bai, J.; Dong, J.; Zhang, B.; Gao, Z.; Wu, J., Doxorubicinloaded dualfunctional hyaluronic acid nanoparticles: Preparation, characterization and antitumor efficacy in vitro and in vivo. (1791-3004 (Electronic)).

27. Quinones, J. P.; Jokinen, J.; Keinänen, S.; Covas, C. P.; Brüggemann, O.; Ossipov, D., Self-assembled hyaluronic acid-testosterone nanocarriers for delivery of anticancer drugs. *European Polymer Journal* **2018,** *99*, 384-393.

28. Mayol, L.; Biondi, M.; Russo, L.; Malle, B. M.; Schwach-Abdellaoui, K.; Borzacchiello, A., Amphiphilic hyaluronic acid derivatives toward the design of micelles for the sustained delivery of hydrophobic drugs. **2014,** *102*, 110-116.

29. Lu, R.; Groer, C.; Kleindl, P. A.; Moulder, K. R.; Huang, A.; Hunt, J. R.; Cai, S.; Aires, D. J.; Berkland, C.; Forrest, M. L., Formulation and preclinical evaluation of a toll-like receptor 7/8 agonist as an anti-tumoral immunomodulator. *Journal of Controlled Release* **2019,** *306*, 165-176.

30. Wei, Y.; Larson, N. R.; Angalakurthi, S. K.; Russell Middaugh, C., Improved Fluorescence Methods for High-Throughput Protein Formulation Screening. *SLAS TECHNOLOGY: Translating Life Sciences Innovation* **2018**, 247263031878062.

31. Cowman, M. K.; Chen, C. C.; Pandya, M.; Yuan, H.; Ramkishun, D.; Lobello, J.; Bhilocha, S.; Russell-Puleri, S.; Skendaj, E.; Mijovic, J.; Jing, W., Improved agarose gel electrophoresis method and molecular mass calculation for high molecular mass hyaluronan. **2011,** *417* (1), 50-56.

32. Falcone, S. J.; Palmeri, D. M.; Berg, R. A., Rheological and cohesive properties of hyaluronic acid. **2006,** *76A* (4), 721-728.

33. Cowman, M. K.; Matsuoka, S., Experimental approaches to hyaluronan structure. **2005,** *340* (5), 791-809.

34. Hoehler, D.; Frohlich, A. A.; Marquardt, R. R.; Stelsovsky, H., Extraction of α-Tocopherol from Serum Prior to Reversed-Phase Liquid Chromatography. *Journal of Agricultural and Food Chemistry* **1998,** *46* (3), 973-978.

35. Bagby, T. R. Development and Optimization of Polymeric Carriers for Lymphatic Imaging and Drug Delivery. University of Kansas, 2011.

36. Magness, K. Biophysical and bioanalytical studies of hyaluronan and lipids. University of Louisville, 2012.

37. Sneharani, A. H., Curcumin as a tool to assess the surface hydrophobicity of proteins. *Spectroscopy Letters* **2016,** *49* (9), 568-572.

38. Jeyachandran, Y. L.; Mielczarski, J. A.; Mielczarski, E.; Rai, B., Efficiency of blocking of non-specific interaction of different proteins by BSA adsorbed on hydrophobic and hydrophilic surfaces. *Journal of Colloid and Interface Science* **2010,** *341* (1), 136-142.

39. Oussoren, C., Liposomes to target the lymphatics by subcutaneous administration. **2001,** *50* (1-2), 143-156.

40. Rao, D. A.; Forrest, M. L.; Alani, A. W. G.; Kwon, G. S.; Robinson, J. R., Biodegradable PLGA based nanoparticles for sustained regional lymphatic drug delivery. **2010,** *99* (4), 2018-2031.

41. Hanke, A. T.; Klijn, M. E.; Verhaert, P. D. E. M.; Van Der Wielen, L. A. M.; Ottens, M.; Eppink, M. H. M.; Van De Sandt, E. J. A. X., Prediction of protein retention times in hydrophobic interaction chromatography by robust statistical characterization of their atomic-level surface properties. **2015**, n/a-n/a.

42. Nicolau Jr, D. V.; Paszek, E.; Fulga, F.; Nicolau, D. V., Mapping Hydrophobicity on the Protein Molecular Surface at Atom-Level Resolution. *PLoS ONE* **2014,** *9* (12), e114042.

43. Wetter, L. R.; Deutsch, H. F., IMMUNOLOGICAL STUDIES ON EGG WHITE PROTEINS: IV. IMMUNOCHEMICAL AND PHYSICAL STUDIES OF LYSOZYME. *Journal of Biological Chemistry* **1951,** *192* (1), 237-242.

44. Tanford, C.; Hauenstein, J. D., Hydrogen Ion Equilibria of Ribonuclease1. *Journal of the American Chemical Society* **1956,** *78* (20), 5287-5291.

45. Righetti Pg Fau - Caravaggio, T.; Caravaggio, T., Isoelectric points and molecular weights of proteins.

46. Kuehl, C.; Zhang, T.; Kaminskas, L. M.; Porter, C. J. H.; Davies, N. M.; Forrest, L.; Berkland, C., Hyaluronic Acid Molecular Weight Determines Lung Clearance and Biodistribution after Instillation. **2016,** *13* (6), 1904-1914.

47. Takahashi, R.; Kubota, K.; Kawada, M.; Okamoto, A., Effect of molecular weight distribution on the solution properties of sodium hyaluronate in 0.2M NaCl solution. **1999,** *50* (1), 87-98.

48. Kaszuba, M.; Connah, M. T.; McNeil-Watson, F. K.; Nobbmann, U., Resolving Concentrated Particle Size Mixtures Using Dynamic Light Scattering. **2007,** *24* (3), 159-162.

49. Cheng, L.; Ji, K.; Shih, T. Y.; Haddad, A.; Giatsidis, G.; Mooney, D. J.; Orgill, D. P.; Nabzdyk, C. S., Injectable Shape-Memorizing Three-Dimensional Hyaluronic Acid Cryogels for Skin Sculpting and Soft Tissue Reconstruction. (1937-335X (Electronic)).

50. Bogdan Allemann, I.; Baumann, L., Hyaluronic acid gel (Juvéderm) preparations in the treatment of facial wrinkles and folds. *Clin Interv Aging* **2008,** *3* (4), 629-634.

51. Chen, W.-Y.; Huang, H.-M.; Lin, C.-C.; Lin, F.-Y.; Chan, Y.-C., Effect of Temperature on Hydrophobic Interaction between Proteins and Hydrophobic Adsorbents: Studies by Isothermal Titration Calorimetry and the van't Hoff Equation. *Langmuir* **2003,** *19* (22), 9395-9403.

Chapter III: Development and biophysical characterization of an extended-delivery platform for Coversin, a C5-specific complement inhibitor

3.1 Introduction

The complement system is a major component of the innate immune system that assists in clearing pathogens and damaged cells. The complement proteins are a family of small inactive precursor proteins that circulate in the blood. Upon activation, the complement proteins undergo a cascade reaction that rapidly amplifies the host immune response. Complement-assisted pathogen death can occur through three known pathways: the classical, alternative and lectin pathways.[1] Each pathway is triggered by recognizing a specific pattern foreign to circulation. In the classical pathway, complement component C1 recognizes antibody, IgG or IgM, bound to a microbial surface leading to a cascade of protease activity and binding. This ultimately leads to the formation of the membrane attack complex (MAC). Once the MAC is formed, it creates a functional pore within the membrane of the target bacterium. The cell is then lysed and killed.[2]

Like many other systems of the innate and adaptive immune system, the complement system relies on complex feedback mechanisms. These feedback mechanisms are known as complement regulators which prevent inadvertent activation. The delicate balance between the identification of foreign substances versus self can be altered through a number of mechanisms. These mechanisms include age-related degeneration, genetic mutations and polymorphisms leading to a variety of disease manifestations.[3]

This type of dysregulation is central to diseases such as atypical hemolytic uremic syndrome (aHUS) and paroxysmal nocturnal hemoglobinuria (PNH); rare genetic mutations leading to complement activation and destruction of blood cells and subsequent damage to vital organs due to blood clot formation.[4, 5] Symptoms of aHUS include acute kidney injury, proteinuria and hematuria. Symptoms of PNH include fatigue, hemolytic anemia and bone marrow hypocellularity. Due to the high mortality rate in both diseases,[6, 7] aggressive therapies were

initially employed including kidney transplantation and plasma replacement therapy for aHUS[5]and allogeneic bone marrow transplantations for PNH[4]. Both treatments resulted in minimal improvement in extension of life despite improved hematological outcomes. Eculizumab (Soliris®, Alexion Pharmaceuticals) is a human monoclonal antibody which inhibits MAC formation by binding C5 of the complement cascade.[8] Eculizumab was approved by the FDA in 2007 for the treatment of patients with PNH[9] and in 2011 for patients with aHUS[10] to reduce complement mediated hemolysis. Treatment with Eculizumab has been shown to drastically reduce symptoms of both diseases while improving survival levels and is now considered a front-line treatment. Recently, the FDA has approved Ravulizumab, Alexion's BLA as a long-acting C5 inhibitor, for the treatment of PNH, with a target approval date in late 2019 for treatment of aHUS.[11, 12] Ravulizumab has been shown to extend the required time between maintenance infusions from 2 weeks to 8 weeks with no inferiority in efficacy when compared to Eculizumab.[13]

Although the emergence of Eculizumab have been a drastic improvement in the treatment of PNH and aHUS, 25-35%[14] of patients suffer from inadequate response to the drug. The inadequate response may be due to phagocytic clearance of opsonized C3-bound erythrocytes.[15, 16] Additionally, the annual treatment cost of Eculizumab is one of the most expensive pharmaceutical therapies to date, projected at $500,000 annually.[17] Given the large patient group who are non-responsive to current drugs and the high cost of treatment, there are strong incentives to develop improved treatments. [18]

Coversin, (*Ornithodoros moubata* complement inhibitor [OmCI], Nomacopan, Akari Therapeutics) is a second-generation C5 complement inhibitor. Coversin was originally discovered within the saliva of the *O. moubata* soft tick, suppressing the host immune response during feeding.[19] Like Eculizumab, Coversin also inhibits formation of the terminal MAC complex

through binding of the C5-component. However, C5 binding site differences between the antibody and Coversin[20] could prove critical in patients with poor response to Eculizumab treatment.[21] Coversin is a lipocalin family protein comprised of 150 amino acids with a molecular weight of 16.8kDa.It has been structurally described as a compact protein composed of a central eight-stranded antiparallel β-barrel and a carboxy-terminal α-helix, similar to human plasma proteins of the same lipocalin family.[22, 23]

In phase II human trials for patients with PNH, Coversin demonstrated efficacy in all patients[24, 25]; however, lapses in sufficient complement inhibition were seen within 24 h following once-daily subcutaneous administrations. In an effort to extend the pharmacokinetics and minimize dosing frequency, Kuhn et. al examined a PASylated version of Coversin in which the N-terminus is recombinantly modified with the addition of a 600 residue peptide composed of proline, alanine and serine (PAS).[14] Similar to the effects of protein PEGylation, PASylation has been shown to dramatically increase the hydrodynamic volume of a protein. PASylation thus reduces the renal clearance of the molecule due to the pore size limit of the glomerular membrane.[26] The terminal plasma half-life of PASylated Coversin following subcutaneous injection was found to be 10.4 h compared to 0.2 h with i.v. infusion of unmodified Coversin. No reduction in complement inhibitory capacity was observed in C5 binding, *in vitro* MAC inhibition or model-PNH *in vitro* hemolysis assays with PASylated Coversin.

The pharmacokinetic improvements presented by PASylated Coversin are substantial. A complete phase I clinical trial is necessary to accurately examine the added benefits or potential harms of this alteration in humans, currently projected as a once weekly s.c. administration.[27] Added complexity to manufacturing and technical development due to the alteration of the drug

must to be addressed to reduce the extremely high cost profile, burdening approved anti-complement treatments.

Prolonging the pharmacokinetic profile of therapeutic proteins following parenteral injections has been a major topic of interest in the pharmaceutical research community, particularly since the approval of recombinant insulin in the early 1980s. Interest has grown rapidly as the prevalence of biological drugs continues to increase.[28] In an effort to reduce healthcare costs and improve patient compliance, at home, self-administration subcutaneous injections has become the new target for proteins therapeutics requiring parenteral delivery.[29] Multiple drug delivery strategies have been employed to create a platform in which a wide-range of biologics could be administered in a rate-controlled manner including PEGylation, polymeric microsphere encapsulation and liposomal formulations.[30] One of the most promising strategies to date is the use of hydrogels to effectively control delivery of protein therapeutics without complex chemical or fabrication strategies which may negatively affect the desired biological effect or stability of the therapeutic.[31] A recently reported[32] nanogel using hyaluronic acid, an endogenous polysaccharide of the extra-cellular matrix, modified with vitamin E, has been shown to associate and extend delivery of intratumorally delivered TLR agonists through a depot-like formation. The following is an investigation the potential of this hyaluronic acid-vitamin E (hyaluronic acid-tocopherol, HAtoco) platform to sustain delivery of unmodified Coversin following subcutaneous injection and its effects on protein structure and biological function.

3.2 Materials and Methods

3.2.1 Materials

Coversin was supplied by Akari Therapeutics (London, UK) lyophilized in phosphate buffered saline. Sodium hyaluronate (HA) was obtained from Lifecore Biomedical (Chaska, MN). Alexa Fluor™ 647 NHS Ester, Rhodamine NHS Ester and SnakeSkin™ dialysis tubing were obtained from Thermo Fisher Scientific (Waltham, MA). Float-A-Lyzer G2 dialysis devices were purchased from Spectrum (Waltham, MA). PD-10 desalting columns with Sephadex G-25 resin were purchased from GE (Pittsburgh, PA). Complement System, Classical Pathway Wieslab ELISA kit COMPLCP310 was purchased from Euro Diagnostica (Malmö, Sweden). Chemical reagents including, (+)-α-tocopherol, 1-ethyl-3-(e-dimethylaminopropyl)carbodiimide hydrochloride (EDC-HCl), N,N'-dicyclohexylcarbodiimide (DCC), 4-dimethylaminopyridine (DMAP), N-(tert-butoxycarbonyl) glycine (Boc-Gly-OH), trifluoroacetic acid (TFA), tetrabutylammonium hydroxide (TBA-OH), and 1-hydroxybenzotriazole hydrate (HOBT-H_2O) were purchased from Sigma Aldrich (St. Louis, MO). Solvents for flash chromatography, HPLC grade solvents and centrifugal filters were purchased from Fisher Scientific (Hampton, NH).

3.2.2 Synthesis of hyaluronan-tocopherol conjugates

Hyaluronan-tocopherol conjugates were synthesized as previously discussed in Chapter II (Scheme 1). Briefly, (+)-α-Tocopherol (Vitamin E) was coupled to a Boc-protected glycine through DCC/DMAP mediated esterification in anhydrous CH_2Cl_2 overnight. The reaction mixture was then cooled to -20°C and filtered. The filtrate was purified by silica gel flash chromatography using a hexane-ethyl acetate gradient and dried *in vacuo*. The product oil was dissolved in CH_2Cl_2, deprotected using TFA and subsequently dried *in vacuo* to remove solvent

and TFA. The gray solid product was purified by silica gel flash chromatography using a hexane-ethyl acetate gradient and again dried to yield a white solid product **1**. Sodium hyaluronate (33 kDa) was fully dissolved to 20 mg/ml in deionized water, followed by addition of Dowex AG 50W-X8 resin (10-fold excess to HA by mass) and stirred overnight at 20°C. The resin was removed by filtration and filtrate was titrated with TBA-OH to pH 8-9, yielding a slightly pink solution. The HA-TBA solution was subsequently frozen and lyophilized to yield a pink-yellow cake **2**. HA-TBA was then dissolved in DMF (20 mg/ml) and subsequently added to a mixture of **1** (10 mg/ml), EDC-HCl (10 mg/ml) and HOBT-H_2O (20 mg/ml) in DMF. The reaction mixture was stirred at 25°C overnight. The crude product was dialyzed (10 kDa MWCO) against 50% ethanol for 12 h, 150 mM sodium chloride for 12 h and water with three changes over 72 h. Dialyzed HAtoco product was lyophilized to yield a white fibrous cake **3**.

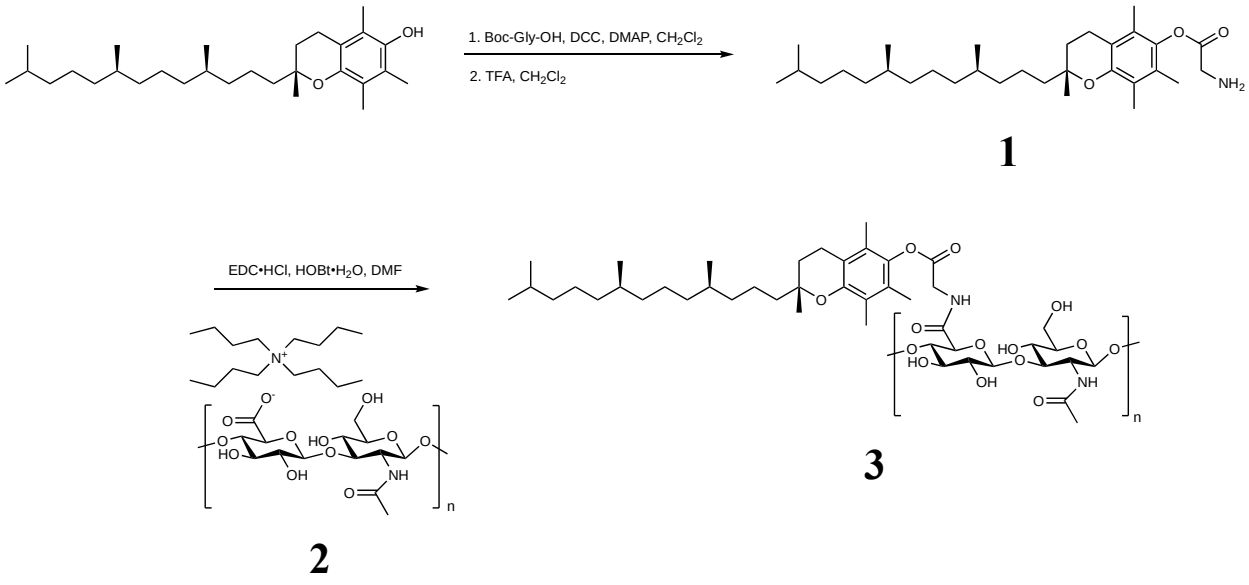

1

2

3

Scheme 1: Synthesis of hyaluronan-Vitamin E (HAtoco).

3.2.3 Subcutaneous-mimicking *in vitro* release

Lyophilized Coversin was dissolved in deionized H_2O to yield 10 mg/ml in PBS and subsequently added to an equal mass of lyophilized HAtoco, 33 kDa HA or 200 kDa HA by pipette. The Coversin/HAtoco solution was mixed overnight at 20°C protected from light. Float-A-Lyzer dialysis cassettes (300 kDa MWCO) were filled with 0.8 ml of 1% (w/v) 622 kDa sodium hyaluronate in PBS, pH 7.4 with 0.05% (w/v) NaN_3 as an anti-microbial agent. Coversin/HAtoco mixture (0.2 ml) was pipetted into the HMW HA solution within the dialysis cassette and dialyzed against 30 ml of PBS, pH 7.4, 0.05% (w/v) NaN_3 in a 50 ml conical centrifuge tube at 37°C while stirring. All release experiments were performed in triplicate. At predetermined intervals, the entire dialysate volume was replaced with fresh buffer and prior dialysate frozen at -80°C for future analysis. Percent Coversin released was determined by HPLC peak area against a standard curve. All chromatography was performed on a Shimadzu LC-2010C HT (Kyoto, Japan) with in-line UV detection (280 nm) using a Phenomenex Aeries 3.6 μm Widepore XB-C18 column (250 x 4.5 mm) at 50°C. Gradient mobile phases were A: 9:1, H_2O:Acetonitrile, 0.05% (v/v) TFA and B: 1:9, H_2O:Acetonitrile, 0.05% (v/v) TFA with an elution gradient of 20-100% B over 6 min at a flow rate of 1.0 ml/min. Formulas for determining percent drug released are as follows:

$$\%DR_t = \frac{Drug\ Concentration\ \left(\frac{mg}{ml}\right) * Dialysate\ Volume\ (ml)}{Drug\ Initially\ Loaded\ (mg)} * 100$$

$$\%CDR_t = \%DR_t + CDR_{t-1}$$

where $\%DR_t$ = percentage of drug released at time (t); $\%CDR_{t-1}$ = cumulative drug released at time point prior to (t); $\%CDR_t$ = cumulative drug released at time (t). Release profiles were fit using a one phase decay nonlinear regression in Prism 6 (Graphpad Software, San Diego, CA).

3.2.4 *In vivo* subcutaneous release

Alexa Fluor™ 647 NHS Ester (0.38 mg, 298 nmol) dissolved in 38 μl of anhydrous DMSO was added to Coversin (1 mg, 59.6 nmol) while stirring in 100 μl of 0.1 M $NaHCO_3$, pH 8.8. Mixing continued for 2 h at 20°C protected from light. The product mixture was first purified over a PD-10 desalting column containing Sephadex G-25 resin with PBS, pH 7.4, as the mobile phase. The first three, 1 mL fractions eluted from the GPC column were pooled together and placed in a 10 kDa MWCO dialysis cassette and dialyzed against PBS, pH 7.4, at 4°C with three bath changes. The final Coversin- Alexa Fluor™ 647 concentration was determined using the manufacturer's instructions as described previously in Chapter II with CF=0.03 and $A_{max}=A_{650}$. Coversin- Alexa Fluor™ 647 conjugate (CovAF647) was diluted with PBS, pH 7.4, to 0.25 mg/ml and used to dissolve HAtoco or 200 kDa HA to 10 mg/ml. Coversin samples without dye were used to dissolve HAtoco and 200 kDa HA at the same concentrations and then used to dilute the fluorescent samples 9-fold to reduce fluorescent intensity. All mixtures mixed overnight at 20°C, protected from light.

All animal studies were approved by the University of Kansas Institutional Animal Care and Use Committee. Female BALB/c mice (16 – 20 g) were purchased from Charles River. Hair in the hind limbs was removed prior to treatment and imaging to reduce autofluorescence using depilatory cream. Mice (3 per group) were anesthetized with isoflurane and injected subcutaneously with 10 μl of CovAF647/HAtoco, CovAF647/200kHA or CovAF647/PBS in the center of the hind footpad. Whole body fluorescent images were acquired at predetermined

timepoints using a CRi Maestro In Vivo Imaging System (Cambridge Research & Instrumentation, Inc., Woburn, MA) equipped with a 615-665 nm excitation bandpass filter and a 645 nm long pass emission filter. All images were acquired at a constant exposure of 1000 ms at 810 nm and equally scaled using the instrument software. Quantification of fluorescent intensity remaining at the injection site was performed by exporting images to ImageJ and adjusting threshold to a pixel intensity greater than 80 based on autofluorescent levels from naïve mice. Integrated density (mean intensity*area) of remaining fluorescent signal was measured from the area of the entire foot to the ankle.

3.2.5 Fluorescence polarization binding isotherm

Rhodamine NHS Ester (1.6 mg, 2.9 μmol) was dissolved in 0.16 ml of anhydrous DMSO and added to Coversin (5 mg, 2.9 μmol) while stirring in 0.5 ml of PBS, pH 7.4, for 2 h at 20°C protected from light. The product mixture was first purified by sequential dilution in PBS, pH 7.4, 0.05% (w/v) NaN_3, followed by concentration using a 3 kDa MWCO centrifugal filter, repeated three times. The concentrate was removed and purified further using a PD-10 desalting column containing Sephadex G-25 resin with PBS, pH 7.4, 0.05% (w/v) NaN_3 as the eluent. The first three 1 mL fractions eluted from the GPC column were pooled together and placed in a 3 kDa MWCO dialysis cassette and dialyzed overnight against PBS, pH 7.4, 0.05% (w/v) NaN_3 at 4°C. Conjugation was verified by HPLC-ESI-TOF acquired on a Waters Synapt G2 (Milford, MA USA) hybrid Quadrupole –Time of Flight mass spectrometer operated in MS mode and acquiring data with the time of flight analyzer. The instrument was operated in resolution mode, 18K resolution. The cone voltage was 45eV and Ar was admitted to the collision (trap) cell. Spectra were acquired over the range of 500-3000 u. Time to mass calibration was made with NaI cluster

ions acquired under the same conditions and lock mass corrected with an auxiliary sprayer presenting the doubly charged ion, 785.84265 m/2z, from Glu-fibrinogen peptide. Lock mass spectra were acquired every 15s. "Zero" charge spectra were generated from the electrospray generated charge states using the "transform routine" in Masslynx post acquisition tools. Spectra are centroided and adjacent ions are assigned as one charge state different and the rest of the charge state "train" are detected and assigned. For the final spectrum, regions of the continuum spectra are multiplied by charge state and shifted to the common mass by subtracting the appropriate number of protons (charge carriers). Samples were desalted on a C4 reverse phase column using a Waters nanoACQUITY UPLC. The column was 0.32mm x 50mm filled with Zora C4 5μM particles. Mobile phase A was 0.08% (v/v) formic acid and B was 1:1:1, methanol:acetonitrile:2-propanol. The desalting/ resolving gradient was 5 to 70% B in 20 min at 25μl/min.

Product purity was assessed by RP-HPLC on a Shimadzu LC-2010C HT (Kyoto, Japan) with in-line UV detection (280 nm) and fluorescence (552 Ex./575 Em.) using a Waters 2475 Multi λ Fluorescence Detector. Chromatography was performed on a Phenomenex Aeries 3.6 μm Widepore XB-C18 column (250 x 4.5 mm) at 50°C. Gradient mobile phases were A: 9:1, H_2O:Acetonitrile, 0.05% (v/v) TFA and B: 1:9, H_2O:Acetonitrile, 0.05% (v/v) TFA with an elution gradient of 5-100% B over 7 min at a flow rate of 1.0 ml/min.

Final Coversin-Rhodamine concentration was determined using the NHS-Rhodamine manufacturer's instructions with the following equation:

$$Protein\ concentration\ (M) = \frac{A_{280} - (A_{max} * CF)}{\varepsilon} * Dilution\ factor$$

$$CF = Correction\ factor = \frac{A_{280}}{A_{max}} = \frac{A_{280}}{A_{555}} = 0.34$$

$$\varepsilon = 22,835\ M^{-1}cm^{-1}$$

Coversin-Rhodamine purified of unreacted dye was serially diluted with PBS, pH 7.4, 0.05% (w/v) NaN_3 to concentrations between 5 – 0.005 mg/ml and used to dissolve HAtoco or 33 kDa HA to 10 mg/ml. All mixtures were allowed to mix overnight at 20°C, protected from light. Fluorescence polarization of all samples was measured in triplicate using a Biotek Synergy H4 Hybrid Reader (Winooski, VT) equipped with a 485/20 nm excitation filter, 620/40 emission filter, and a 510 nm cutoff dichroic mirror. All measurements were made in triplicate and data fitted using a sigmoidal, 4PL non-linear regression in Prism 6.

3.2.6 Intrinsic tryptophan fluorescence spectroscopy

Coversin steady-state intrinsic tryptophan fluorescence was acquired using a fluorescence plate reader manufactured by Fluorescence Innovations Inc. (Minneapolis, MN). Excitation wavelength was set at 295 nm coupled with a 310 nm long-pass dichroic mirror. Emission spectra was acquired from 300 – 400 nm with an integration time of 100 ms. Spectra was acquired from 10 to 90°C with a 2.5°C step and 30 s equilibration time. Coversin in PBS/NaN_3 at 0.25 mg/ml was used to dissolve lyophilized HAtoco or 33 kDa HA to 10 mg/ml and allowed to mix overnight at 20°C, protected from light. All samples were analyzed on a 384-well plate (n=6) with silicon oil added onto samples to avoid evaporation during heating. Spectra contributions from HAtoco, HA or buffer were subtracted from raw data and processed using Python to derive the spectral moment as a function of temperature as described by Wei et al.[33] to calculate Coversin melting temperature (T_m). Melting curves were fitted using an asymmetric 5PL, non-linear regression with Prism 6.

3.2.7 Differential scanning calorimetry

Differential scanning calorimetry of Coversin (0.25 mg/ml) formulated in PBS/NaN_3 alone or in HAtoco (10 mg/ml) was acquired in duplicate using a Malvern MicroCal VP-Capillary DSC (Malvern, UK). All samples were held in an autosampler tray at 4°C prior to analysis. Temperature was ramped from 20°C to 90°C with a scan rate of 1°C/min. Apparent transition temperature was derived using a non-two state equilibrium model with Origin 7.0 (OriginLab, Northhampton, MA).

3.2.8 Fourier-transform infrared spectroscopy (FTIR)

FTIR spectra were collected using a Bruker Tensor 27 FTIR spectrometer (Billerica, MA) equipped with a liquid nitrogen cooled detector, KBr beam splitter and nitrogen purged interferometer. Coversin at 1, 2, 5, 10 and 30 mg/ml with and without HAtoco at 10 mg/ml were analyzed using a Bio-ATR cell with 250 scans between 4000 and 600 cm^{-1} with 4 cm^{-1} resolution. All measurements were made in triplicate at 25°C. Spectral contributions from HAtoco or PBS buffer alone were subtracted from sample spectra along with atmospheric water and baseline corrections using OPUS v6.5 (Bruker Optics, Billerica, MA). The absorbance spectrum of the Amide I region (1700-1600 cm^{-1}) was normalized and deconvoluted using a mixed Gaussian and Lorentzian function resulting in 8 fitted peaks with the area corresponding to relative percentage of secondary structure based on previously assigned contributions by Yang et al[34].

3.2.9 Classical complement pathway inhibition

To assess the biological activity of Coversin upon release from the HAtoco formulation, selected samples from the subcutaneous-mimicking *in vitro* release assay described above were examined for classical complement pathway inhibition using the Complement System, Classical Pathway Wieslab ELISA kit. All reagent diluents and buffers were prepared fresh, autoclaved and filtered with a 0.2 μm sterile filter, and all procedures were performed under aseptic conditions unless otherwise noted to prevent inadvertent microbial activation. Naïve human serum (positive control, PC) and heat-inactivated human serum (negative control, NC) were reconstituted, diluted and aliquoted for storage as directed by the manufacturer. Coversin standards were freshly dissolved in PBS, pH 7.4, 0.05% (w/v) NaN_3 and serially diluted to a final concentration of 1000, 200, 100, 75, 50 and 25 nM. Standards and release samples were plated into a low-protein binding Nunc™ 96-well polypropylene storage plate (Thermo Fisher Scientific) and diluted 10-fold with PC serum. Blank buffer diluted 10-fold in PC serum or NC serum was taken as the positive and negative controls, respectively. All samples and controls were incubated at room temperature for 15 min to allow inhibitory activity to reach equilibrium. Following mixing and incubation, all samples were added to microplate wells precoated with the classical complement pathway precursor, human IgM, provided with the kit using a multi-channel pipette and incubated for 1 h at 37°C, covered to prevent evaporation. Following ELISA plate incubation, wells were aspirated by tapping onto sorbent paper and wash solution added for three total cycles. After the final aspiration, alkaline phosphatase anti-human C5b-C9 antibody conjugate was added to all wells and incubated, covered from light for 30 min at room temperature and washed as done previously. Lastly, p-nitrophenyl phosphate substrate was added to all wells, developed for 30 min at room temperature, covered from light and absorbance measured at 405 nm with pathlength correction

using a Biotek Synergy H1 Spectrophotometer. Absorbance data were fitted using a sigmoidal, 4PL, non-linear regression with Prism 6. Release sample Coversin concentrations were determined by RP-HPLC as described previously.

3.3 Results

3.3.1 Synthesis and characterization of HA-tocopherol

HAtoco was synthesized through the coupling of a Boc-protected glycine to the chromane ring hydroxyl of α-tocopherol (vitamin E), deprotection and subsequent carbodiimide-mediated amidation to the carboxylate of 33 kDa sodium hyaluronate. Unreacted tocopherol was removed by exhaustive dialysis against a 10 kDa MWCO membrane. Disaccharide molar substitution was characterized by ^{1}H NMR using the peak area ratio of the HA N-acetyl protons (2.0 ppm) and the tocopherol side chain methyl protons (0.8 ppm) (Figure 3.1). Tocopherol substitution on a disaccharide molar basis was calculated at 7%.

3.3.2 Extended release of Coversin by HA-tocopherol

In vitro subcutaneous-mimicking release of Coversin was examined by sampling release dialysate at predetermined time intervals and analyzing for protein concentration by correlating the peak area determined by RP-HPLC against known concentration standards (Figure 3.2). Release profiles of Coversin incubated with 33 kDa HAtoco10 (1% w/v), 33 kDa HA, 200 kDa HA in PBS, pH 7.4, 0.05% (w/v) NaN_3 or buffer alone are shown in Figure 3.3. All release profiles were well fit by one-phase decay non-linear regression. Coversin formulated in PBS buffer alone was released from the high molecular weight hyaluronan matrix within the dialysis bag with a half-

life of approximately 5.4 h (4.9 h – 6.1 h, 95% CI). 33 kDa HA and 200 kDa HA formulated Coversin exhibited a release half-life of 6.1 h (5.1 h – 7.5 h, 95% CI) and 4.4 h (3.4 h – 6.4 h, 95% CI) respectively. In comparison, Coversin formulated with HAtoco had a release half-life of 11.3 h (9.9 h – 13.3 h, 95% CI). Coversin was detected within the release dialysate for 9 days in the buffer only sample and 24 days for the HAtoco formulated sample.

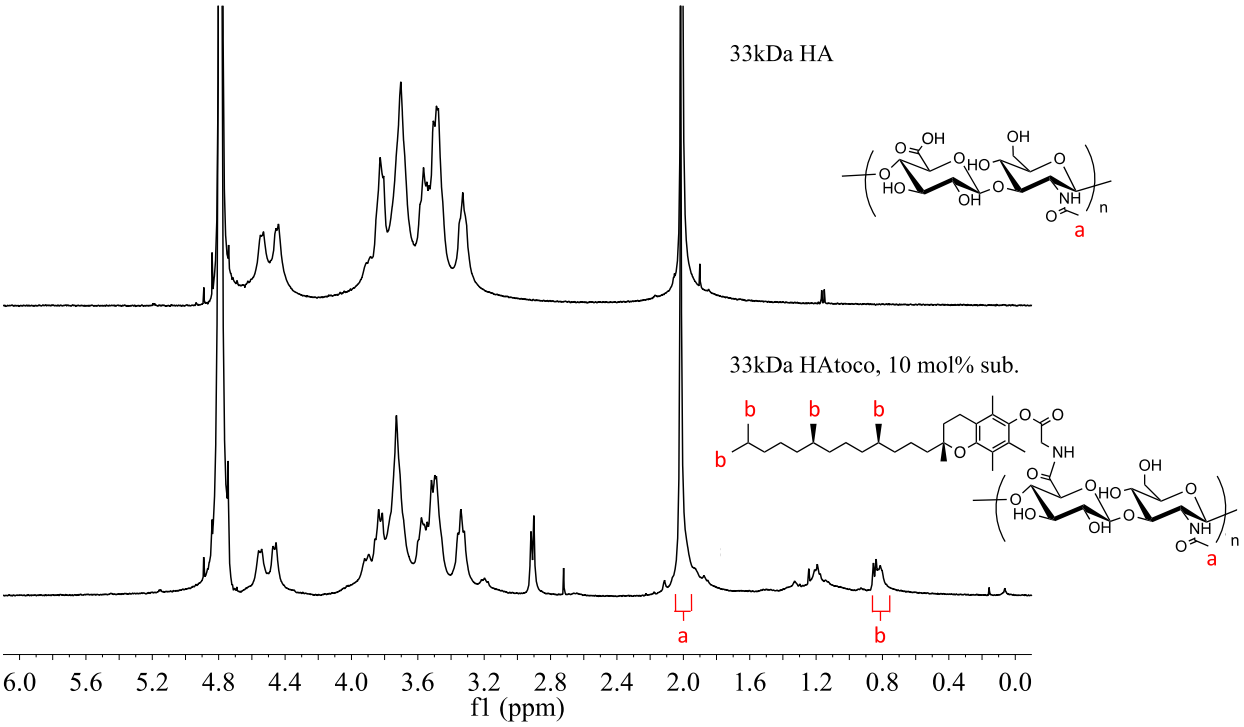

Figure 3.1: 1H NMR of 33 kDa HA (above) and 33 kDa HA-tocopherol, 10 mol% disaccharide substitution (below).

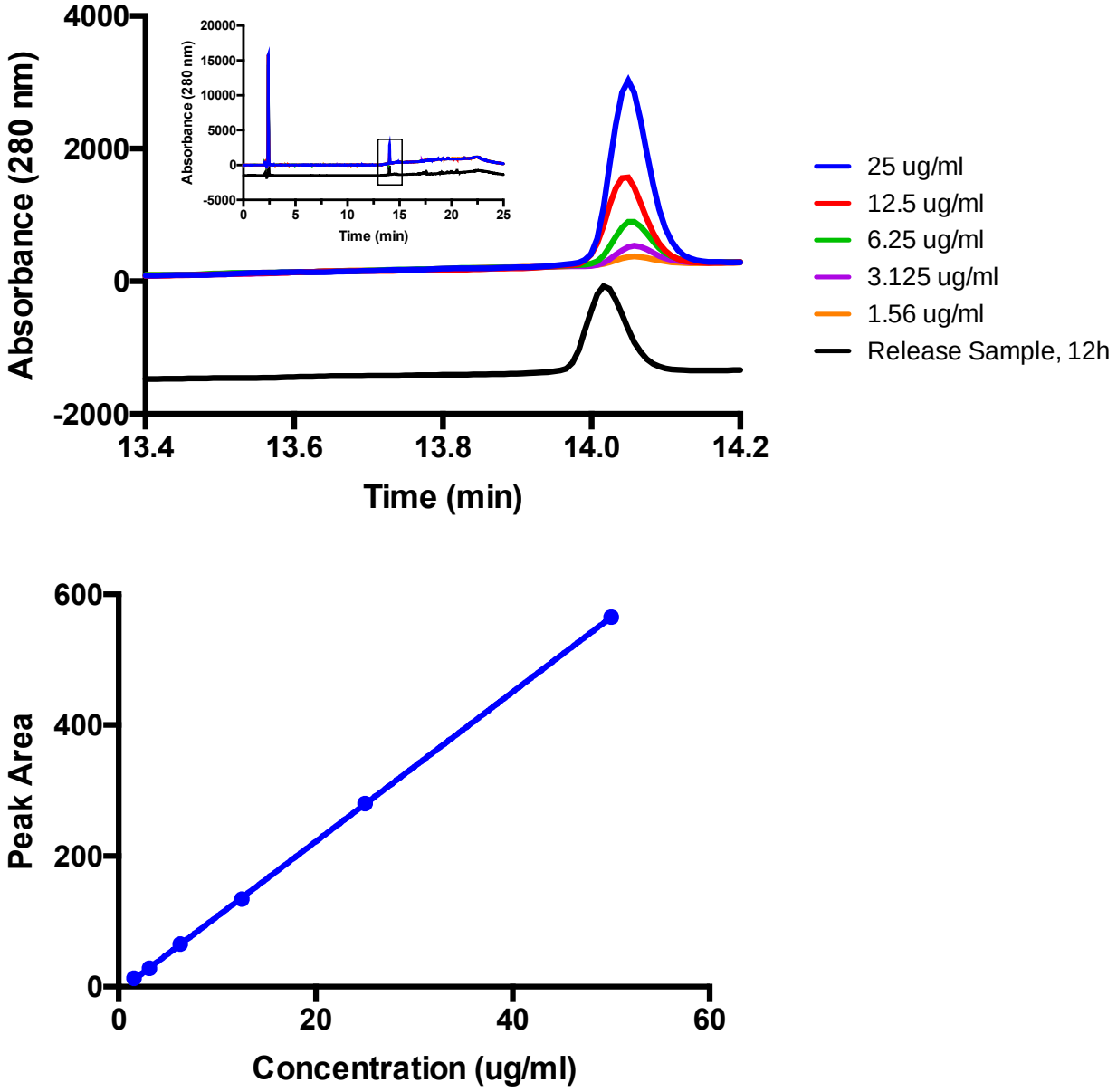

Figure 3.2: RP-HPLC chromatogram (280 nm) of Coversin standards vs. representative in vitro release sample (above) and calibration of curve of peak area at 14.0 min (below).

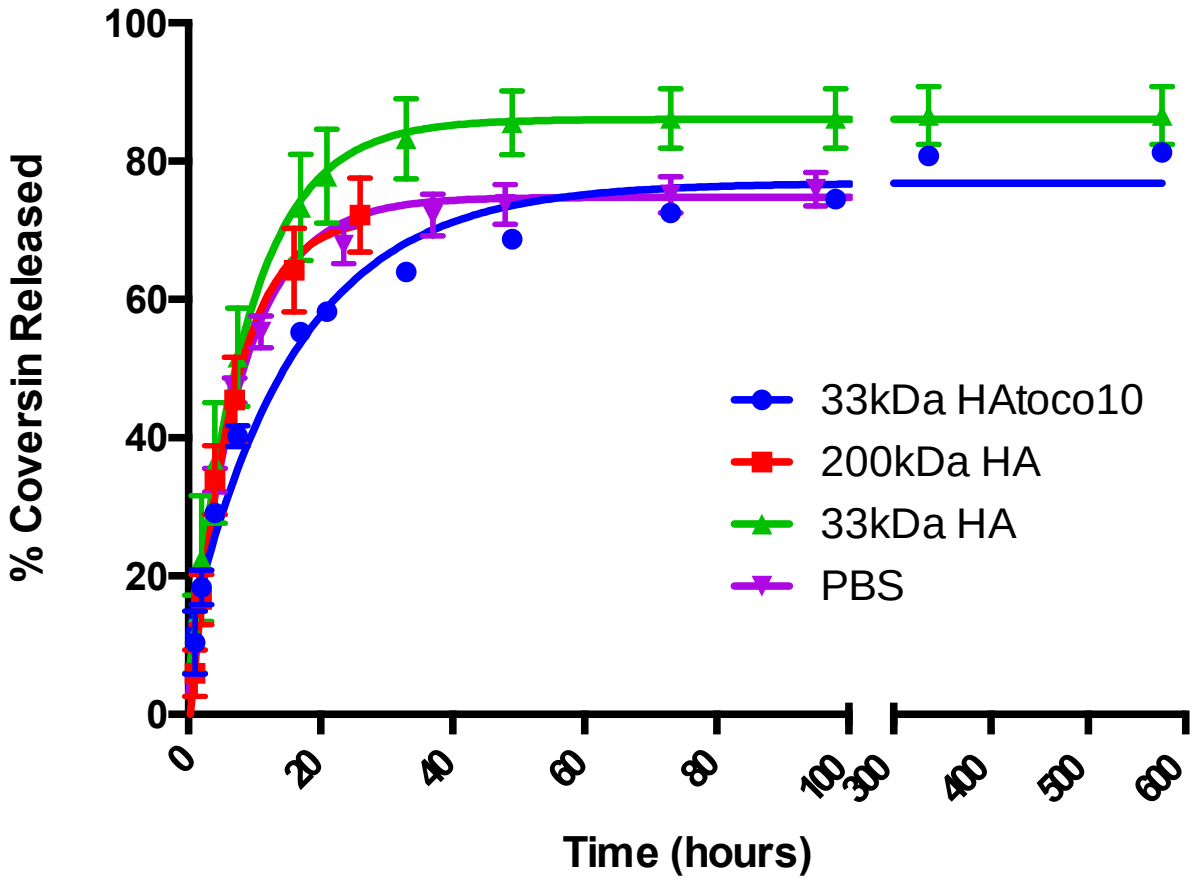

Sample	$t_{1/2}$ (h)	95% CI	R^2
33kDa HAtoco10	11.33	9.89 to 13.25	0.9748
200kDa HA	4.42	3.37 to 6.39	0.9669
33kDa HA	6.08	5.11 to 7.49	0.9633
PBS	5.44	4.88 to 6.14	0.9871

Figure 3.3: *In vitro* release of Coversin in 1% (w/v) test formulations of 33 kDa HA-tocopherol, 10 mol% subst. (33 kDa HAtoco10), 200 kDa HA, 33 kDa HA or PBS alone. Release profiles fit using a one-phase decay non-linear regression.

3.3.3 *In vivo* subcutaneous release

The *in vivo* release profile of Coversin complexed with HAtoco was assessed by subcutaneous administration of a fluorescently labeled Coversin at equal concentrations formulated within 33 kDa HAtoco10, 200 kDa HA or PBS into the hind limb footpad of female BALB/c mice (N=3). After injection, fluorescence at the injection site was monitored at predetermined intervals for 8 days. All images were taken at constant exposure times, equally threshold adjusted to minimize autofluorescent contributions (Figure 3.4) and reported as integrated density (mean intensity x area) and fit using a one-phase decay, non-linear regression (Figure 3.5). Coversin injected in PBS alone or 200 kDa HA had release half-lives of 6.7 h and 5.3 h respectively and both had essentially no signal remaining at the injection site after 24 h. Coversin associated with HAtoco had a half-life of 10 h and persisted at the injection site for up to 3 days. Overall, the relative release half-lives of all the formulations patterned those found within the *in vitro* system with slight reductions likely due to the presence of endogenous hyaluronidase which is capable of degrading HAtoco and 200 kDa HA, pressure differences due to endogenous tissue pressure and walking contact and other hydrogel deterioration brought on by in vivo conditions not present within the model *in vitro* system. HAtoco again was able to provide a nearly 2-fold extended release of the Coversin protein with simple mixing and room temperature incubation prior to injection.

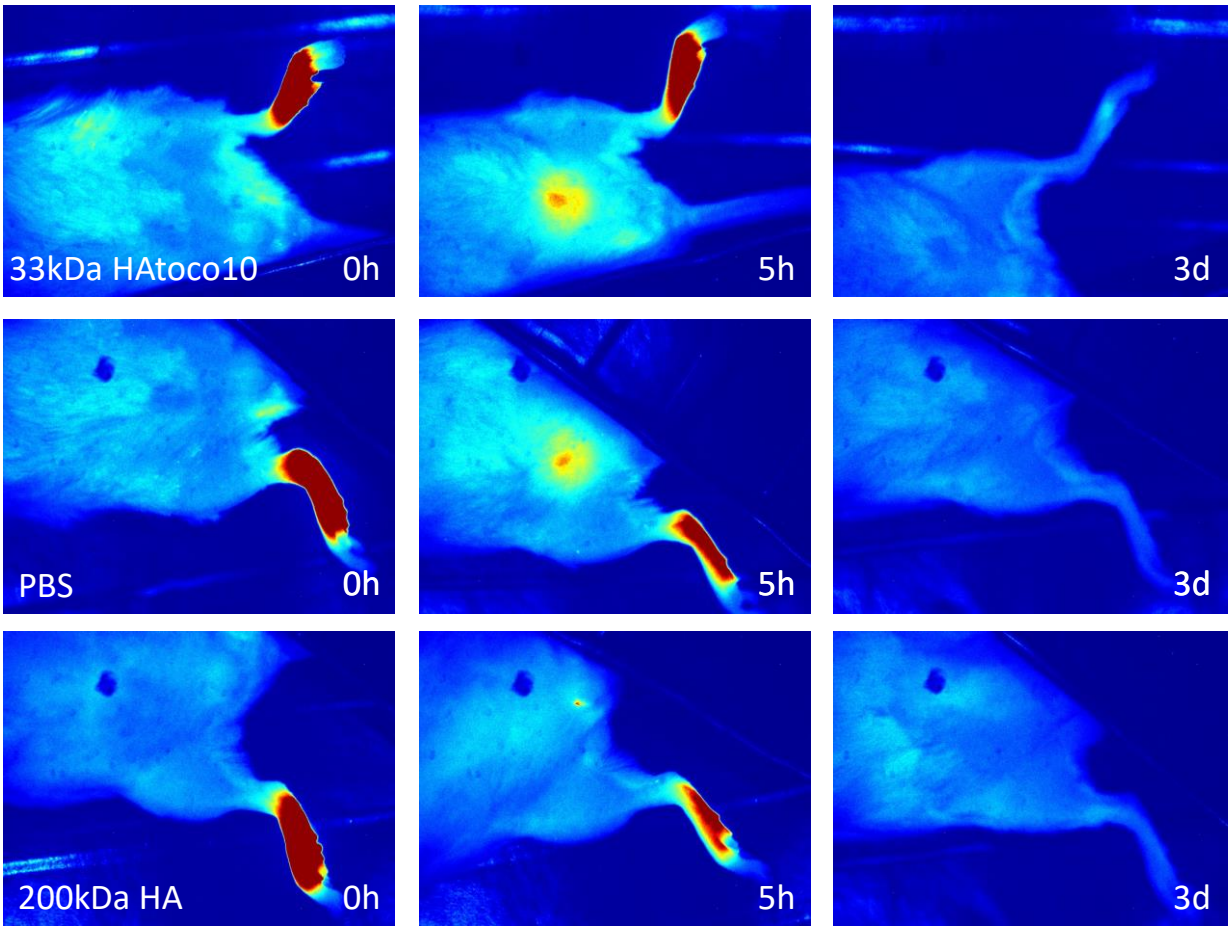

Figure 3.4: *In vivo* release of formulated Coversin-Alexa Fluor 647 conjugates injected subcutaneously into the hind footpad of a mouse immediately following injection (left), at peak absorption (middle) and at the terminal elimination phase (right).

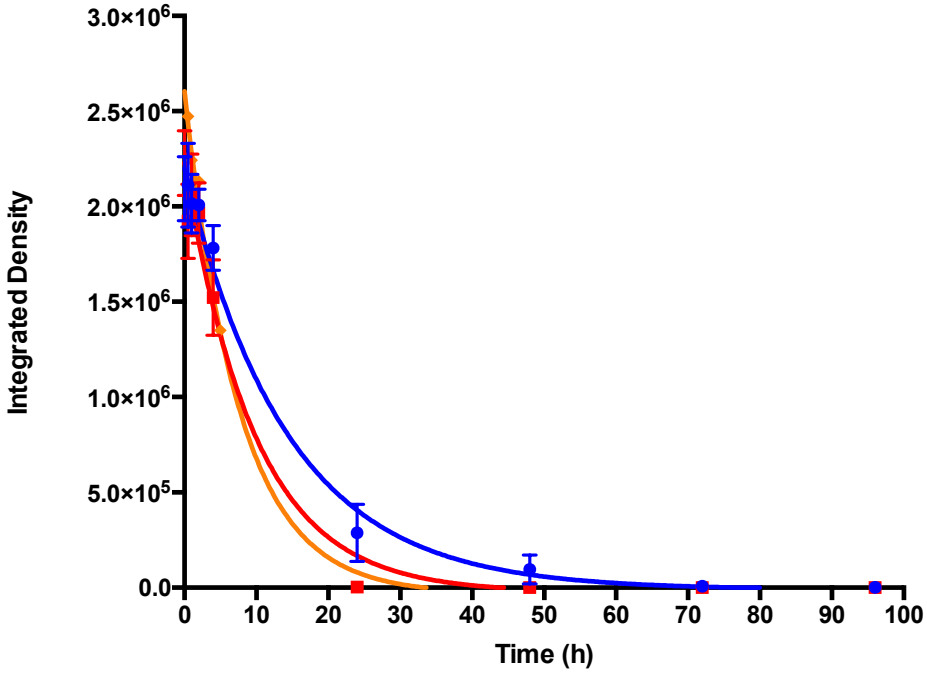

Sample	$t_{1/2}$ (h)	95% CI	R^2
33kDa HAtoco10	9.97	8.88 to 11.37	0.9824
200kDa HA	5.29	4.88 to 5.77	0.9964
PBS Only	6.76	5.86 to 7.98	0.9763

Figure 3.5: In vivo release profile of subcutaneously injected Coversin- Alexa Fluor conjugates formulated in 33 kDa HAtoco10, 200 kDa HA or PBS alone. Release data fit to a one phase decay non-linear regression. Integrated density = cumulative pixel intensity x area.

3.3.4 Assessing HAtoco and Coversin binding by intrinsic fluorescence

In order to assess Coversin association with HAtoco, intrinsic tryptophan (Trp) fluorescence was used to probe polarity of the tryptophan microenvironment. Emission spectra were collected between 300 – 400 nm formulated in 1% (w/v) 33 kDa HAtoco or 33 kDa HA (Figure 3.6). Emission spectra were also collected with increasing amounts of 33 kDa HAtoco10 (Figure 3.7) and moment and area under the curve (intensity) plotted versus polymer concentration (Figure 3.8a, 3.8b). No shift in the Coversin emission moment was observed in either formulation as was seen in previous studies with model-protein BSA, suggesting no alteration in tryptophan environment polarity. However, clear decreases in overall peak area were observed with increasing amounts of HAtoco which were not observed with addition of unmodified HA. To assess the mechanism of fluorescent quenching using the Stern-Volmer equation (Equation 1), a plot of the ratio of the initial fluorescence intensity (F_0) to the quenched fluorescence intensity (F) versus quencher concentration (Q) (Figure 3.8c) was made resulting in a non-linear, downward curved plot suggesting differing accessibilities of the three tryptophan residues within Coversin.[35] Using a modified Stern-Volmer plot (Figure 3.8d) derived from equation 2, the y-intercept was taken as the inverse of the freely accessible fraction of the tryptophan fluorophore (f_a) and was found to equal 23 ± 3 %. Variance in the tryptophan accessibility suggests one reason why shifts in Coversin fluorescent moment are not observed with increasing HAtoco concentration as was seen in similar studies performed in Chapter II with model-protein BSA. Further experiments monitoring the fluorescent lifetime or absorption spectra with increasing HAtoco would be required in order to assess more detailed quenching mechanisms such as collision (dynamic) or complex formation (static).[35]

(1) $\frac{F_0}{F} = 1 + K_D[Q]$

(2) $\frac{F_0}{\Delta F} = \frac{1}{f_a K_a[Q]} + \frac{1}{f_a}$

$\Delta F = F_0 - F$

$K_D(K_a) = Stern - Volmer\ quenching\ constant\ (accessible\ fraction)$

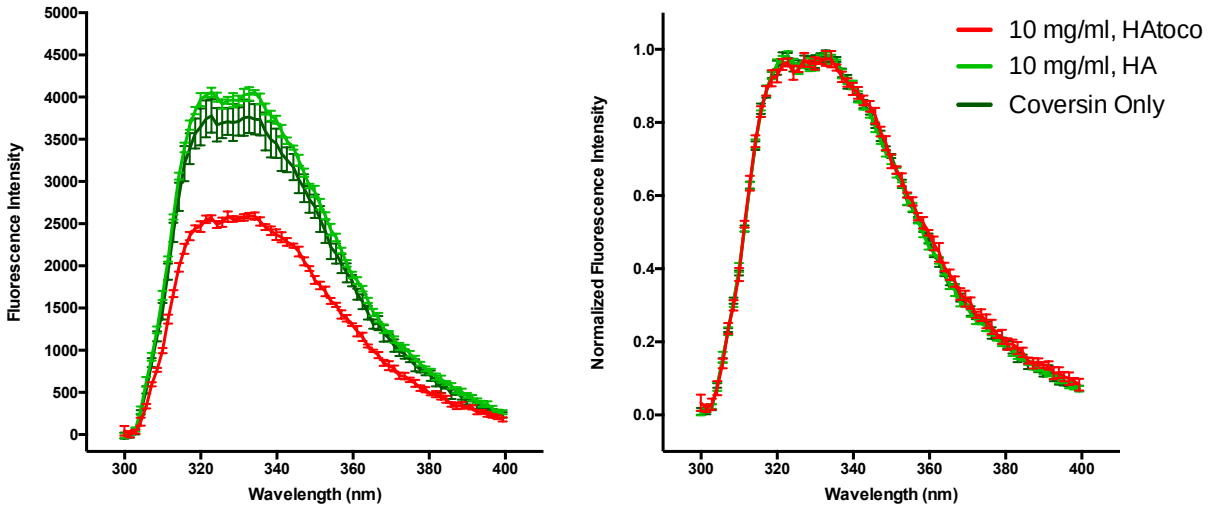

Figure 3.6: Intrinsic tryptophan fluorescence spectra of Coversin (0.25 mg/ml) with and without HAtoco (10mg/ml) or HA (10mg/ml) at 20°C. (Left) raw spectra, (right) normalized spectra.

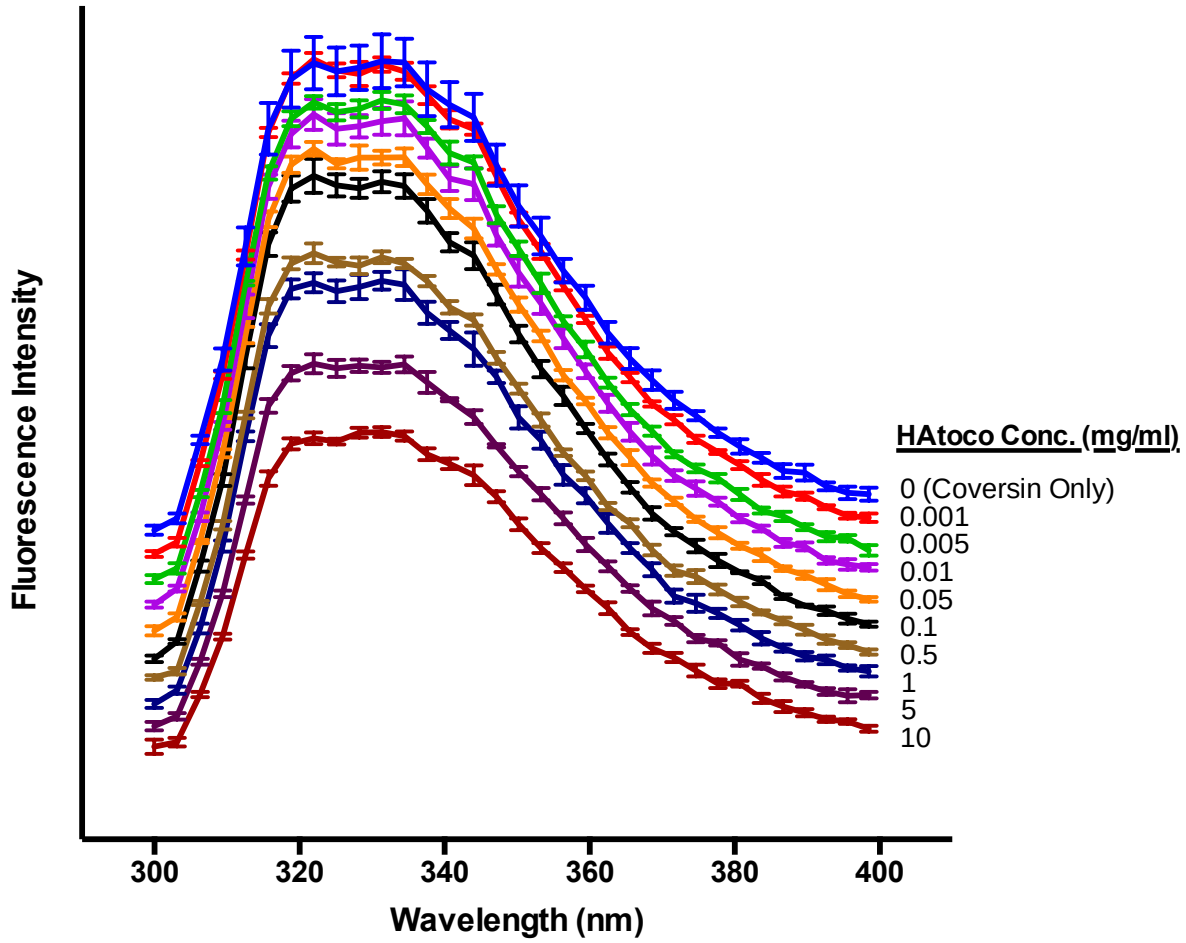

Figure 3.7: Coversin (0.25 mg/ml) intrinsic tryptophan fluorescence versus HAtoco concentration (10 mg/ml to 0.001 mg/ml), error bars represent SD (*N*=6). Spectra are equally offset for visual clarity.

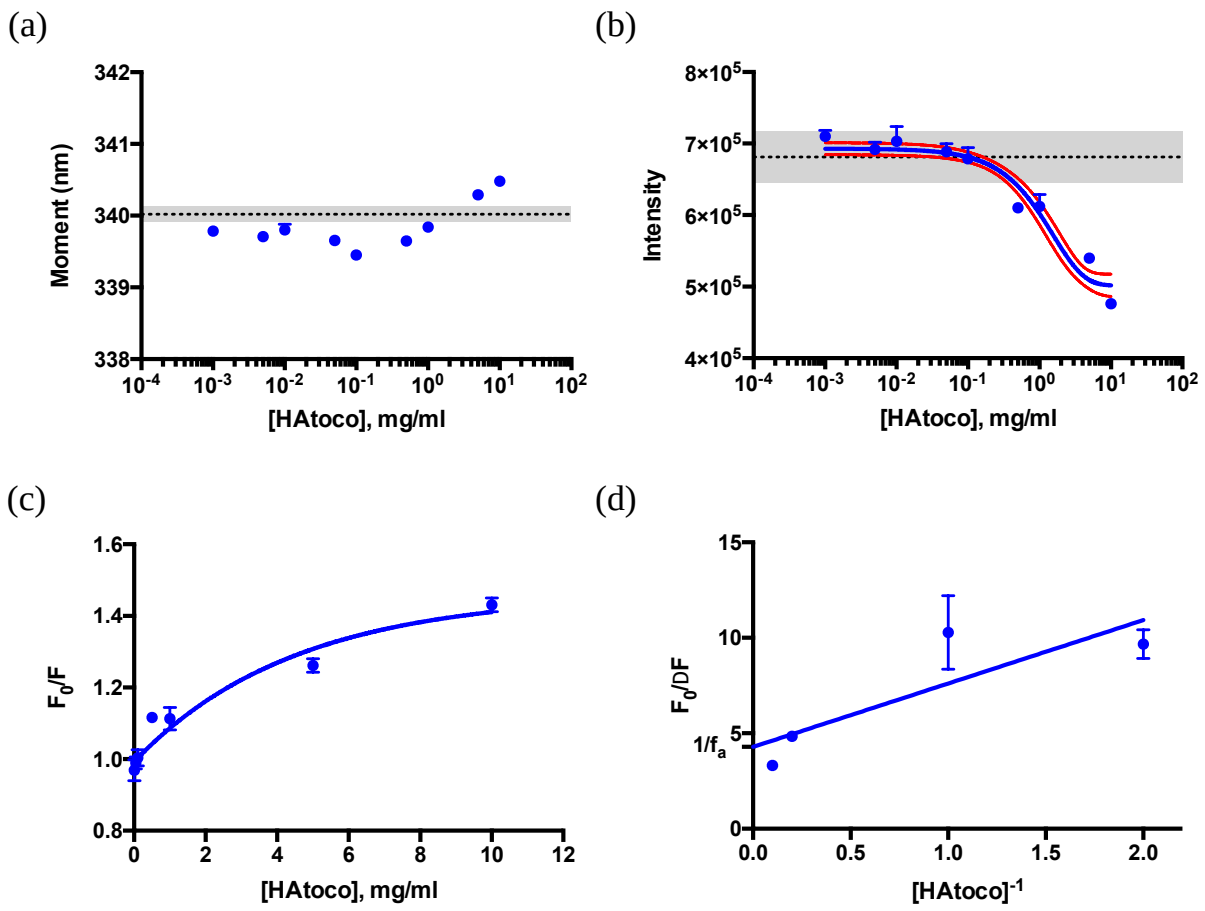

Figure 3.8: (a) Coversin (0.25 mg/ml) intrinsic tryptophan fluorescence moment and (b) intensity versus HAtoco concentration, error bars represent SD (*N*=6). Black-dotted line represents average moment or intensity of Coversin alone with gray area equal to ± SD (*N*=6). Intensity versus HAtoco concentration fit using a one-phase decay non-linear regression with Graphpad Prism 6, red-dotted line represents 95% confidence interval of fit. (c) Stern-Volmer plot and (d) modified Stern-Volmer plot with y-intercept depicting inverse fraction of accessible fluorophore (23 ± 3 %).

3.3.5 Fluorescence polarization binding isotherm

To assess the binding stoichiometry of Coversin and HAtoco further, Coversin was fluorescently labelled to permit measurement of polarization changes when incubated with HAtoco. Free amines of Coversin were covalently modified with NHS-Rhodamine (NHS-Rh), purified by GPC and subsequently dialyzed. To verify conjugation of dye and to assess labelling degree, samples were analyzed by UPLC-ESI-MS, with +413.1 u corresponding to a rhodamine addition. Rhodamine substitution was verified and the degree of substitution was found to be a distribution of 1 to 4 dye molecules per protein (Figure 3.9). Purity of Coversin-Rhodamine (Coversin-Rh) was assessed by gradient RP-HPLC coupled with an in-line fluorescent detector. NHS-Rh standards were found to elute with a multiple peak pattern (Figure 3.10) possibly due to succinimidyl ester hydrolysis during storage. Purified Coversin-Rh was found to elute at a similar retention time (13.6 min) as unmodified Coversin standards (13.5 min). Assessment of peak area of free dye associated peaks and Coversin-Rh associated peaks suggests >95% purity of the Coversin-Rh conjugate from free dye.

After verifying dye conjugation and purity, 33 kDa HAtoco10 or 33 kDa HA were dissolved to 1% (w/v) in decreasing concentrations of Coversin-Rh, PBS, pH 7.4 and sample polarity was assessed by polarized fluorescent spectroscopy (Figure 3.11). No change in polarization occurred with increasing ratios of HA to Coversin (i.e. decreasing amounts of Coversin) or in buffer only controls. When formulated with HAtoco, Coversin was found to have a distinguishable increase in polarization beginning at about 1 mg/ml Coversin (10:1 (w/w), HAtoco:Coversin) and plateauing at about 0.2 mg/ml Coversin (50:1 (w/w), HAtoco:Coversin).

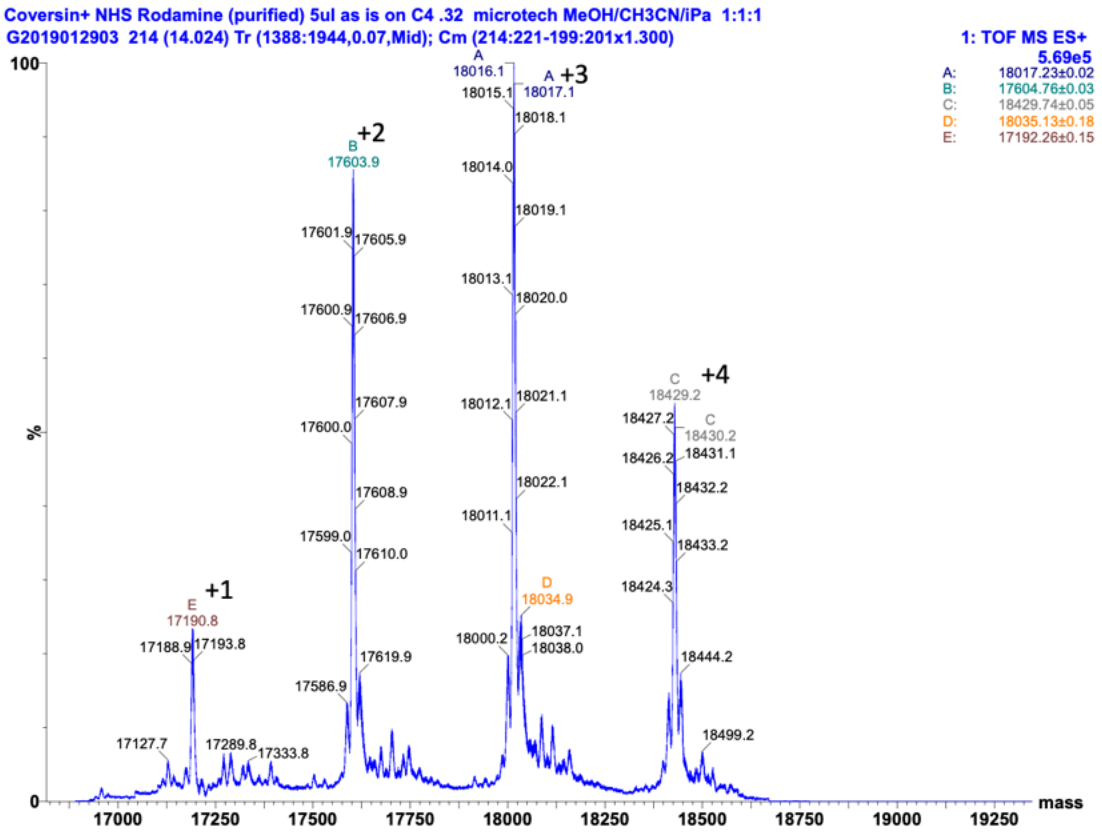

Figure 3.9: Mass spectra of purified Coversin-Rhodamine conjugates with +1, +2, +3 and +4 rhodamine substitions.

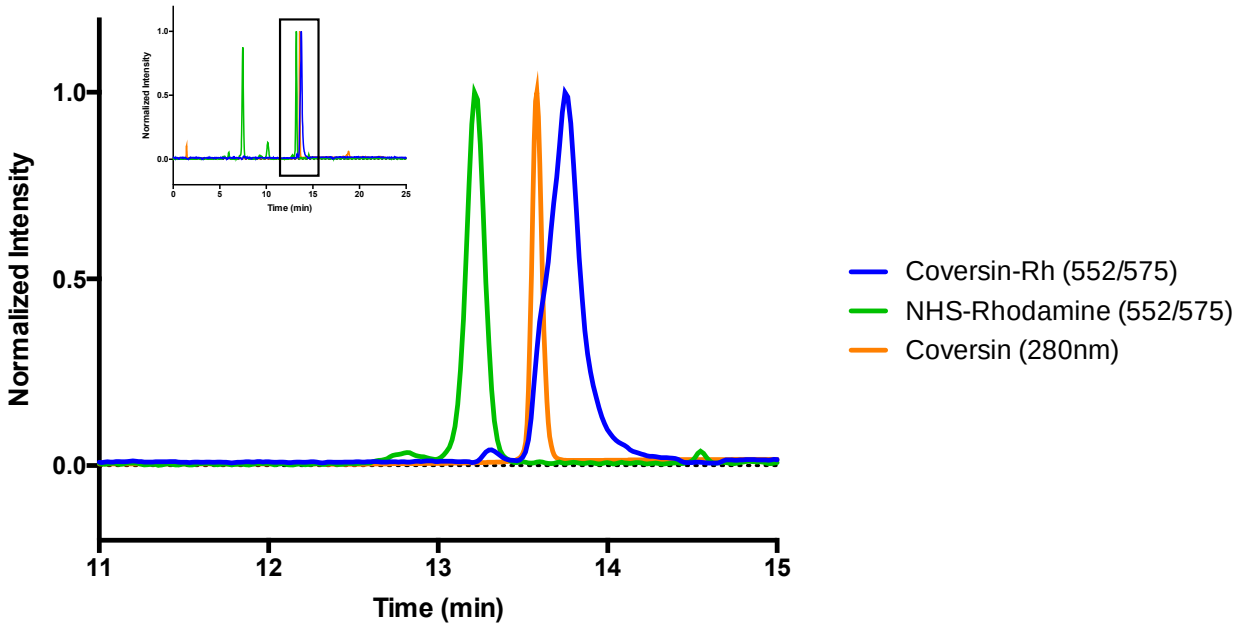

Figure 3.10: RP-HPLC-Fluorescence-UV of GPC/dialysis purified Coversin-Rhodamine conjugate, NHS-Rhodamine or Coversin (280 nm detection).

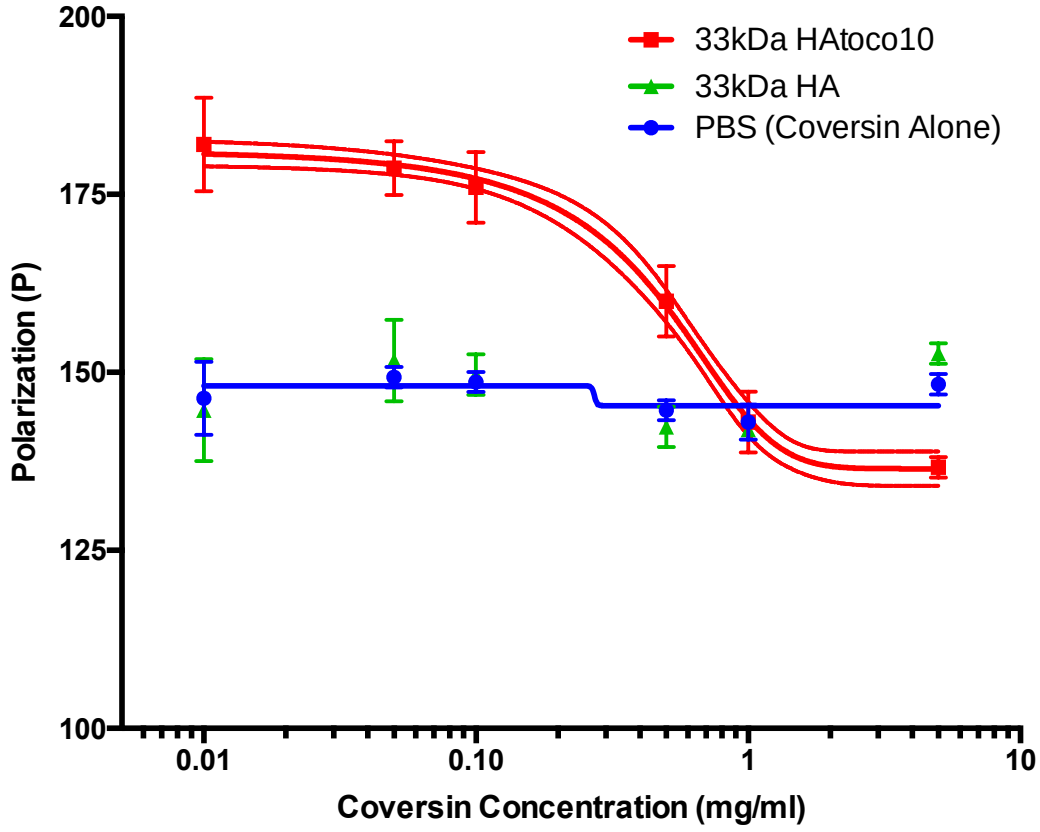

Figure 3.11: Fluorescence polarization versus concentration of Coversin-Rhodamine formulated in 1% (w/v) 33 kDa HAtoco10, 33 kDa HA or PBS alone (*N*=3). Polarization curves were fit using a sigmoidal 4PL non-linear regression, red-dotted line equals 95% confidence interval of regression.

3.3.6 Coversin tertiary structure temperature stability assessment by intrinsic tryptophan fluorescence

The tertiary structure stability of Coversin in HAtoco was studied by monitoring intrinsic steady-state tryptophan (Trp) fluorescence with increasing temperature. Fluorescence was assessed at >90% bound Coversin based on stoichiometric ratios determined by fluorescence polarization binding isotherms. Raw spectra were background subtracted (Figure 3.12) and the moment, also known as mean spectral center of mass (MSM), was plotted against temperature (Figure 3.13). Upon heating, moment position for Coversin steadily increased from an initial 343 nm at 10°C to 50°C, at which a significant thermal transition occurred with T_m at 60.3°C. HAtoco bound Coversin spectral moment remained relatively steady (340 nm) until an earlier thermal transition of 55.2°C. Both transitions exhibited a similar slope of change in the thermal transitions, but with post-transition moment of Coversin alone at 355 nm and in HAtoco at 349 nm. Overall, differences in tertiary structure thermal transitions suggests that when bound to the HAtoco platform, Coversin's tertiary structure is significantly destabilized when compared to protein alone in solution.

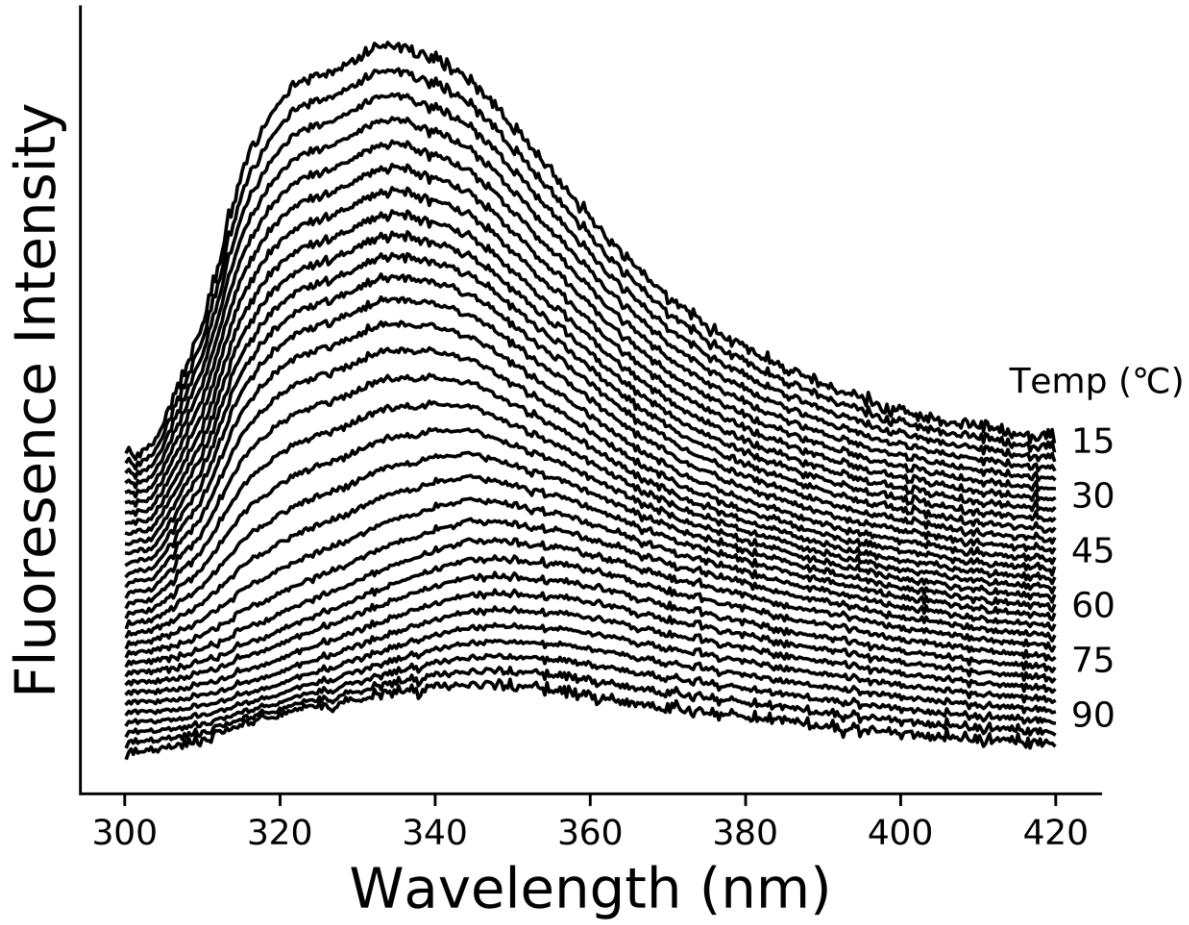

Figure 3.12: Intrinsic tryptophan spectra of Coversin at increasing temperature. Samples were excited at 295 nm to produce >95% tryptophan fluorescence.

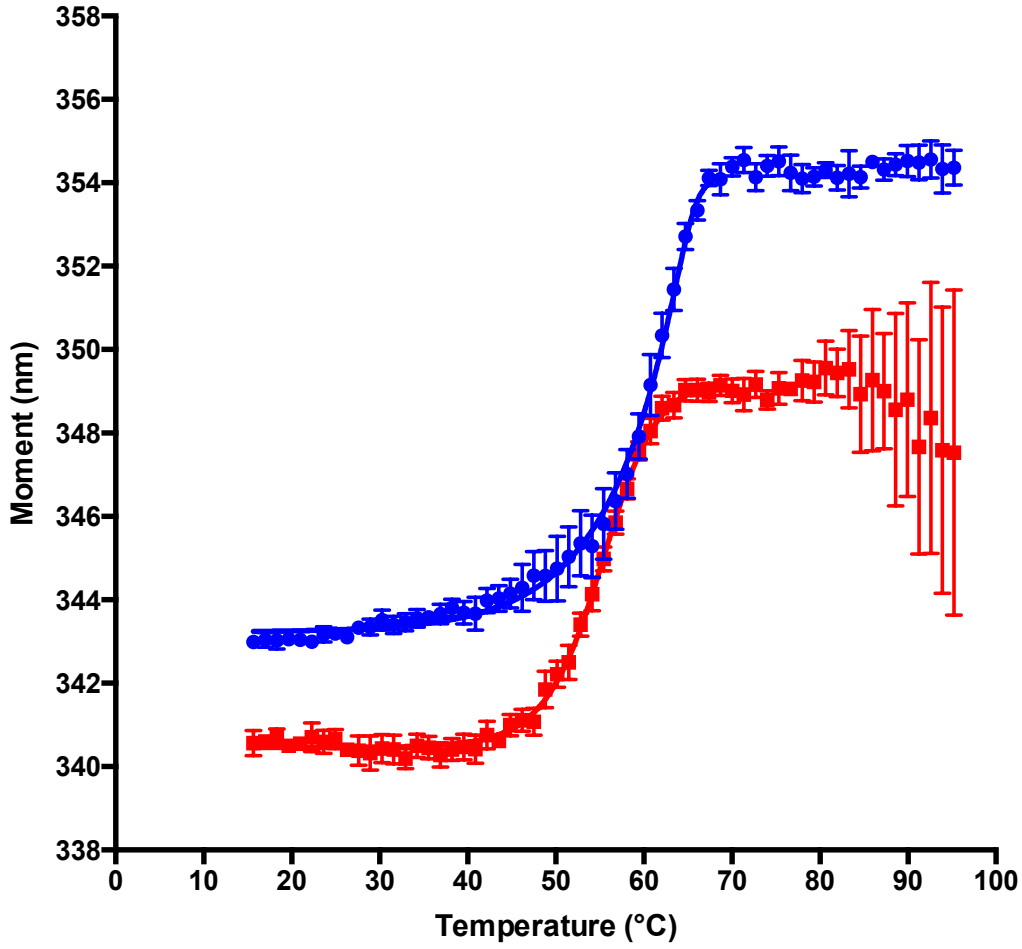

Sample	Tm, (°C) ± SD
PBS (Coversin Alone)	60.31 ± 0.15
33kDa HAtoco10	55.21 ± 0.10

Figure 3.13: Coversin (0.25 mg/ml) intrinsic tryptophan fluorescence moment versus temperature formulated with and without 33 kDa HAtoco10 at 1% (w/v). Melt curves fit with asymmetric 5-parameter logistic fit non-linear regression and curve EC_{50} reported as the T_m (N=6). Data reported as mean ± SD.

3.3.7 Differential scanning calorimetry

DSC was used to assess the overall conformational stability of binding Coversin to the HAtoco platform. One major transition was observed for both Coversin alone and when bound (>90%) to HAtoco (Figure 3.14). Slight differences in T_m values and thermograms were observed, mirroring findings of the fluorescent thermal melts. The T_m of Coversin alone was found to be ~63.7°C while the T_m when bound to HAtoco was found to be ~60°C. A clear reduction in overall AUC of the thermogram, and thus the apparent ΔH_{cal}, when bound to HAtoco was observed suggesting an overall reduction in the energy required to denature the protein present and thus an overall reduction in the presence of native state protein. Reductions in stored energy (apparent ΔH_{cal}) and subsequently the equilibrium temperature between native and denatured protein (i.e. T_m) have been previously documented for partially unfolded proteins, and could be a result of protein structure alterations as a result of association with the HAtoco conjugate or protein aggregation.

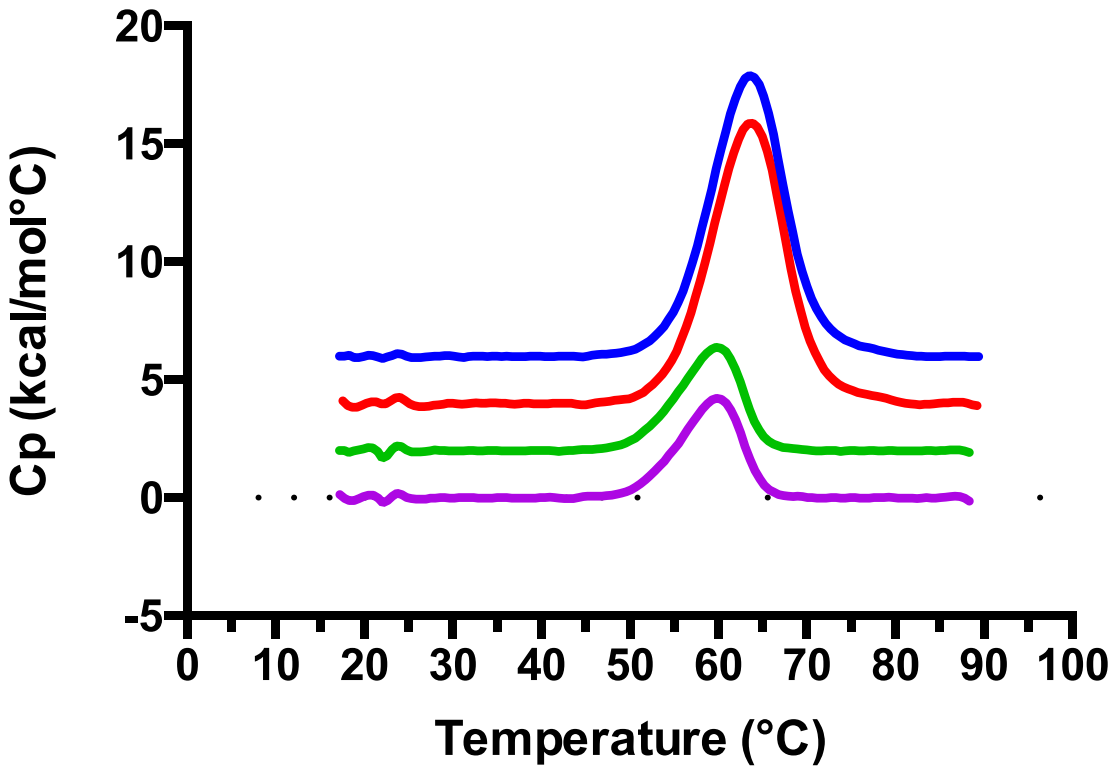

Sample	T_m (°C)	ΔH_{cal} (cal/mol)
Coversin, 1	63.5	1.26×10^5
Coversin, 2	63.9	1.27×10^5
Coversin + HAtoco, 1	59.8	3.90×10^4
Coversin + HAtoco, 2	59.8	3.67×10^4

Figure 3.14: Differential scanning calorimetry of Coversin (0.25 mg/ml) in PBS or formulated with 33 kDa HAtoco10 (1% w/v), (*N*=2). Individual sample traces are equally offset for visual clarity.

3.3.8 Fourier-transform infrared spectroscopy (FTIR)

The secondary structure of Coversin in solution and when bound to HAtoco were assessed by FTIR. Due to the limits of detection within the Amide I region of the FTIR spectra (Figure 3.15), Coversin was measured down to 1mg/ml with and without HAtoco at 10 mg/ml. Absorption spectra within the Amide I region were atmospheric and baseline corrected, normalized and deconvoluted for component secondary structures using a mixed Gaussian and Lorentzian function (Figure 3.16). Clear differences can be seen in the absorption spectra of the HAtoco bound versus solution Coversin, particularly within the 1700 cm^{-1} to 1667 cm^{-1} range generally associated with β-turn and β-sheet contributions. After calculating component peak area contributions of the total absorption peak area, β-turn and β-sheet contributions in samples with increasing fraction of bound protein (i.e. lower protein concentrations) begin to deviate from the buffer only control (Figure 3.17). At 1 mg/ml Coversin, β-turn and β-sheet cumulative contributions are 22% and 62% respectively, but when formulated with HAtoco they are 11% and 72% respectively (Figure 3.18). Alterations in these specific structures may be indicative of the particular location on the Coversin surface with which HAtoco preferentially associates or a general conformational change upon binding.

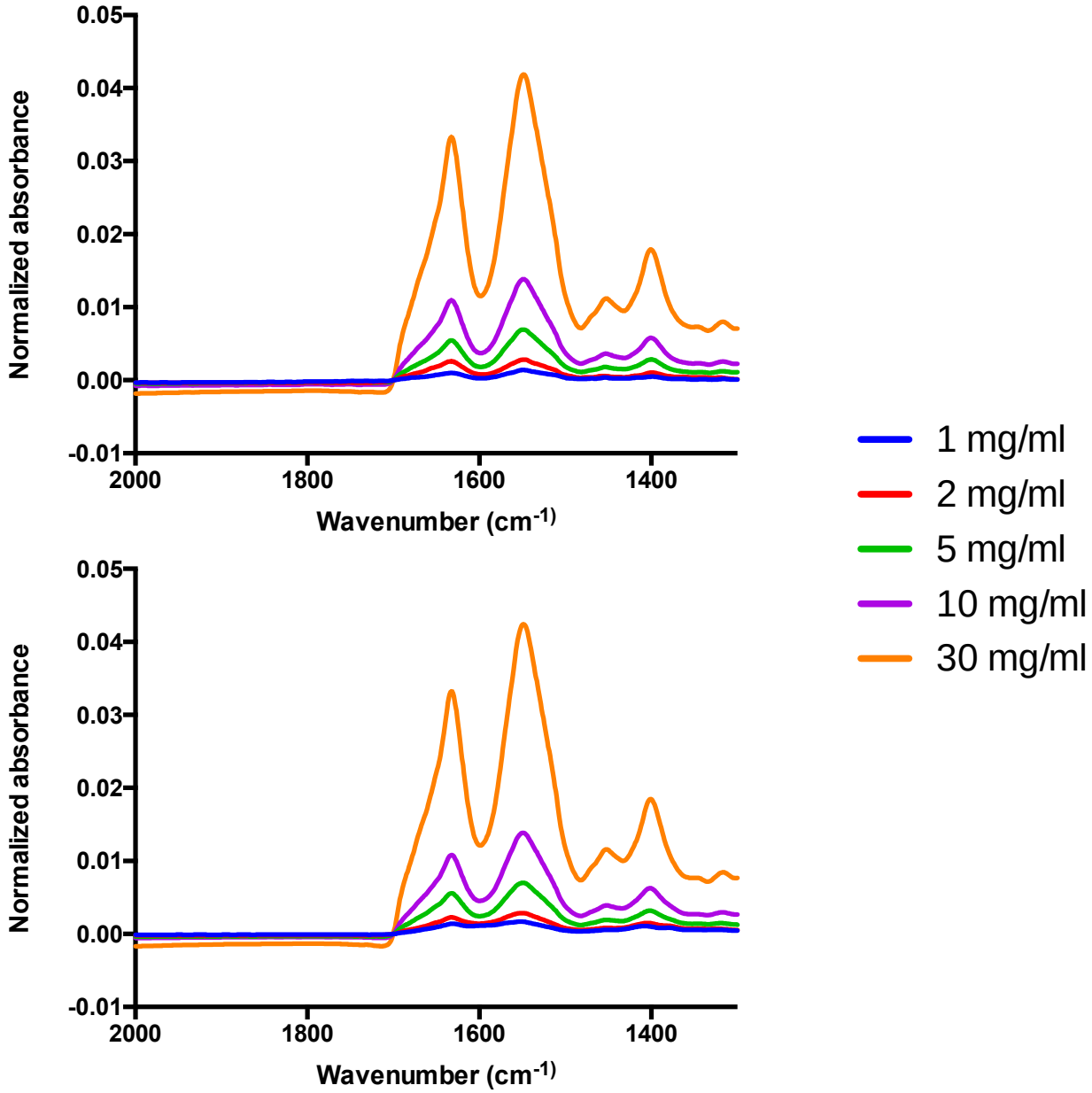

Figure 3.15: Amide I/II regions of Coversin (1 mg/ml) in PBS (above) and Coversin in 10 mg/ml HAtoco (below).

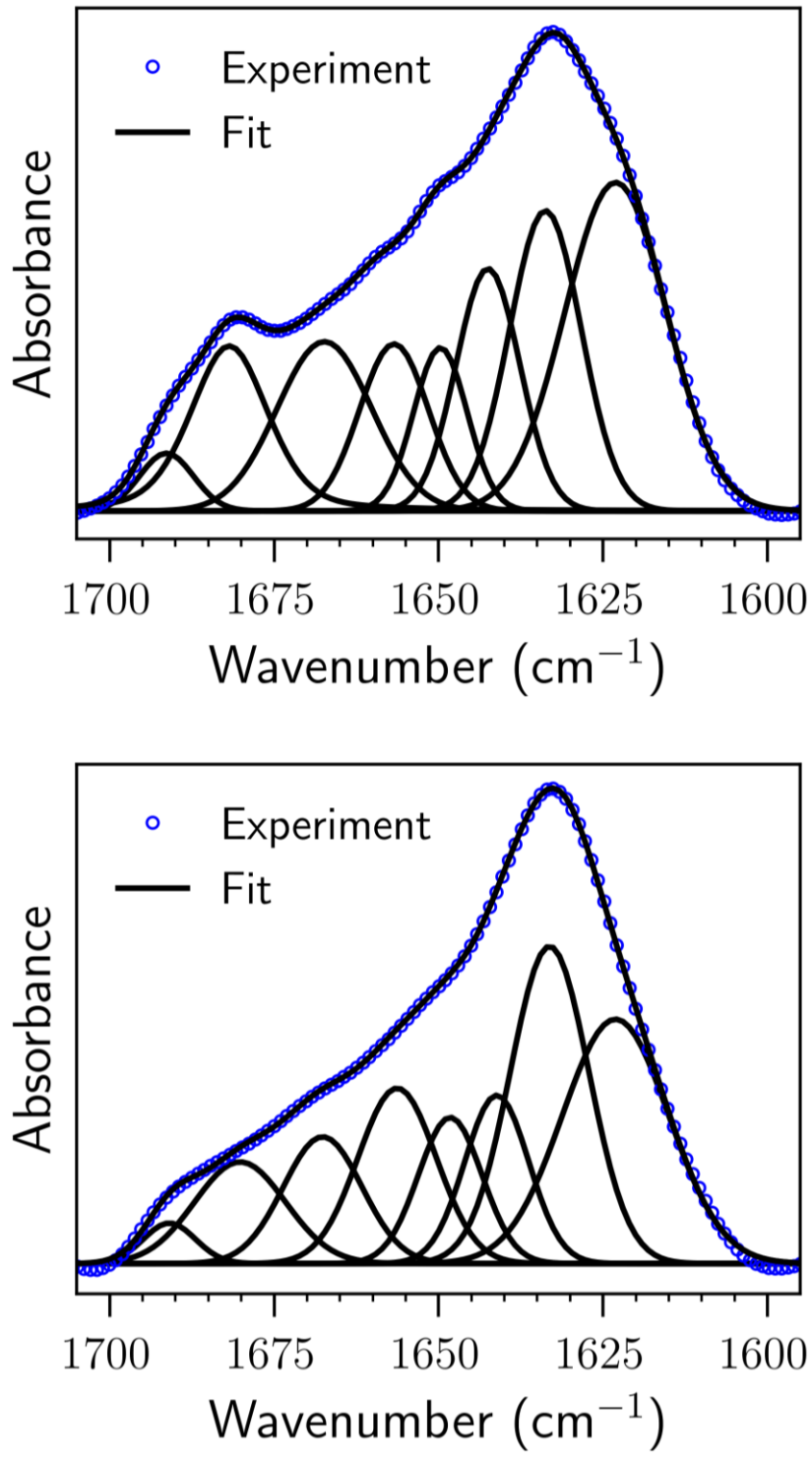

Figure 3.16: Deconvolution of Amide I FTIR absorption spectra for Coversin (1 mg/ml) in PBS (above) or Coversin (1mg/ml) with HAtoco (10 mg/ml) (below).

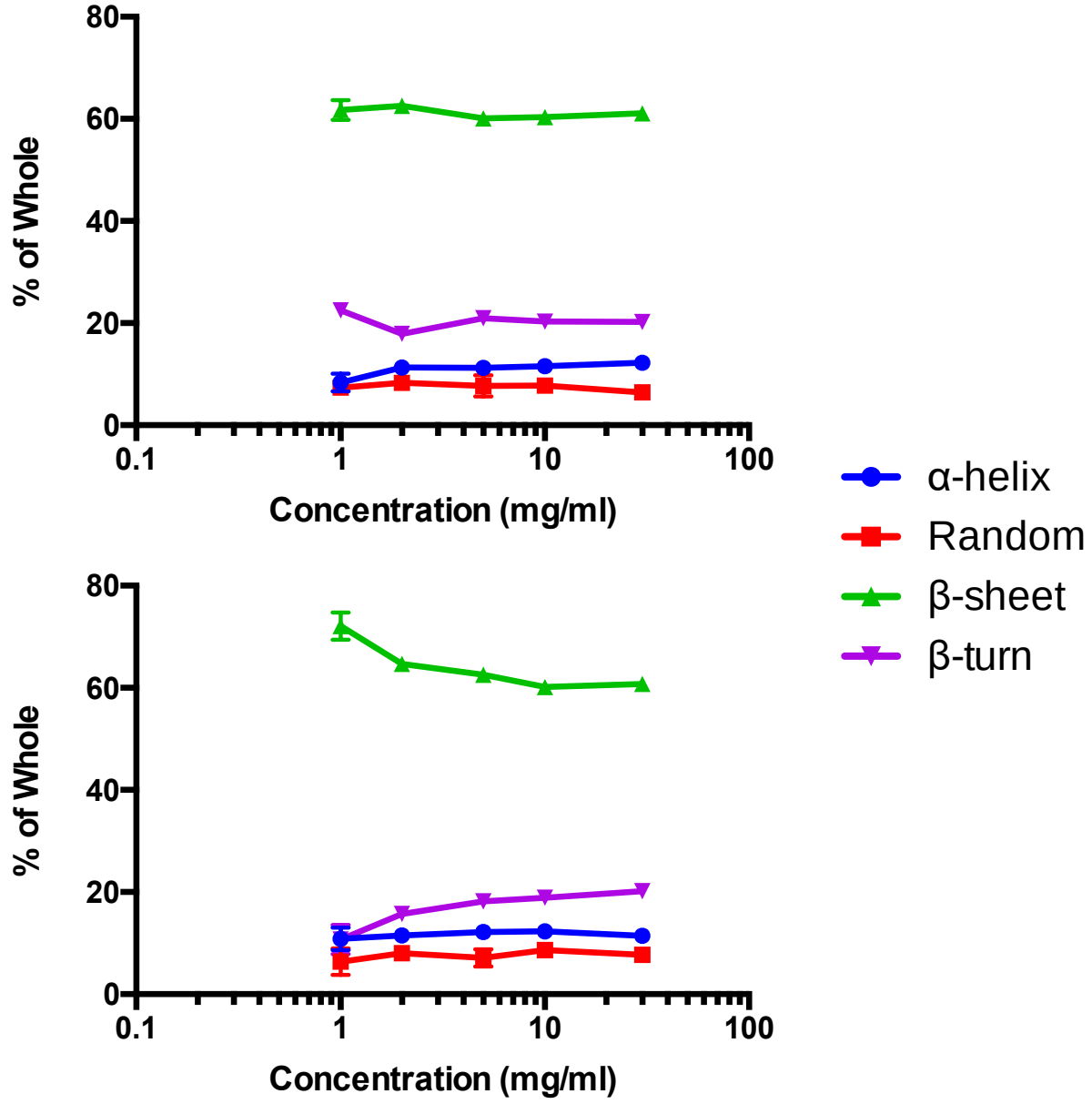

Figure 3.17: Component secondary structure contribution to overall secondary structure based on peak area of deconvoluted amide I band of Coversin (30 to 1 mg/ml) in PBS (above) or in HAtoco, 10 mg/ml (below). All measurements made in triplicate. Error bars represent standard deviation.

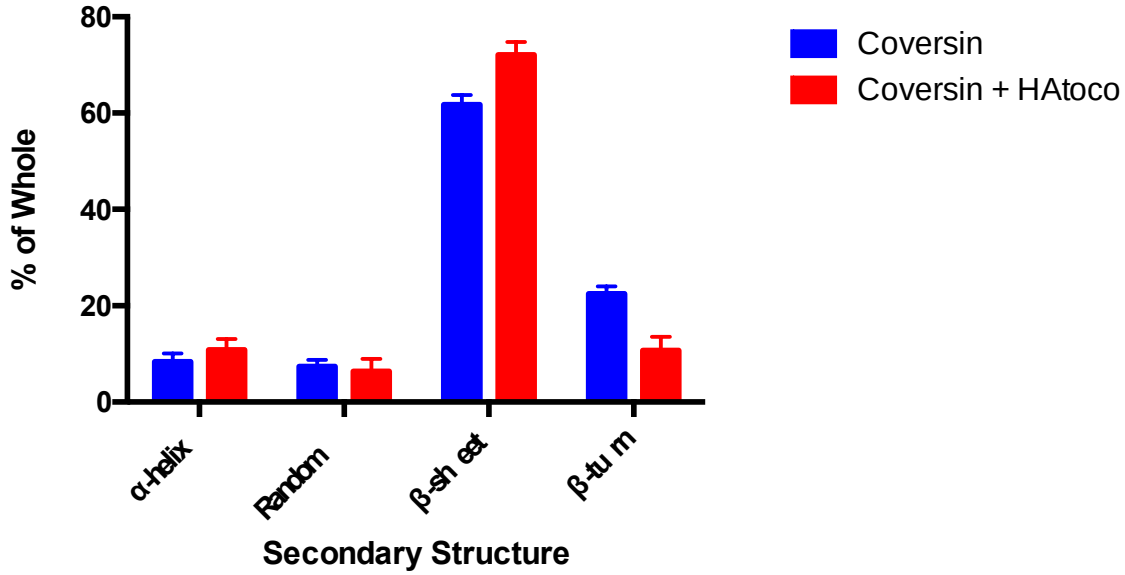

Figure 3.18: Component secondary structure analysis of Coversin (1mg/ml) with and without HAtoco (10mg/ml), (*N*=3), error bars = ± SD.

3.3.9 Classical complement pathway inhibition screening by ELISA

Retention of Coversin's biological functionality after release from HAtoco was examined using a commercially available ELISA which measures the development of the terminal membrane attack complex (MAC) following initiation of the classical complement pathway. Complete inhibition was defined as the MAC formation in heat-inactived serum (NC) while full complement activity was defined as the MAC formation in naïve serum (PC). *In vitro* release samples of Coversin formulated in PBS alone (37h and 73h) or in HAtoco (33h and 73h) were mixed with naïve serum for 15 min prior to initiation of the classical complement cascade through exposure to IgM coating the wells of the micro-plate. All samples were found to provide full inhibition of the complement cascade (Figure 3.19). To determine the theoretical minimum amount of biologically active Coversin within each release sample, a dose-response curve of fresh Coversin was tested and the plateau of the sigmoidal response taken as the minimum concentration required to fully inhibit ($MinC_{FI}$) the response within this system which was determined to be 24.6 nM. The theoretical minimum biological protein content of each sample is dependent on the concentration tested within all samples. Completely biologically active protein may exist within each sample; however, it is important to note that due to the small dynamic range and limited plate capacity, 100% inhibition does not equate to 100% retainment of biologically active protein content. With these caveats in mind, retainment of biologically active protein following 73 h of release both within the PBS control and within the HAtoco formulated samples is surprising based on documented lapses in biological activity *in vivo* within 24 h post-subcutaneous delivery in human clinical trials. These results coupled with *in vitro* and *in vivo* release profiles suggest HAtoco is capable of extending the delivery of Coversin following subcutaneous injection and that Coversin retains its biological activity upon disassociation with the matrix.

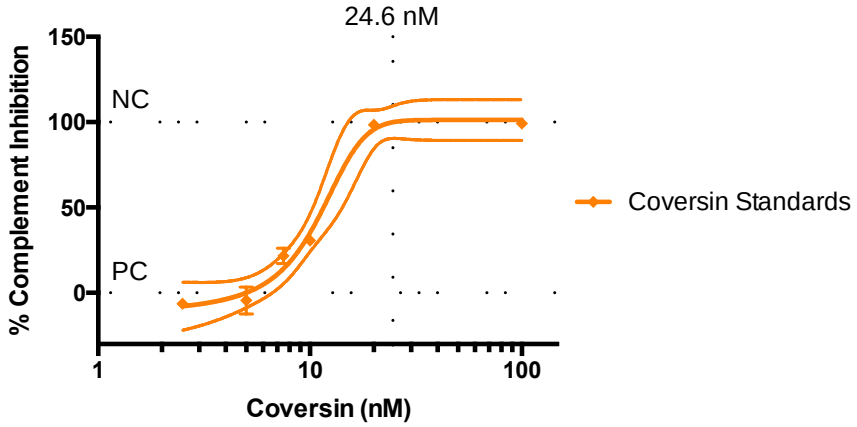

Coversin Formulation	Release Time (h)	Complement Inhibition[a] (%)	Concentration (nM)	Biologically Active[b] (%, Min.)
PBS Only	37	100.1 ± 0.03	87.0 ± 6.2	28.4 ± 2.1
	73	100.5 ± 0.35	27.9 ± 5.4	90.4 ± 17.0
HAtoco, PBS	33	100.0 ± 0.30	113.0 ± 8.9	21.9 ± 1.6
	73	99.8 ± 0.03	76.4 ± 3.0	32.2 ± 1.3

$$(1) \qquad \%\ \boldsymbol{Complement\ Inhibition} = \left(1 - \left(\frac{\boldsymbol{Sample - NC}}{\boldsymbol{PC - NC}}\right)\right) * \mathbf{100}$$

$$(2) \qquad \%\ \boldsymbol{Minimum\ Biologically\ Active} = \left(\frac{\boldsymbol{MinC_{FI}}}{\boldsymbol{Sample\ Concentration}}\right) * \mathbf{100}$$

Figure 3.19: (Above) Coversin dose response complement classical pathway MAC inhibition by ELISA with bounds determined by heat-inactivated serum (PC) and naïve serum (NC) responses. Minimum Coversin concentration required for 100% inhibition was found to be 24.6 nM by non-linear regression of the Coversin standard curve. Orange dotted-line represent 95% confidence interval of non-linear regression. (Below) [a]Complement inhibition activity of *in vitro* release samples formulated in PBS only (37h, 73h release time points) or HAtoco, PBS (33h, 73h time points) determined by PC and NC bounds (equation 1). [b]In order to assess the minimum percentage of biologically active protein present within each release sample, the measured concentration of

protein by RP-HPLC was compared to the measured concentration of fresh protein required for 100% inhibition ($MinC_{FI}$ = 24.6 nM) using equation 2. Error values are standard deviation (N = 3).

3.4 Discussion

Unwanted overactivation of the complement system underlies the core of a number of life-threatening diseases such as PNH and aHUS, which until recently did not have any available pharmacological treatment. Fortunately, with the development of potent complement system inhibitors such as Eculizumab, many lives have been saved and the quality of these patients' lives dramatically altered. However, available pharmacotherapies are limited, ineffective in many patients, and costly. There is a substantial need to develop new medicines to address and expand treatment efficacy within this patient population, while simultaneously reducing the cost associated with treatment to those who respond to currently approved drugs.

Coversin is a second-in-class C5-complement inhibitor shown to effectively treat patients with PNH and is currently being evaluated in multiple clinical trials. Based on initial human clinical data, a clear need exists for improved technical development of Coversin, because as it is currently formulated, greater than once-daily dosing would be required to maintain necessary complement inhibition. To reduce the burden associated with multiple daily injections, a simple release platform which effectively extends release of the therapeutic beyond 24 h and which does not compromise its biological activity is desperately needed.

A recently reported hyaluronic-Vitamin E (HAtoco) conjugate was shown to effectively release small molecule TLR agonists through a depot-like effect following intratumoral injections, and as a consequence was shown to effectively reduce tumor size in both a mice xenograft trial and pilot canine study.[32] In this study, HAtoco is examined for its capacity to sustain delivery of biologically active Coversin following subcutaneous injections and its effects on the protein's structural characteristics and thermal stability.

Following the synthesis and purification of 33 kDa HAtoco with a 10 mol% disaccharide substitution, the extended release of Coversin was initially evaluated using an *in vitro* system composed of a molecular weight dialysis bag and high molecular weight hyaluronan intended to mimic the environment of a subcutaneous injection site.[36] Against buffer alone and viscosity-matched controls (200 kDa HA), HAtoco at equal mass to loaded Coversin, extended release by greater than 2-fold by the release half-life and depot duration. Similarly, under *in vivo* conditions, Coversin labelled with fluorescent dye was loaded into the HAtoco matrix and release was extended nearly 2-fold by half-life and greater than 2-fold by depot duration. These results suggest HAtoco at ratios up to 1:1 Coversin:HAtoco (m/m) will extend release of the therapeutic to a level where multiple daily injections would not be required. Instead, potentially bi-weekly injections based on comparable release half-lives seen in PASylated coversin preclinical pharmacokinetic data and human projections are possible.[14, 27] Complications to this claim include the translatability of both *in vitro* and fluorescently labeled *in vivo* data towards a therapeutic pharmacokinetics profile and also the high dosing requirements currently in use at the clinic. Current clinical dosing regimens include a single ablating dose of 0.57 mg/kg with daily repeat maintenance doses set initially at 25% of the ablating dose.[25] To dose an average male patient (90 kg x 0.57mg/kg = 51.3 mg) subcutaneously with a volume of less than 1.5 ml (51.3 mg/1.5 ml = 34.2 mg/ml) to limit pain, a ratio of 3.42:1 (m/m), Coversin:HAtoco (i.e. 34.2 mg Coversin:10 mg HAtoco per ml) would be required for the ablating dose based on current viscosity limits syringeable through a 30-gauge needle (<50 cP).[37] The viscosity of the 10 mg/ml HAtoco used in this study is equal to 16.4 cP as discussed in Chapter II.

Based on binding isotherms determined by intrinsic tryptophan fluorescence signal quenching (Figure 3.8) and fluorescence polarization (Figure 3.10), >90% binding of Coversin to

HAtoco occurs near a ratio of 40:1 (m/m). This suggests the greatest increase in half-life release would be seen at ratios much lower than the 1:1 (m/m) tested in the *in vitro* assay, however when such ratios were used within the *in vivo* assay no increase in release half-life was observed. It is possible that *in vivo* factors such as higher surfactant concentrations could have weakened the binding between the HAtoco matrix and Coversin even at these lower ratios subsequently decreasing the observed release half-life.

Reductions in the melting temperature (T_m) of Coversin when >90% bound to HAtoco measured by both DSC and intrinsic tryptophan fluorescence, suggests destabilization of the Coversin native structure when associated with the HAtoco matrix, perhaps due to surface adsorption to the tocopherol moieties. It has been shown that hydrophobically-driven surface adsorption is energetically favorable due to the negative entropic contribution ($+\Delta S$) to the Gibbs free energy when water or counter ions are excluded from the protein surface upon binding.[38] Energetic effects on protein binding are largely dependent on the protein and surface of interest and their particular characteristics. BSA was reported to bind Alhydrogel® through apolar driven interactions and was found to have a considerably altered calorimetric thermogram with transitions occurring up to 39°C lower than the native protein.[39] BSA is however known to contain a large hydrophobic binding site which has shown the ability to self-associate[40] and may represent the extreme of such binding when coupled with *in vitro* release data from Chapter II where HAtoco bound BSA released less than 20% over 25 days.

The lipocalin family of proteins, of which Coversin (OmCI) is a member, are known to bind a wide-range of small hydrophobic ligands as part of their natural function as extracellular transport proteins.[41] These ligands include molecules with critical biological function such as long-chain fatty acids, triacylglycerols, steroids and recently vitamin A and E (e.g. (+)-α-tocopherol).[23,

[42] Vitamin E in its water-soluble form of D-α-tocopheryl polyethylene glycol succinate (TPGS), was recently shown to decrease antibiotic resistance *in vitro* by binding the lipocalin protein BcnA produced by the gram-negative bacteria *Burkholderia cenocepacia* and subsequently inhibiting its function as a global extracellular mechanism of antimicrobial resistance.[43] Similarly, Coversin has been shown to bind the fatty acid derivatives ricinoleic acid, palmitic acid, stearic acid and tetraethylene glycol diethylether within the lipocalin conserved, central, eight-stranded antiparallel β-barrel.[22] This structure, known as the lipocalin fold or pocket, is widely accepted as the primary binding region of hydrophobic ligands for all proteins of the lipocalin family. Similar to our results seen upon HAtoco binding to Coversin, structural studies on the effects of hydrophobic ligand binding to the β-barrel pocket within human tear lipocalin protein have shown reversible increases in β-sheet structure.[44-46] In addition, extensive x-ray crystallography, NMR and site-directed mutagenesis studies coupled with docking models have shown that the therapeutic inhibition of C5 by Coversin (OmCI) occurs through binding on the opposite face from the characteristic β-barrel pocket.[20, 22] These studies have also found that Coversin is capable of binding its other therapeutic ligand, the proinflammatory leukotriene LTB4 which binds within the β-barrel fold, simultaneous to binding C5 in a noncooperative manner.[47, 48] Overall, these results coupled with the observed preservation of the C5 inhibitory function of Coversin upon release from HAtoco suggest that the tocopherol moieties of HAtoco bind to Coversin within the characteristic β-barrel ligand pocket without perturbation of the C5 binding site on its opposite face. Further studies are required to assess the reversibility in secondary structure alterations within the β-barrel pocket upon binding to HAtoco and its effects on LTB4 therapeutic binding upon release.

3.5 Conclusion

Coversin, a second-in-class C5 inhibitor, has shown promise in the continued development of the breakthrough therapies inhibiting complement activation for patients suffering from PNH and aHUS. In an effort to reduce the injection frequency of Coversin, HAtoco was shown to extend the release of Coversin in both *in vitro* and *in vivo* models. In addition, C5 inhibitory activity was observed following release of Coversin from the HAtoco matrix for at least 73 h. Structural studies suggest Coversin binding to HAtoco occurs through hydrophobically driven surface adsorption with binding likely occurring within the characteristic lipocalin β-barrel opposite the Coversin-C5 interface. Overall, HAtoco may be considered as a simple platform capable of extending the release of biologically active Coversin following subcutaneous injection. Extension of the release would reduce dosing frequency and thus improve Coversin's potential as a cheaper, efficacious therapeutic option for atypical hemolytic uremic syndrome and paroxysmal nocturnal hemoglobinuria patients.

3.6 References

1. Murphy, K.; Travers, P.; Walport, M.; Janeway, C., *Janeway's immunobiology*. 8th ed.; Garland Science: New York, 2012; p xix, 868 p.
2. Nesargikar, P.; Spiller, B.; Chavez, R., The complement system: History, pathways, cascade and inhibitors. *European Journal of Microbiology and Immunology* **2012,** *2* (2), 103-111.
3. Ricklin, D.; Lambris, J. D., Complement in Immune and Inflammatory Disorders: Pathophysiological Mechanisms. *The Journal of Immunology* **2013,** *190* (8), 3831-3838.
4. Brodsky, R. A., Paroxysmal nocturnal hemoglobinuria. *Blood* **2014,** *124* (18), 2804-2811.
5. Afshar-Kharghan, V., Atypical hemolytic uremic syndrome. *Hematology* **2016,** *2016* (1), 217-225.
6. Socié, G.; Mary, J.-Y.; de Gramont, A.; Rio, B.; Leporrier, M.; Rose, C.; Heudier, P.; Rochant, H.; Cahn, J.-Y.; Gluckman, E., Paroxysmal nocturnal haemoglobinuria: long-term follow-up and prognostic factors. *The Lancet* **1996,** *348* (9027), 573-577.
7. Hill, A.; Kelly, R. J.; Hillmen, P., Thrombosis in paroxysmal nocturnal hemoglobinuria. *Blood* **2013,** *121* (25), 4985-4996.
8. Thomas, T. C.; Rollins, S. A.; Rother, R. P.; Giannoni, M. A.; Hartman, S. L.; Elliott, E. A.; Nye, S. H.; Matis, L. A.; Squinto, S. P.; Evans, M. J., Inhibition of complement activity by humanized anti-C5 antibody and single-chain Fv. *Mol Immunol* **1996,** *33* (17-18), 1389-401.
9. Kelly, R. J.; Hill, A.; Arnold, L. M.; Brooksbank, G. L.; Richards, S. J.; Cullen, M.; Mitchell, L. D.; Cohen, D. R.; Gregory, W. M.; Hillmen, P., Long-term treatment with

eculizumab in paroxysmal nocturnal hemoglobinuria: sustained efficacy and improved survival. *Blood* **2011,** *117* (25), 6786-6792.

10. Legendre, C. M.; Licht, C.; Muus, P.; Greenbaum, L. A.; Babu, S.; Bedrosian, C.; Bingham, C.; Cohen, D. J.; Delmas, Y.; Douglas, K.; Eitner, F.; Feldkamp, T.; Fouque, D.; Furman, R. R.; Gaber, O.; Herthelius, M.; Hourmant, M.; Karpman, D.; Lebranchu, Y.; Mariat, C.; Menne, J.; Moulin, B.; Nürnberger, J.; Ogawa, M.; Remuzzi, G.; Richard, T.; Sberro-Soussan, R.; Severino, B.; Sheerin, N. S.; Trivelli, A.; Zimmerhackl, L. B.; Goodship, T.; Loirat, C., Terminal Complement Inhibitor Eculizumab in Atypical Hemolytic–Uremic Syndrome. *New England Journal of Medicine* **2013,** *368* (23), 2169-2181.

11. FDA approves ravulizumab-cwvz for paroxysmal nocturnal hemoglobinuria. FDA: fda.gov, 2018.

12. U.S. FDA Accepts Supplemental Biologics License Application (SBLA) For ULTOMIRIS® (Ravulizumab-Cwvz) Under Priority Review For The Treatment Of Atypical Hemolytic Uremic Syndrome (AHUS). Alexion Pharmaceuticals: news.alexion.com, 2019.

13. Lee, J. W.; Sicre De Fontbrune, F.; Wong Lee Lee, L.; Pessoa, V.; Gualandro, S.; Füreder, W.; Ptushkin, V.; Rottinghaus, S. T.; Volles, L.; Shafner, L.; Aguzzi, R.; Pradhan, R.; Schrezenmeier, H.; Hill, A., Ravulizumab (ALXN1210) vs eculizumab in adult patients with PNH naive to complement inhibitors: the 301 study. *Blood* **2019,** *133* (6), 530-539.

14. Kuhn, N.; Schmidt, C. Q.; Schlapschy, M.; Skerra, A., PASylated Coversin, a C5-Specific Complement Inhibitor with Extended Pharmacokinetics, Shows Enhanced Anti-Hemolytic Activity in Vitro. *Bioconjugate Chemistry* **2016,** *27* (10), 2359-2371.

15. Risitano, A. M.; Notaro, R.; Marando, L.; Serio, B.; Ranaldi, D.; Seneca, E.; Ricci, P.; Alfinito, F.; Camera, A.; Gianfaldoni, G.; Amendola, A.; Boschetti, C.; Di Bona, E.; Fratellanza, G.; Barbano, F.; Rodeghiero, F.; Zanella, A.; Iori, A. P.; Selleri, C.; Luzzatto, L.; Rotoli, B., Complement fraction 3 binding on erythrocytes as additional mechanism of disease in paroxysmal nocturnal hemoglobinuria patients treated by eculizumab. *Blood* **2009,** *113* (17), 4094-4100.

16. Lin, Z.; Schmidt, C. Q.; Koutsogiannaki, S.; Ricci, P.; Risitano, A. M.; Lambris, J. D.; Ricklin, D., Complement C3dg-mediated erythrophagocytosis: implications for paroxysmal nocturnal hemoglobinuria. *Blood* **2015,** *126* (7), 891-894.

17. Ariceta, G., Optimal duration of treatment with eculizumab in atypical hemolytic uremic syndrome (aHUS)—a question to be addressed in a scientific way. *Pediatric Nephrology* **2019**.

18. Thomson, N.; Ulrickson, M., Maintenance eculizumab dose adjustment in the treatment of atypical hemolytic uremic syndrome: a case report and review of the literature. *Clinical Case Reports* **2016,** *4* (8), 773-776.

19. Nunn, M. A.; Sharma, A.; Paesen, G. C.; Adamson, S.; Lissina, O.; Willis, A. C.; Nuttall, P. A., Complement Inhibitor of C5 Activation from the Soft Tick Ornithodoros moubata. *The Journal of Immunology* **2005,** *174* (4), 2084-2091.

20. Jore, M. M.; Johnson, S.; Sheppard, D.; Barber, N. M.; Li, Y. I.; Nunn, M. A.; Elmlund, H.; Lea, S. M., Structural basis for therapeutic inhibition of complement C5. *Nature Structural & Molecular Biology* **2016,** *23* (5), 378-386.

21. Nishimura, J.-I.; Yamamoto, M.; Hayashi, S.; Ohyashiki, K.; Ando, K.; Brodsky, A. L.; Noji, H.; Kitamura, K.; Eto, T.; Takahashi, T.; Masuko, M.; Matsumoto, T.; Wano, Y.; Shichishima, T.; Shibayama, H.; Hase, M.; Li, L.; Johnson, K.; Lazarowski, A.; Tamburini, P.; Inazawa, J.; Kinoshita, T.; Kanakura, Y., Genetic Variants in C5 and Poor Response to Eculizumab. *New England Journal of Medicine* **2014,** *370* (7), 632-639.

22. Roversi, P.; Lissina, O.; Johnson, S.; Ahmat, N.; Paesen, G. C.; Ploss, K.; Boland, W.; Nunn, M. A.; Lea, S. M., The Structure of OMCI, a Novel Lipocalin Inhibitor of the Complement System. *Journal of Molecular Biology* **2007,** *369* (3), 784-793.

23. Schiefner, A.; Skerra, A., The Menagerie of Human Lipocalins: A Natural Protein Scaffold for Molecular Recognition of Physiological Compounds. **2015,** *48* (4), 976-985.

24. Risitano, A. M.; Marotta, S., Toward complement inhibition 2.0: Next generation anticomplement agents for paroxysmal nocturnal hemoglobinuria. *American Journal of Hematology* **2018,** *93* (4), 564-577.

25. Coversin in Paroxysmal Nocturnal Haemoglobinuria (PNH). FDA, Ed. Clinicaltrials.gov, 2018.

26. Schlapschy, M.; Binder, U.; Borger, C.; Theobald, I.; Wachinger, K.; Kisling, S.; Haller, D.; Skerra, A., PASylation: a biological alternative to PEGylation for extending the plasma half-life of pharmaceutically active proteins. *Protein Engineering Design and Selection* **2013,** *26* (8), 489-501.

27. Akari Therapeutics Announces New Data Highlighting Differentiation of Drug Candidate Coversin. Akari Therapeutics: investor.akaritx.com, 2018.

28. Mitragotri, S.; Burke, P. A.; Langer, R., Overcoming the challenges in administering biopharmaceuticals: formulation and delivery strategies. *Nature Reviews Drug Discovery* **2014,** *13* (9), 655-672.

29. Jones, G. B.; Collins, D. S.; Harrison, M. W.; Thyagarajapuram, N. R.; Wright, J. M., Subcutaneous drug delivery: An evolving enterprise. *Science Translational Medicine* **2017,** *9* (405), eaaf9166.

30. Patel, A.; Cholkar, K.; Mitra, A. K., Recent developments in protein and peptide parenteral delivery approaches. *Therapeutic Delivery* **2014,** *5* (3), 337-365.

31. Vermonden, T.; Censi, R.; Hennink, W. E., Hydrogels for Protein Delivery. **2012,** *112* (5), 2853-2888.

32. Lu, R.; Groer, C.; Kleindl, P. A.; Moulder, K. R.; Huang, A.; Hunt, J. R.; Cai, S.; Aires, D. J.; Berkland, C.; Forrest, M. L., Formulation and preclinical evaluation of a toll-like receptor 7/8 agonist as an anti-tumoral immunomodulator. *Journal of Controlled Release* **2019,** *306*, 165-176.

33. Wei, Y.; Larson, N. R.; Angalakurthi, S. K.; Russell Middaugh, C., Improved Fluorescence Methods for High-Throughput Protein Formulation Screening. *SLAS TECHNOLOGY: Translating Life Sciences Innovation* **2018**, 247263031878062.

34. Yang, H.; Yang, S.; Kong, J.; Dong, A.; Yu, S., Obtaining information about protein secondary structures in aqueous solution using Fourier transform IR spectroscopy. *Nature Protocols* **2015,** *10*, 382.

35. Quenching of Fluorescence. In *Principles of Fluorescence Spectroscopy*, Lakowicz, J. R., Ed. Springer US: Boston, MA, 2006; pp 277-330.

36. Kinnunen, H. M.; Sharma, V.; Contreras-Rojas, L. R.; Yu, Y.; Alleman, C.; Sreedhara, A.; Fischer, S.; Khawli, L.; Yohe, S. T.; Bumbaca, D.; Patapoff, T. W.; Daugherty, A. L.; Mrsny, R. J., A novel in vitro method to model the fate of subcutaneously administered biopharmaceuticals and associated formulation components. *Journal of Controlled Release* **2015,** *214*, 94-102.

37. Miller, M. A.; Engstrom, J. D.; Ludher, B. S.; Johnston, K. P., Low Viscosity Highly Concentrated Injectable Nonaqueous Suspensions of Lysozyme Microparticles. **2010,** *26* (2), 1067-1074.

38. Roach, P.; Farrar, D.; Perry, C. C., Interpretation of Protein Adsorption: Surface-Induced Conformational Changes. **2005,** *127* (22), 8168-8173.

39. Jones, L. S.; Peek, L. J.; Power, J.; Markham, A.; Yazzie, B.; Middaugh, C. R., Effects of Adsorption to Aluminum Salt Adjuvants on the Structure and Stability of Model Protein Antigens. **2005,** *280* (14), 13406-13414.

40. Bulone, D.; Martorana, V.; San Biagio, P. L., Effects of intermediates on aggregation of native bovine serum albumin. **2001,** *91* (1), 61-69.

41. Flower, D. R., The lipocalin protein family: structure and function. *Biochemical Journal* **1996,** *318* (1), 1-14.

42. El-Halfawy, O. M.; Klett, J.; Ingram, R. J.; Loutet, S. A.; Murphy, M. E. P.; Martín-Santamaría, S.; Valvano, M. A., Antibiotic Capture by Bacterial Lipocalins Uncovers an Extracellular Mechanism of Intrinsic Antibiotic Resistance. **2017,** *8* (2), e00225-17.

43. Naguib, M. M.; Valvano, M. A., Vitamin E Increases Antimicrobial Sensitivity by Inhibiting Bacterial Lipocalin Antibiotic Binding. *mSphere* **2018,** *3* (6).

44. Gasymov, O. K.; Abduragimov, A. R.; Yusifov, T. N.; Glasgow, B. J., Structural changes in human tear lipocalins associated with lipid binding. *Biochim Biophys Acta* **1998,** *1386* (1), 145-156.

45. Dartt, D. A., Tear Lipocalin: structure and Function. **2011,** *9* (3), 126-138.

46. Norde, W.; Horbett, T. A.; Brash, J. L., Proteins at Interfaces III: Introductory Overview. In *Proteins at Interfaces III State of the Art*, American Chemical Society: 2012; Vol. 1120, pp 1-34.

47. Roversi, P.; Ryffel, B.; Togbe, D.; Maillet, I.; Teixeira, M.; Ahmat, N.; Paesen, G. C.; Lissina, O.; Boland, W.; Ploss, K.; Caesar, J. J. E.; Leonhartsberger, S.; Lea, S. M.; Nunn, M. A., Bifunctional Lipocalin Ameliorates Murine Immune Complex-induced Acute Lung Injury. **2013,** *288* (26), 18789-18802.

48. Macpherson, A.; Liu, X.; Dedi, N.; Kennedy, J.; Carrington, B.; Durrant, O.; Heywood, S.; Van Den Elsen, J.; Lawson, A. D. G., The rational design of affinity-attenuated OmCI for the purification of complement C5. *Journal of Biological Chemistry* **2018,** *293* (36), 14112-14121.